Report
R-21-18
February 2022

Potential effects of concrete plugs on the near-field flow in SFR

Alvaro Sainz-Garcia
Diego Sampietro
Elena Abarca
Jorge Molinero

SVENSK KÄRNBRÄNSLEHANTERING AB

SWEDISH NUCLEAR FUEL
AND WASTE MANAGEMENT CO

Box 3091, SE-169 03 Solna
Phone +46 8 459 84 00
skb.se

SVENSK KÄRNBRÄNSLEHANTERING

ISSN 1402-3091
SKB R-21-18
ID 1689100

February 2022

Potential effects of concrete plugs on the near-field flow in SFR

Alvaro Sainz-Garcia, Diego Sampietro, Elena Abarca, Jorge Molinero
Amphos 21 Consulting S.L.

Abstract

The present work is an extension of the analysis of the hydrological behaviour of the near-field carried out as part of the long-term safety assessment for the SFR extension application (Abarca et al. 2013, 2014).

The initial design of the extended SFR considered sealed sections of bentonite for closure of both facilities (SFR1 and SFR3) after operation (Abarca et al. 2013, 2014). However, using bentonite as sealing material requires complex installation, the support of concrete structural plugs and put requirements on tunnel dimensions and mechanical stability of the surrounding rock. For those reasons, concrete is considered as an alternative material for the sealing plugs.

In this report, the work in Abarca et al. (2013) is extended to include concrete sealing plugs in the repository-scale models of the existing facility (SFR1) and the planned extension (SFR3). Recent advances in the assessment of the temporal evolution of the hydraulic properties of chemically degrading concrete for the SFL repository (Idiart and Shafei 2019, Idiart and Laviña 2019) is used to better conceptualize the hydraulic properties of the degrading plugs. A set of cases of homogeneous and axial concrete degradation are evaluated using the repository-scale models of SFR1 and SFR3. Flow rates through predefined control volumes are calculated and transferred to radionuclide transport calculations following the procedure in Abarca et al. (2013).

Sammanfattning

Detta arbete är en utvidgning av analysen av närfältets hydrologiska egenskaper som genomförts som en del av den långsiktiga säkerhetsanalysen för ansökan om utbyggnad av SFR (Abarca et al. 2013, 2014).

Den initiala utformningen av SFR innefattar användning av bentonitpluggar för försegling av sektioner vid förslutning av båda anläggningarna (SFR1 och SFR3) efter drift (Abarca et al. 2013, 2014). Installationen av bentonitpluggar är komplex och medför behov av stödjande betongpluggar och ställer krav på tunneldimensioner och den mekaniska stabiliteten hos det omgivande berget. Av dessa skäl betraktas betong som ett alternativt material till bentonit för tätningspluggarna.

I denna rapport har arbetet i Abarca et al. (2013) utökats till att omfatta tätningspluggar av betong i förvarsmodellerna för den befintliga anläggningen (SFR1) och den planerade utbyggnaden (SFR3). I studien har nya kunskaper om de hydrauliska egenskaperna hos betong under kemisk degradering framtagits för SFL-förvaret (Idiart och Shafei 2019, Idiart och Laviña 2019) använts för att bättre beskriva hydrauliska egenskaper hos degraderade betongpluggar. En uppsättning beräkningsfall av homogen och axiell betongnedbrytning har utvärderats med hjälp av förvarsmodellerna för SFR1 och SFR3. Flödeshastigheterna genom fördefinierade kontrollvolymer har beräknats och använts till radionuklidtransportberäkningar i enlighet med metodiken i Abarca et al. (2013).

Contents

1 Introduction and objectives 7
1.1 Objectives 8

2 Methodology 9
2.1 Definition of the simulation cases 10
2.2 Data transfer to Ecolego 11
2.3 Outline of the report 11

3 Description of the models 13
3.1 Geometry 13
3.1.1 Repository-scale model 13
3.1.2 Single plug model 14
3.2 Initial state of the repository materials 15
3.2.1 Repository-scale model 15
3.2.2 Single plug model 16
3.3 Properties of the host rock 17
3.4 Governing equations 18
3.4.1 Groundwater flow 18
3.4.2 Concrete leaching 19
3.4.3 Impact of concrete leaching in the hydrodynamic properties of concrete 20
3.5 Boundary conditions 23
3.5.1 Repository-scale models 23
3.5.2 Single plug model 23
3.6 Mesh discretization 24
3.6.1 Repository-scale model 24
3.6.2 Single plug model 24

4 Repository closure with concrete plugs 25
4.1 SFR1 25
4.1.1 Groundwater streamlines 26
4.1.2 Total flow rates through the vaults and waste 29
4.1.3 Comparison with alternative closure case 30
4.2 SFR3 31
4.2.1 Groundwater streamlines 31
4.2.2 Total flow through the vaults and waste 34

5 Homogeneous concrete degradation 35
5.1 Degradation cases 35
5.2 SFR1 38
5.3 SFR3 40
5.4 Discussion 42

6 Shrinking core plug degradation 43
6.1 Single plug model 43
6.1.1 Studied cases 43
6.1.2 Results 44
6.2 Repository scale model 47
6.2.1 Degradation cases 47
6.2.2 SFR1 49
6.2.3 SFR3 50
6.3 Discussion 53

7 Conclusion 55

References 57

Appendix A Homogeneous concrete degradation 59
Appendix B Single plug model with the stepwise degradation front 63
Appendix C Axial concrete degradation 67

1 Introduction and objectives

The Swedish Nuclear Fuel and Waste Management Company (SKB) operates the repository for low- and intermediate-level radioactive operational waste (SFR) located in Forsmark. The rock vaults of the existing facility are located approximately 60 m below the seabed. An extension of the SFR is planned to mainly accommodate waste arising from the decommissioning of Swedish nuclear power plants. The SFR extension will be excavated, at a depth of around 120 m. A schematic view of the repository and its extension is shown in Figure 1-1.

The hydrological behaviour of the near-field of extended SFR was analysed as part of the long-term safety assessment for the SFR extension application, SR-PSU. The future hydrogeological conditions of the SFR1 (the existing facility) and the SFR3 (the planned extension) were explored in Abarca et al. (2013, 2014). The term near-field refers to the engineered barrier system (EBS) components that are designed to contain the waste, and the host rock in the vicinity of the repository.

In Abarca et al. (2013, 2014), numerical models were set up and solved in COMSOL Multiphysics to increase the understanding of the near-field hydrology and to generate consistent input data to radionuclide transport calculations. Two repository-scale models, one for the SFR1 and another for the SFR3 were developed.

In SR-PSU, repository closure considers sealed sections of bentonite to restrict groundwater flow through the vaults. The bentonite sections are mechanically supported by ”earth dam plugs”. ”Earth dam plugs” consist in transition material composed by a 30 % bentonite and 70 % crushed rock that do not require local mechanical support from the rock walls. Bentonite installations also put requirements on tunnel dimensions and on the mechanical stability of the surrounding rock. In this work, concrete is being considered as an alternative material for sealing plugs. The potential advantages are that the complexity of the sealing system is reduced to only one component and that the requirements on supporting tunnel length are reduced. However, concrete plugs are susceptible to degradation and they may lose their sealing capacity with time.

In this report, the work in Abarca et al. (2013) is extended to include concrete sealing plugs in the repository-scale models of SFR1 and SFR3. Recent advances in the assessment of the temporal evolution of the hydraulic properties of chemically degrading concrete for the SFL repository (Idiart and Shafei 2019) will be used to better conceptualize the hydraulic properties of the degrading plugs.

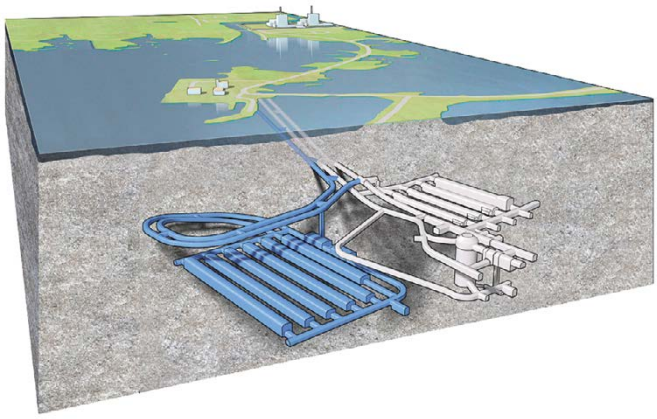

Figure 1-1. *Schematic view of the SFR repository in Forsmark: SFR1 (gray) and SFR3 (blue).*

1.1 Objectives

The objective of this work is to evaluate the implications of using concrete as sealing material on the near-field hydrogeology of SFR.

A second objective of this project is to improve the conceptualization of the hydraulic properties of a degrading concrete plug using recent results of reactive transport models of concrete degradation (Idiart and Shafei 2019).

A set of cases of homogeneous and axial concrete degradation are computed using the repository-scale models of SFR1 and SFR3. The flow rates through predefined control volumes are computed and tabulated as input to radionuclide transport calculations following the procedure in Abarca et al. (2013).

2 Methodology

This work analyses the impact of concrete plugs on the groundwater flow in SFR1 and SFR3. The methodology is that applied in Abarca et al. (2013). The two repositories are represented in separate models (Figure 2-1). The commercial finite element code COMSOL Multiphysics (COMSOL 2015) has been used for the analysis. In addition to the geometry of the repository itself, the models also include a volume of surrounding rock. This volume is chosen such that any change of the hydraulic properties of the repository after closure, is expected to leave the reginal pressure field largely unaffected at the model boundary.

The pressure field at the boundaries is extracted from the regional hydrogeology model implemented in DarcyTools (Odén et al. 2014), as detailed in Abarca et al. (2013). Three different pressure fields are considered to represent the time-evolution of the groundwater flow due to land rise (Figure 3-13). Land rise causes the shoreline position to move and consequently changes the conditions above the repository from being initially submerged to land conditions. Land rise is the main contributor to changing groundwater flow over time.

The rock conductivity field corresponds with the Base_Case1_DFN_R85 in Odén et al. (2014).

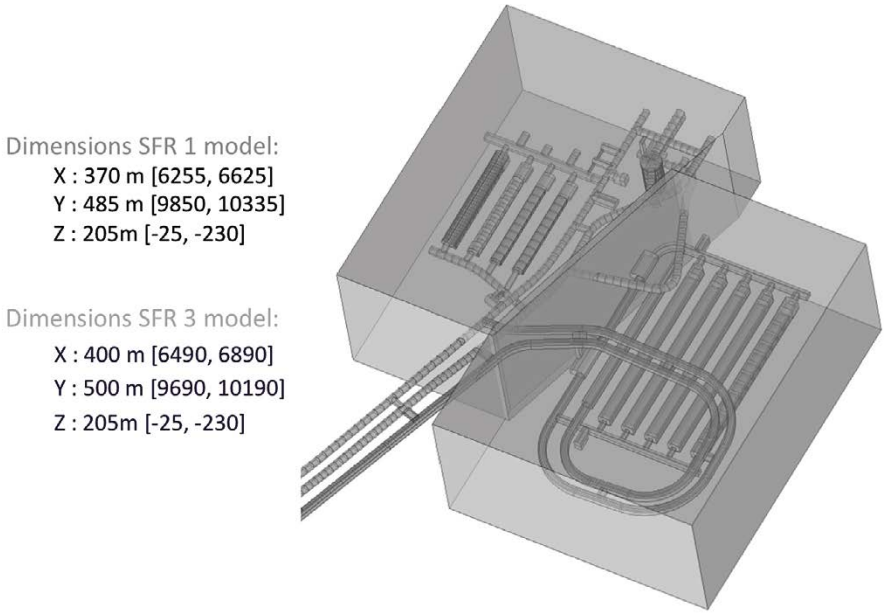

Figure 2-1. *3D model domains of the COMSOL model of the SFR1 and SFR3 repositories (Abarca et al. 2013).*

2.1 Definition of the simulation cases

A case of an alternative closure with concrete plugs is simulated with the SFR1 and SFR3 models for all three shoreline positions. The distribution of the plugs is that of the alternative closure case in Abarca et al. (2013) (Figure 2-2). All the models are steady-state models except the single plug model (see Table 2-1). The evolution of the flow in the repository is characterized by the flow rates through control volumes in which the vaults have been divided.

Recent reactive transport models of concrete chemical degradation (Höglund 2014, Idiart and Shafei 2019, Idiart and Laviña 2019) have shown that the leaching of calcium causes a gradual deterioration of concrete. This deterioration starts at the interface rock/concrete and penetrates into the concrete, resulting in a weakly weathered zone where portlandite is depleted, and a severely weathered zone where both portlandite and CSH are consumed. For this reason, a more sophisticated degradation approach has been considered for the plugs. Hereafter, this approach is referred as axial degradation. It consists of the following steps:

- The Wall distance physics in COMSOL Multiphysics (COMSOL 2015) is used to calculate the minimum distance to the rock/concrete interface at all points in the plug domain.
- The depth of the degradation front is computed with a 1D analytical solution for a shrinking core model (SCM) (Levenspiel 1972, Höglund 2014) assuming diffusion-control transport and dissolution of mineral phases under thermodynamic equilibrium conditions.
- Then, a porosity function is defined as a function of the depth of the degradation front. Here, two porosity functions are considered: a step porosity function characteristic of a step degradation front and a more realistic gradual increase in porosity characteristic of a gradual calcium leaching.
- The hydraulic conductivity of the concrete plugs can be defined as a function of porosity. Here, the modified Kozeny-Carman relation between the hydraulic conductivity of the concrete and the porosity changes is used to calculate the spatial distribution of the concrete conductivity.
- A groundwater flow simulation is computed with the spatial distribution of the plugs hydraulic conductivity previously calculated.

The axial degradation of plugs is first evaluated using a model of a single plug. The model represents a plug in a BLA vault in SFR3. This small-scale model is used to simulate a transient evolution of groundwater flow through a concrete plug degrading during 100 000 years with pressure field conditions corresponding to shoreline position 3. Subsequently, the axial degradation of the plugs is implemented in the repository-scale models of both SFR1 and SFR3 for shoreline position 3. Here, the degradation of the concrete plugs is determined by the penetration depth of degradation. The remaining concrete structures in the repository degrade homogeneously, as in the previous studies (Abarca et al. 2013). Six degradation cases are analysed considering three homogeneous concrete degradation states (moderate, severe and complete) for the concrete structures and four penetrations depths for the axial plug degradation (Table 2-1).

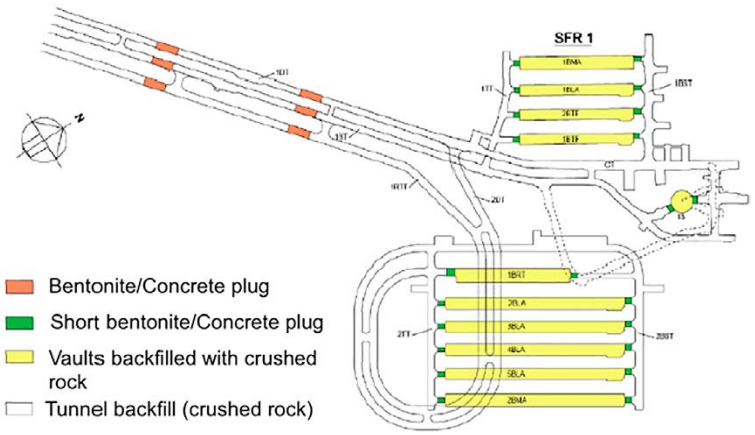

Figure 2-2. *Location of the plugs of the alternative closure case considered in this study. Modified from Abarca et al. (2013).*

2.2 Data transfer to Ecolego

The results of the groundwater flow simulations performed with the repository-scale models are tabulated to serve as input for radionuclide transport calculations with Ecolego. The data transfer from COMSOL to Ecolego is based on commonly defined control volumes. The partitioning of each vault into control volumes for Ecolego is described in detail in Abarca et al. (2013). This procedure results in a total of 280 control volumes used to calculate groundwater flow rates:

- 233 control volumes for SFR1
- 47 control volumes for SFR3

2.3 Outline of the report

Section 3 describes the repository-scale and single plug models. The geometry and material properties of the repository structures and the surrounding rock are defined. The model equations, boundary conditions and discretization are also detailed.

Section 4 describes the results of the groundwater flow simulations for the repository closure with concrete plugs at their initial state (Table 2-1). Groundwater flow streamlines and total flow rates through the vaults and waste domains for SFR1 and SFR3 repositories are described for three different shoreline positions.

Section 5 analyses the effects of the homogeneous degradation of concrete materials (Table 2-1) on the groundwater flow. Tunnel and waste flow rates for the three shoreline positions are presented and compared with the initial state results of the Section 4.

Section 6 studies the effect of the axial concrete leaching (Table 2-1) on the groundwater flow in the near field of the SFR1 and SFR3. The influence of axial degradation is first explored in a model of a single plug and then evaluated in the repository-scale models. The groundwater streamlines and the tunnel and waste flow rates are calculated.

Table 2-1. Table of simulation cases.

ID		Case definition	Geometry	Temporal span	
1		Concrete plugs closure (initial state)	SFR1	Shoreline position 1	
2				Shoreline position 2	
3				Shoreline position 3	
4			SFR3	Shoreline position 1	
5				Shoreline position 2	
6				Shoreline position 3	
7	Homogeneous concrete degradation	Moderate concrete degradation	SFR1	Shoreline position 1	
8				Shoreline position 2	
9				Shoreline position 3	
10			SFR3	Shoreline position 1	
11				Shoreline position 2	
12				Shoreline position 3	
13		Severe concrete degradation	SFR1	Shoreline position 1	
14				Shoreline position 2	
15				Shoreline position 3	
16			SFR3	Shoreline position 1	
17				Shoreline position 2	
18				Shoreline position 3	
19		Complete concrete degradation	SFR1	Shoreline position 1	
20				Shoreline position 2	
21				Shoreline position 3	
22			SFR3	Shoreline position 1	
23				Shoreline position 2	
24				Shoreline position 3	
25		Single plug model	Single plug	Transient (0–100 000 years)	Step degradation front
26					Gradual degradation front
27	Axial concrete degradation	Repository-scale model	SFR1	3 000 years	Gradual degradation front
28			SFR3		
29			SFR1	> 12 000 years	
30			SFR3		
31			SFR1	> 12 000 years	
32			SFR3		
33			SFR1	> 22 000 years	
34			SFR3		
35			SFR1	> 22 000 years	
36			SFR3		
37			SFR1	52 000 years	
38			SFR3		

3 Description of the models

This section describes the set-up of the repository-scale and the single plug models that have been used for the simulations. The full description of the repository-scale models of the SFR1 and SFR3 is presented in detail in Abarca et al. (2013). The information reported here focusses on the modifications carried out to simulate the repository closure with concrete plugs.

3.1 Geometry

3.1.1 Repository-scale model

The hydrogeological interaction between the SFR1 and SFR3 is assumed to be modest (Öhman et al. 2014). Therefore, two repository-scale models, one for the SFR1 and another for the repository extension, SFR3 were developed (Figure 2-1).

The SFR1 repository is composed of four vaults: 1BMA, 1BLA, 1BTF, and 2BTF and a Silo (Figure 3-1). The SFR3 will be composed of six additional vaults: 2BMA, 2BLA, 3BLA, 4BLA, 5BLA, and BRT. A detailed summary of the characteristics of the different vaults and engineering elements that form the SFR1 and SFR3 is detailed in Abarca et al. (2013).

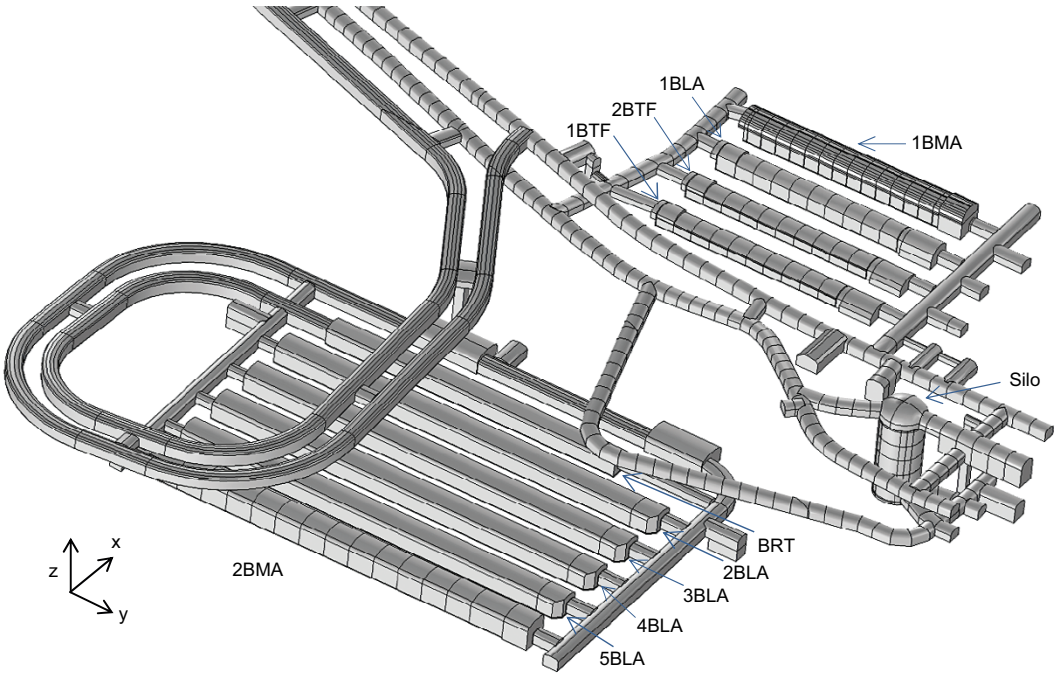

Figure 3-1. *Geometry of SFR1 (on the right) and SFR3 (on the left) from the CAD files as imported into COMSOL. The different configurations of the vaults are also considered.*

In addition to the geometry of the repository itself, the models also include a volume of surrounding rock. This volume is chosen such that any change of hydraulic properties of the repository will leave the regional pressure field unaffected. The dimensions and geometries of the SFR1 and SFR3 models are presented in Figure 2-1. The SFR1 model domain is defined by the local coordinates presented in Table 3-1 and the SFR3 model domain, by the coordinates in Table 3-2. The reference coordinate system (position and orientation) is consistent with the one used in the SDM report (SKB 2013).

Table 3-1. Local coordinates of the vertices defining the SFR1 COMSOL model.

X (m)	Y (m)	Z_{max} (m)	Z_{min} (m)
6625.00	10335.00	−25	−230
6625.00	10271.00	−25	−230
6496.12	9850.00	−25	−230
6255.00	9850.00	−25	−230
6255.00	10335.00	−25	−230

Table 3-2. Local coordinates of the vertices defining the SFR3 COMSOL model.

X (m)	Y (m)	Z_{max} (m)	Z_{min} (m)
6890.00	9690.00	−25	−230
6490.00	9690.00	−25	−230
6490.00	9865.96	−25	−230
6589.19	10190.00	−25	−230
6890.00	10190.00	−25	−230

3.1.2 Single plug model

A model of a representative plug in SFR is set up to study the axial degradation of a concrete plug. The plugs in SFR have similar geometry (Figure 3-4), and the southern plug of the 4BLA vault at the SFR3 is selected for the single plug model. The model domain is 35.5 × 24 × 36.4 m (Figure 3-2). The model includes the plug and 15 m (half distance between consecutive plugs) of rock in the x and z direction. In the y direction, half of the access tunnel (located at the south of the plug) and half of the loading area of BLA are included in the model. The loading area is located at the end of the vaults to allow the load and storage of the waste. The access tunnel and loading area are filled with crushed rock (macadam). The high permeability of this material controls the pressure field and gradient in the surroundings of the plug.

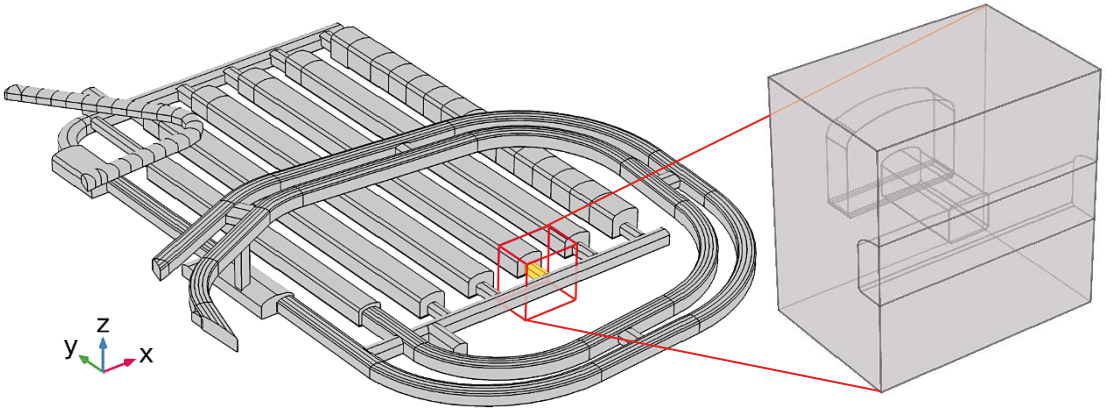

Figure 3-2. *3D view of the SFR3 repository and 4BLA southern plug used in the single plug model.*

The total volume of the model is 31 230 m^3, from which 28 141 m^3 corresponds to the host rock and 603.12 m^3 to the concrete plug. The coordinates of the model vertices are given in Table 3-3. The local coordinate system is consistent with the repository scale model and with SKB (2013).

Table 3-3. Local coordinates of the vertices defining the single plug model domain (external box).

X (m)	Y (m)	Z_{max} (m)	Z_{min} (m)
6711.12	9827.56	−112.21	−148.61
6746.72	9827.56	−112.21	−148.61
6711.12	9851.66	−112.21	−148.61
6746.72	9851.66	−112.21	−148.61

3.2 Initial state of the repository materials

3.2.1 Repository-scale model

Table 3-4 and Table 3-5 contain the values of hydraulic conductivity of the materials at the initial state for SFR1 and SFR3, respectively. The distribution of the repository materials is represented graphically in Figure 3-3 and Figure 3-4 for SFR1 and SFR3, respectively.

Two scenarios are considered for the beams and drainage system beneath the 1BMA concrete floor as in Abarca et al. (2013). In the High Permeability Beams (HPB) case, the beams are considering highly conductive ($K = 1.0 \times 10^{-3}$ m/s). In the Low Permeability Beams case (LPB), an effective conductivity of the beams equal to the structural concrete conductivity ($K = 8.3 \times 10^{-10}$ m/s) is considered. The results presented in the main report correspond to the LPB, whereas the results of the HPB are presented in Appendix A.

Table 3-4. Hydraulic conductivity values for the materials in the SFR1 repository.

Repository components	Materials		K (m/s)
Tunnels	Backfill		1.00E−03
Vaults	Structural concrete		8.30E−10
	Concrete Backfill (BTF vaults)		8.30E−09
	1BMA high permeable beams*		1.00E−03
	1BMA low permeable beams		8.30E−10
	Waste 1–2BTF vaults	K_x	3.79E−09
		K_y	6.65E−09
		K_z	6.79E−09
	Waste 1BLA		1.00E−03
	Waste (BMA)		8.30E−07
	Sand layer		1.00E−07
Silo	Top layer (90 % sand, 10 % bentonite)		1.00E−09
	Bottom layer (90 % sand, 10 % bentonite)		1.00E−09
	Waste		8.30E−07
	Silo concrete lid with gas evacuation pipes	$K_x = K_y$	8.30E−10
		K_z	3.00E−07
	Silo bentonite Walls		1.54E−12 × z (m) + 2.11E−10
Plugs	Concrete		8.30E−10

* High permeable beams considered as an alternative case. Its results are shown in Appendix A.

Table 3-5. Hydraulic conductivity values for the materials in SFR3.

Materials	K (m/s)
Concrete	8.30E−10
Backfill	1.00E−03
BRT grouted waste	8.30E−09
2BMA waste	8.30E−07
Sand layer	1.00E−07
2BMA gravel layer	1.00E−03
Concrete plugs	8.30E−10

3.2.2 Single plug model

The single plug model respresents the southern plug of the 4BLA vault in SFR3. The material properties of the repository included in the model domain corresponds to that of the 4BLA vault plus the concrete plug and the access tunnels (Figure 3-5).

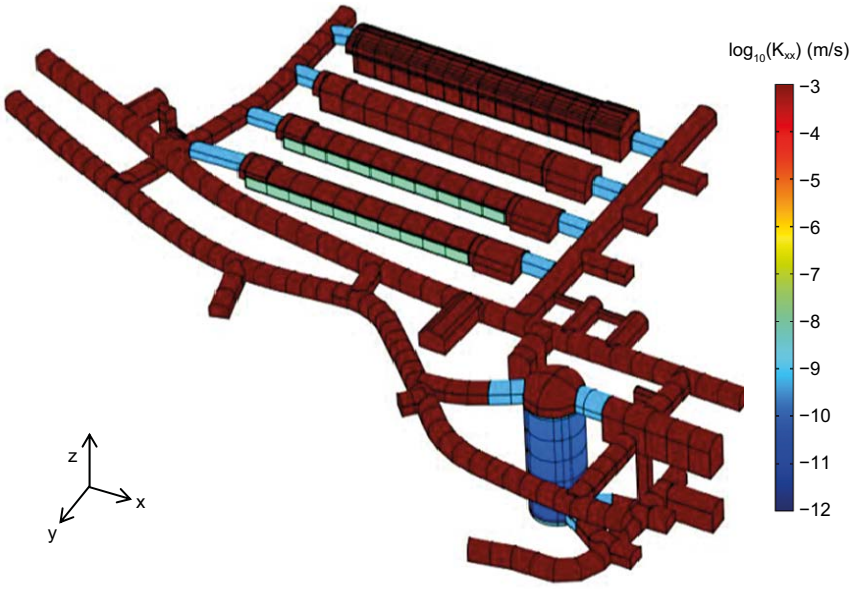

Figure 3-3. *Hydraulic conductivity in x direction of the SFR1 materials. The concrete plug location is shown in light blue.*

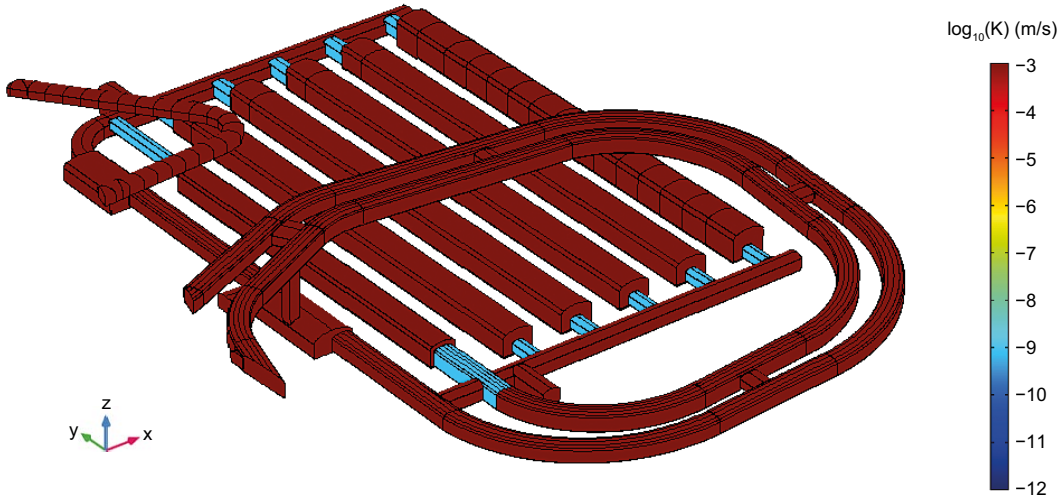

Figure 3-4. *Hydraulic conductivity of the SFR3 materials. The concrete plug location is shown in light blue.*

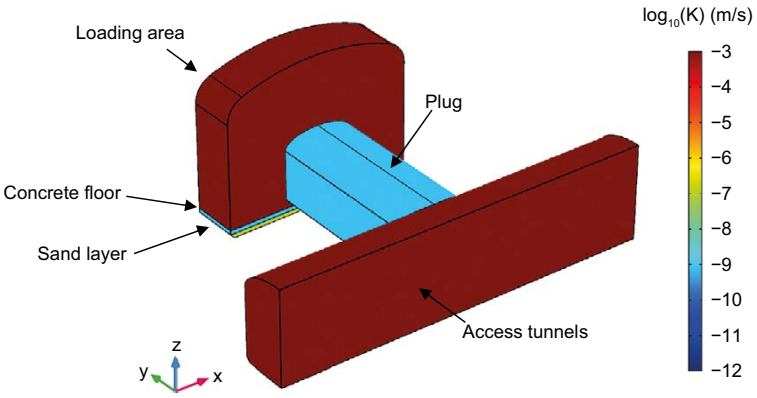

Figure 3-5. *Hydraulic conductivity of the materials in the single plug model.*

3.3 Properties of the host rock

SFR is located at Forsmark, situated in crystalline rock. Groundwater moves preferentially through deformation zones and small-scale fractures. The distribution, connectivity and transmissivity of these features determine the hydraulic properties of the rock mass. The hydraulic conductivity field data is extracted from the regional hydrogeology model. The data corresponds to the Case 1 (Base_Case1_DFN_R85), presented in Odén et al. (2014). Figure 3-6 and Figure 3-7 show the hydraulic conductivity of the rock surrounding SFR1 and SFR3, respectively. More detailed information can be found in Abarca et al. (2013).

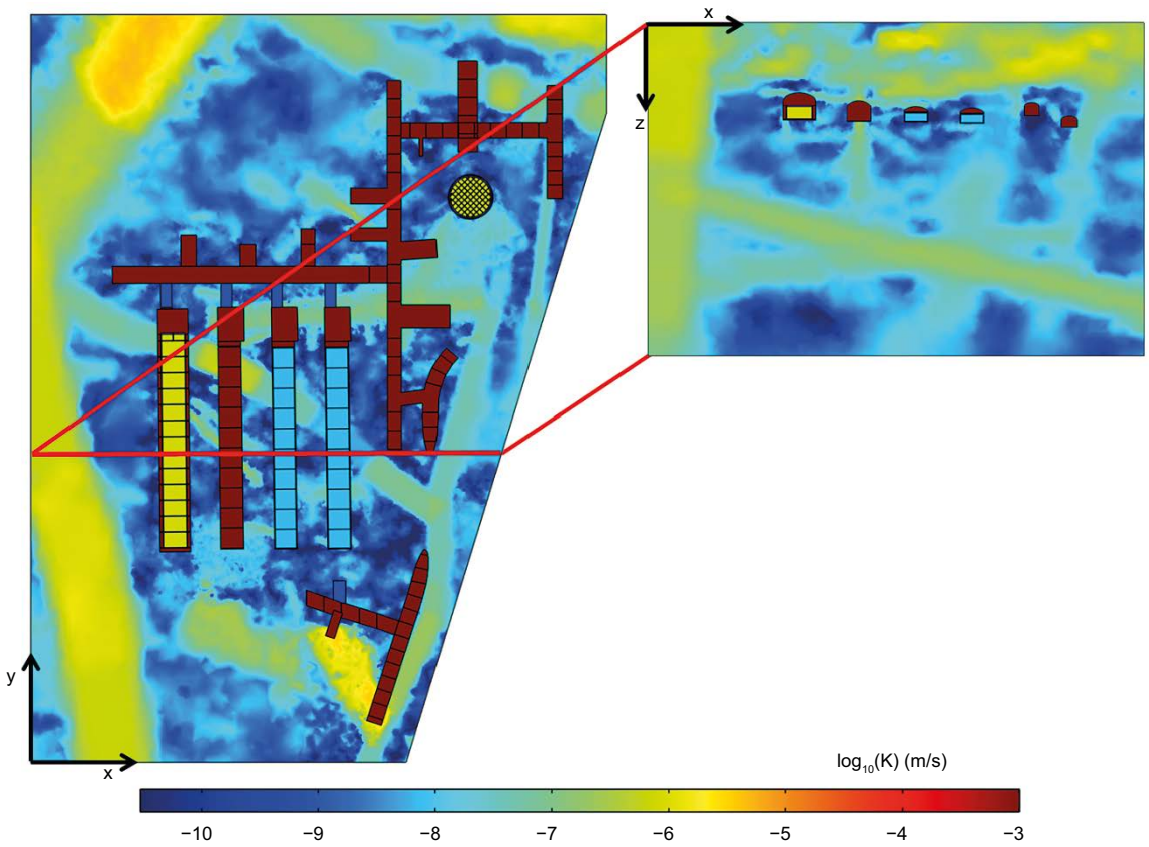

Figure 3-6. *Rock conductivity field (log10, m/s) in two orthogonal sections of the model domain (z = −82.5 m, and x = 10 050 m), and hydraulic conductivity of the rock vaults and tunnels for the initial state case. The horizontal conductivity is displayed.*

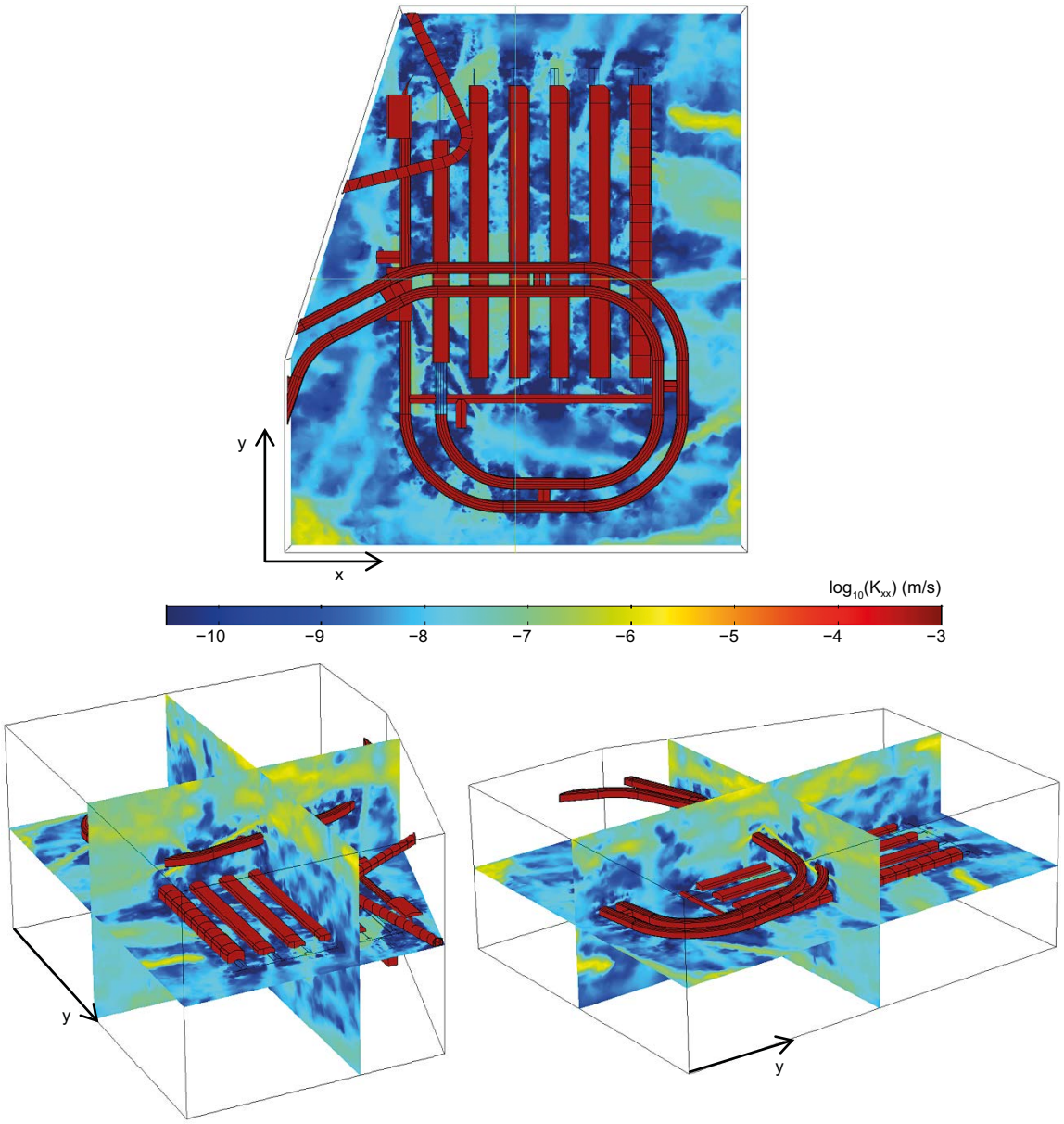

Figure 3-7. *Rock conductivity field (log10, m/s) in three orthogonal planes in the rock in the middle sections of the model domain and hydraulic conductivity of the rock vaults and tunnels at the initial state. The horizontal conductivity is displayed.*

3.4 Governing equations

3.4.1 Groundwater flow

The groundwater flow in porous media is modelled using the Subsurface Flow Module of COMSOL Multiphysics (COMSOL 2015). The water mass conservation is written as:

$$\frac{\partial(\rho\phi)}{\partial t} = -\nabla \cdot (\rho q) + Q \qquad \text{Equation 3-1}$$

Where, $\boldsymbol{q}$ is the Darcy velocity (m/s), ρ the water density (kg/m^3), ϕ the porosity of the media (–) and Q represents a sink/source term (m^3/s). The Darcy velocity can be expressed as:

$$\boldsymbol{q} = -\boldsymbol{k}/\boldsymbol{\mu}\,(\nabla \boldsymbol{p}) \qquad \text{Equation 3-2}$$

where k is the rock permeability (m^2), μ the dynamic viscosity (Pa/s) and p is the driving pressure (Pa), defined as the difference between the liquid pressure and the hydrostatic contribution ($\rho \cdot g \cdot z$), with g = –9.81 m/s^2 and z the elevation (negative in the present model). In this work, the repository scale

simulations are performed under steady-state conditions, so that the time derivative is equal to zero. Furthermore, constant water density is assumed and no sink/source terms are considered. As a result, Equation 3-3 reduces to its divergence free form:

$$\nabla \cdot (q) = \mathbf{0}$$ Equation 3-3

3.4.2 Concrete leaching

Groundwater leaches calcium from concrete, first from portlandite ($Ca(OH)_2$/CH) and then from silicate hydrate gel (CSH). Portlandite leaches faster than the less soluble CSH gel. Two zones could tentatively be defined in the degraded concrete (Höglund 2014); the weakly weathered zone, where portlandite is depleted, and the severely weathered zone where both portlandite and CSH are exhausted.

The penetration depth of the weakly weathered zone in a concrete slab has been represented by linear 1D shrinking core models (SCM) (Levenspiel 1972, Höglund 2014). A variety of analytical solutions (Höglund 2014) evaluate the penetration depth of the degradation front depending on the process controlling solute transport: diffusion, advection, fractures, etc.

In this study, the model of diffusion-controlled leaching of portlandite is applied to calculate the weakly weathered zone penetration (Höglund 2014). The model assumes diffusion-driven transport and dissolution of mineral phases under thermodynamic equilibrium conditions. The concentration of dissolved Ca at the boundary layer is consider equal to 0 (Figure 3-8). That assumption assumes that a high groundwater flow, parallel to the surface of the weathered concrete, flushes out the dissolved calcium. The groundwater flow in repository conditions will be lower and the concentration of Ca in the boundary layer higher than 0, following a diffusive profile. Therefore, for a diffusion driven leaching, this assumption is conservative for the first thousands of years because it maximizes the concentration gradient between the weathered zone and the surrounding rock. With these assumptions, the advance of the degradation front is decoupled from the groundwater flow through the weathered concrete. This is reasonable for the first thousands of years of degradation (Höglund 2014), although an advection controlled leaching would lead to larger penetration of the degradation front at later times.

The diffusive-controlled SCM for portlandite is expressed as:

$$h_{CH} = \sqrt{2\frac{D_{eff,deg} \cdot Ca_{sol}^{CH} \cdot t}{q_0^{CH}}}$$ Equation 3-4

where h_{CH} (m) is the leaching depth, $D_{eff,deg}$ (m^2/s) is a representative value of the effective diffusion coefficient of the degraded region, Ca_{sol}^{CH} is the solubility of portlandite (0.02 mol/l water) and q_0^{CH} is the initial concentration of portlandite in concrete (1.6016 mol/l medium). The values of the concentration and solubility of portlandite are assumed equal to those in Idiart and Laviña (2019) for the evaluation of concrete degradation in SFL.

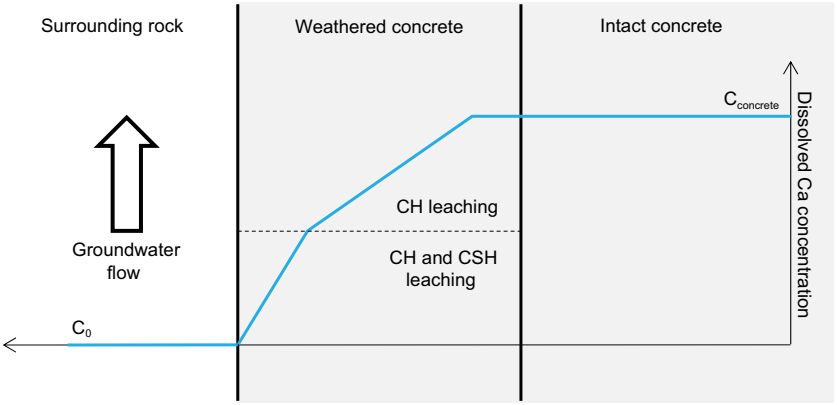

Figure 3-8. *Diagram of the diffusion-controlled shrinking core model in concrete. The blue line corresponds to the profile of dissolved concentration of calcium along the system.*

The penetration depth of the concrete leaching process is implemented in COMSOL through the Wall distance physics interface (COMSOL 2015), which evaluates the closest distance of any point within a volume to the border of that volume (Figure 3-9).

3.4.3 Impact of concrete leaching in the hydrodynamic properties of concrete

Concrete leaching leads to a gradual transformation of the concrete properties. When calcium minerals are depleted, the concrete can no longer act as alkaline buffer, and the mechanical strength decrease. Furthermore, leaching will increase the porosity of the concrete, in turn leading to higher hydraulic conductivity and effective diffusivity.

Porosity

The evolution of the concrete porosity due to leaching is a complex process that depends on the solubility of portlandite and CSH and the mass transport conditions. Typically, concrete porosity ranges from an initial value of 0.11 to a value of 0.3 for a totally degraded material (Höglund 2014, Idiart and Shafei 2019). In this study, two porosity functions are considered: a step porosity function characteristic of a step degradation front and a gradual increase in porosity (Figure 3-10).

The step function considers that concrete leaching leads to an immediate rise of the porosity to its maximum value (0.3). It is assumed that both portlandite and CSH weathers simultaneously, leaving a skeleton of the initial ballast material. This assumption is conservative, and it should be seen as a bounding case.

The gradual function is more realistic and is based on the reactive transport models of concrete degradation developed on Idiart and Shafei (2019) and Idiart and Laviña (2019). In the gradual function two leaching fronts are accounted for (Figure 3-10). The first corresponds to the leaching of portlandite, which increases the porosity from 0.11 to 0.165. The second increases the porosity from 0.175 to 0.3 and corresponds to the CSH leaching. The porosities between these two fronts coincide with the weakly weathered zone, while the severely weathered zone has a porosity of 0.3. In the gradual function, the transition zone between the intact concrete and the severely weathered zone has an extension of 1.2 m. It should be noticed that the actual evolution of porosity depends on many factors and this relation should be seen as a reasonable approximation.

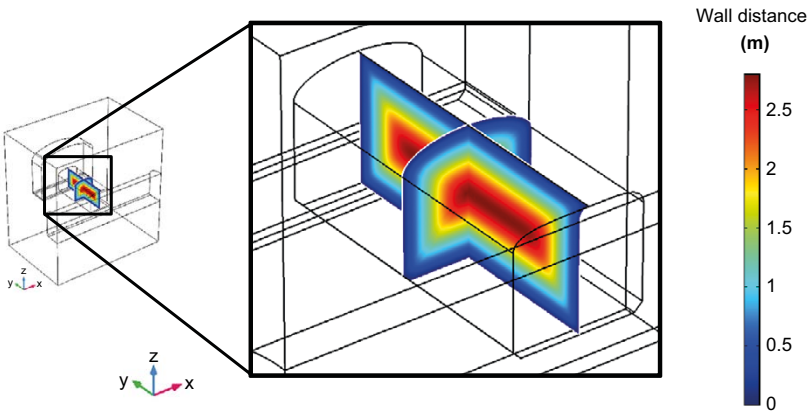

Figure 3-9. *Result of the wall distance function in the plug domain. It evaluates the closest distance, in meters, from any point of the plug to the plug boundaries.*

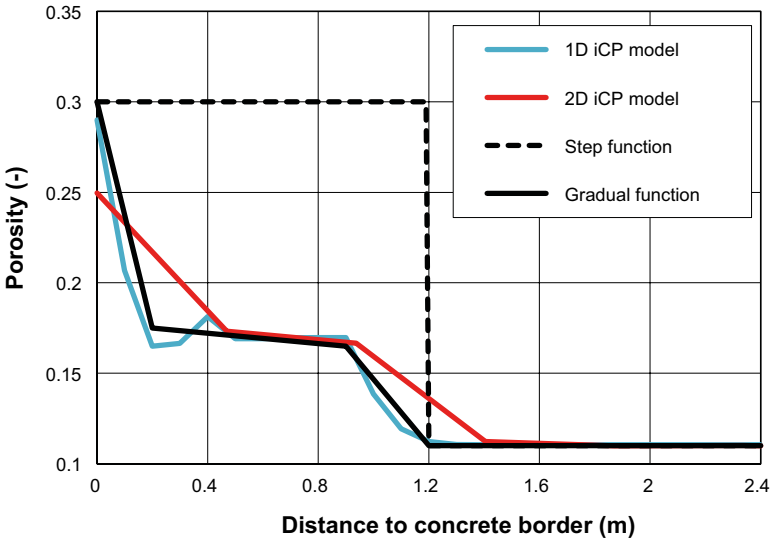

Figure 3-10. *Porosity spatial distribution due to concrete leaching. The concrete outer border is located at coordinate 0. Results from the 2D reactive transport model in Idiart and Shafei (2019) (red); results from the 1D reactive transport model in Idiart and Laviña (2019) (blue), the step porosity function (dash black) and the gradual porosity function (black) used in this study. Both reactive transport models show the porosity distribution after 100 000 years. The gradual and step functions consider a leaching front penetration of 1.2 m. In the gradual function, the transition zone between intact and totally degraded concrete is of 1.2 m.*

Hydraulic conductivity

The lack of sufficient experimental data on the relation between hydraulic conductivity and porosity for severely leached concrete, leads to a certain degree of uncertainty. Usually, the Kozeny-Carman (KC) equation (Carman 1937) has been used to evaluate hydraulic conductivity as a function of porosity (Höglund 2014, Idiart and Shafei 2019, Idiart and Laviña 2019). In this study the modified Kozeny-Carman, as proposed by Benbow et al. (2005), is implemented.

The difference between these two relations is that the modified KC scales between the initial conductivity of the intact concrete and the final conductivity where all calcium minerals have been depleted whereas the Kozeny-Carman relation depends uniquely on the concrete initial state. The KC relation does not reach the assumed values for the hydraulic conductivity of the severely weathered concrete (Figure 3-11). The more aggressive modified KC relationship is applied in this study as a conservative approach.

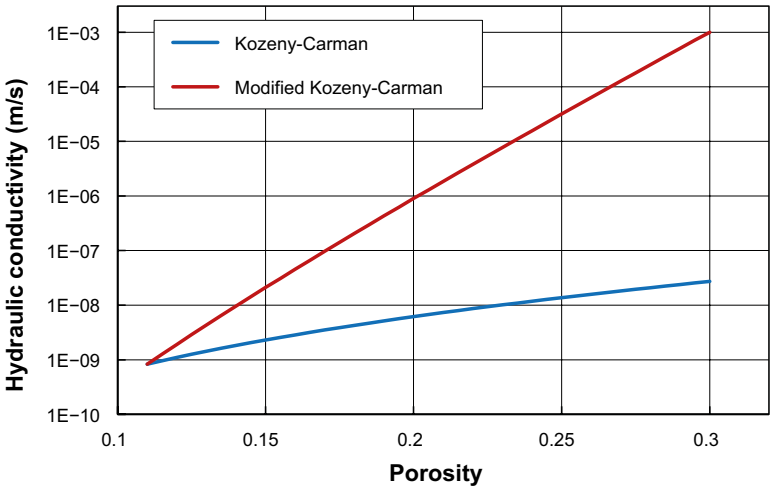

Figure 3-11. *Hydraulic conductivity of the degraded concrete calculated by the Kozeny-Carman and the modified Kozeny-Carman relations. The conductivity of intact concrete is assumed to be 8.3×10^{-10} m/s and the conductivity of fully degraded concrete 1×10^{-3} m/s.*

The Kozeny-Carman equation is defined as: is a log-linear relation expressed as

$$\boldsymbol{K = K(\varphi_0)\frac{(1-\varphi_0)^2}{\varphi_0{}^3}\frac{\varphi^3}{(1-\varphi)^2}}$$ Equation 3-5

where this equation, $K(\phi_0)$ is the hydraulic conductivity (m/s) associated with the initial porosity (ϕ_0).

The modified Kozeny-Carman is a log-linear relation expressed as:

$$\boldsymbol{K = C(\vartheta_c)\frac{\varphi^3}{(1-\varphi)^2}}$$ Equation 3-6

where

$$\boldsymbol{log\, C(\vartheta_c) = \left(1 - \frac{\vartheta_c}{\vartheta_{c,0}}\right) logC_{ballast} + \frac{\vartheta_c}{\vartheta_{c,0}} logC_{conc}}$$ Equation 3-7

$\vartheta_{c,0}$ and ϑ_c are the volume fractions of the cement minerals in intact concrete and partially leached concrete, respectively. $C_{ballast}$ and C_{conc} are given by:

$$\boldsymbol{C_{ballast} = K(\varphi_{ref})\frac{(1-\varphi_{ref})^2}{\varphi_{ref}{}^3}}$$ Equation 3-8

$$\boldsymbol{C_{conc} = K(\varphi_0)\frac{(1-\varphi_0)^2}{\varphi_0{}^3}}$$ Equation 3-9

where, φ_0 is the initial state porosity, φ_{ref} is the porosity for the severely weathered concrete and $K(\varphi_\alpha)$ is the hydraulic conductivity corresponding the φ_α porosity. Similar to Höglund (2014) and Idiart and Shafei (2019): $\varphi_0 = 0.11$, $\varphi_{ref} = 0.3$ and $K(\varphi_0) = 8.3 \times 10^{-10}$ m/s. The conductivity of the initial state concrete corresponds to the initial state of the 2BMA concrete barriers in Abarca et al. (2013). The maximum conductivity of the weathered concrete ($K(\varphi_{ref})$) is 1×10^{-3} m/s, i.e., the value of the "completely degraded concrete" in Abarca et al. (2013). The hydraulic conductivities corresponding to the step and gradual functions of the porosity are shown in Figure 3-12.

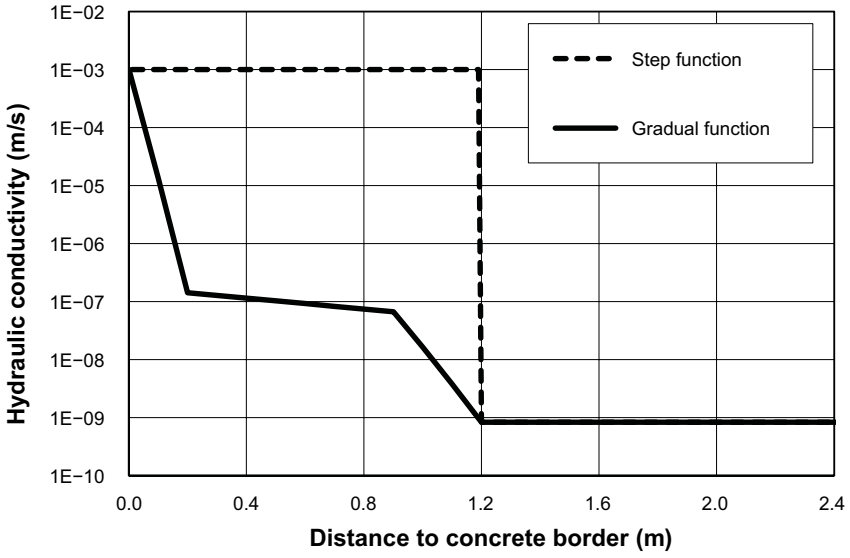

Figure 3-12. *Hydraulic conductivity of the degraded concrete calculated using the modified Kozeny-Carman relation for both the step and gradual porosity functions described in Figure 3-10. The concrete external border is located at coordinate 0. Both, the gradual and the step function, consider a leaching front penetration of 1.2 m. In the gradual function, the transition zone between intact and totally degraded concrete is of 1.2 m.*

3.5 Boundary conditions

3.5.1 Repository-scale models

At the time of closure, SFR is submerged beneath the Baltic Sea (Figure 3-13 (a)). Land rise shifts the shoreline such that land conditions are expected above the repository approximately 5000 AD (Figure 3-13 (c)). When land conditions are established above the repository the groundwater flow approached steady-state conditions (Odén et al. 2014).

The evolution of groundwater flow due to land rise is captured in the flow modelling by implementing three pressure different boundary conditions, representing different shoreline position. Steady-state groundwater flow is solved for each position. This is the identical approach used in Abarca et al. (2013).

3.5.2 Single plug model

The boundary and initial conditions of the single plug model are imported from the SFR3 repository model at shoreline position 3 (see Section 4). The driving pressure from the repository-scale model is imposed at the boundaries of the domain (Figure 3-14).

It is expected that a large variation in the hydraulic properties of the concrete plug will affect the boundaries due to the small size of the single plug model. Imposing a prescribed pressure field at the boundaries will give reasonable results for the initial states of the plug degradation. However, for advanced degradation states it will exaggerate groundwater fluxes through the model. The objective of this model is not to compute accurate fluxes during the whole plug degradation process but rather to gain insight about the concrete leaching at the plugs. This knowledge will be used later to evaluate the influence of concrete degradation on the flow in the repository scale models. The shrinking core models are evaluated under shoreline position 3, where the highest flow rates occur (Abarca et al. 2013).

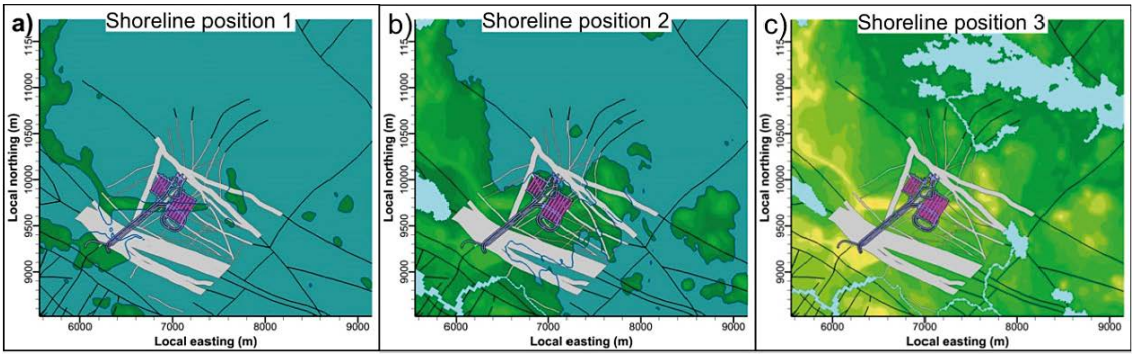

Figure 3-13. *Shoreline positions above SFR at the time of closure 2000 AD (a), at shore dominated conditions 3000 AD (b), and land dominated conditions 5000 AD (c).*

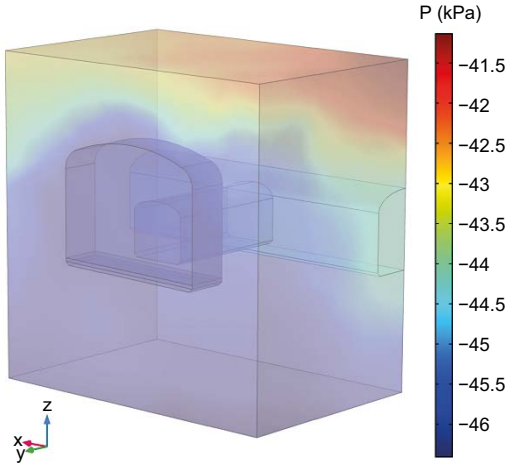

Figure 3-14. *Driving pressure field (P-ρ·g·z) in the single plug model.*

3.6 Mesh discretization

3.6.1 Repository-scale model

The spatial discretization of the repository models of SFR1 and SFR3 is that presented in Abarca et al. (2013). The meshes consist in tetrahedral quadratic finite elements: 10,748,580 (14,380,723 degrees of freedom) for SFR1 and 11,548,320 (15,435,799 degrees of freedom) for SFR3 (Figure 3-15).

The time and memory needed to solve a model is strongly related to the number of degrees of freedom in the model. The number of degrees of freedom depends on the number of elements, the number of variables to be solved and the type of mesh elements in the model. It can be calculated roughly as the number of elements multiplied by the number of variables and multiplied by a factor depending on the element type (e.g., linear triangular elements have a factor of 1, while quadratic tetrahedral elements have a factor of 4).

3.6.2 Single plug model

The single plug model preserves the same meshing settings of the repository scale model except in the plug, where the mesh has been refined. The mesh has 929,834 tetrahedral quadratic elements and 3,029,702 degrees of freedom (Figure 3-16).

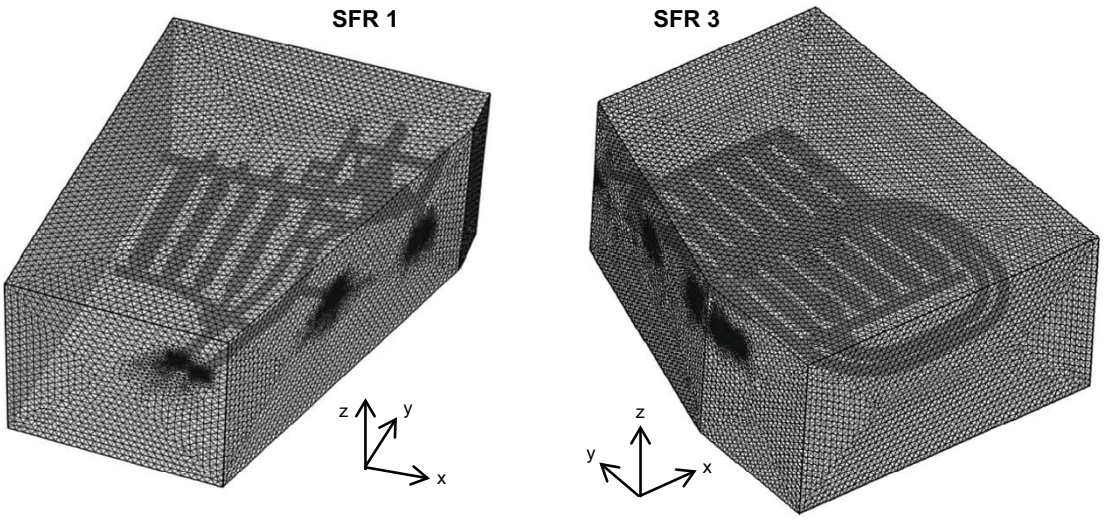

Figure 3-15. *Three-dimensional finite element meshes (tetrahedral) of the SFR1 (left, 10,748,580 elements) and SFR3 (right, 11,548,320 elements) repository-scale models.*

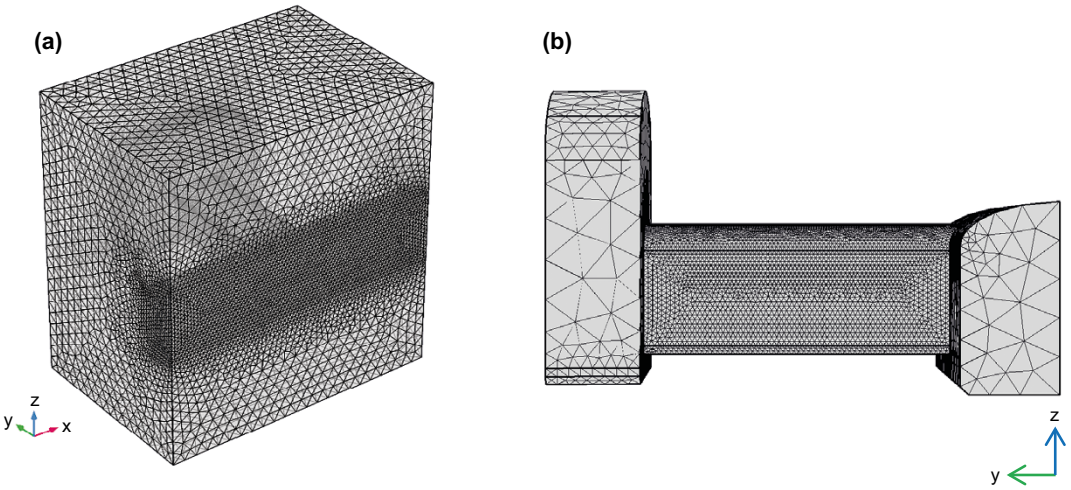

Figure 3-16. *Three-dimensional finite element mesh (tetrahedral) of the single plug model in the whole domain (a) and in the repository materials (b).*

4 Repository closure with concrete plugs

This section presents the results of the groundwater flow simulations for the repository closure with concrete plugs at their initial state. The hydraulic properties for the different materials of the repository for the initial state case are given in Table 3-4 and Table 3-5. The three shoreline positions are studied with the SFR1 and the SFR3 repository-scale models.

The water pathways and flow rates are determined by the hydraulic conductivity of the repository materials and by the highly permeable areas around the repositories. The permeability field for the rock around the SFR1 and the SFR3 is shown in Figure 3-6 and Figure 3-7, respectively.

The behaviour of the groundwater flow in the areas near the repository for the different shoreline positions is analysed with the same parameters and variables as in Abarca et al. (2013). The streamlines illustrate the water flow paths in the vicinity of the repository, while the total flow rates through the vaults and waste domains quantifies the groundwater flow. The calculation methodology of both variables is further explained in Abarca et al. (2013).

4.1 SFR1

This section contains the results of the SFR1 with low permeable beams in 1BMA (Table 3-4). However, the total flow rates through the vaults and waste at 1BMA for the case of high permeable beams has been added in Section 4.1.2 for completeness. The groundwater flow rates entering all vaults and tunnels for that the case with high permeable beams is fully reported in Appendix A.

4.1.1 Groundwater streamlines

For shoreline position 1, the repository is submerged and located below the regional groundwater discharge area. The groundwater crosses the repository from the bottom towards the top (Figure 4-1). The water that enters all the vaults except the silo comes from the south–east area. In these vaults, the water enters mainly through the bottom of the vaults and leaves through the top. The main discharge area is located above the vaults (Figure 4-1). The outflowing streamlines show a vertical and distributed flow towards the surface. The groundwater coming from the eastern model boundary reaches the silo at different depths and leaves it through the top. The main difference with the base case in Abarca et al. (2013) is due to the different distribution of the plugs. The volume of concrete sealing sections is significantly lower than in the base case. The reduced volume of low permeability material in the access tunnels redirects the groundwater to these tunnels. For a closure with concrete plugs, part of the groundwater flow arriving to the vaults come from the access tunnels (Figure 4-1 right).

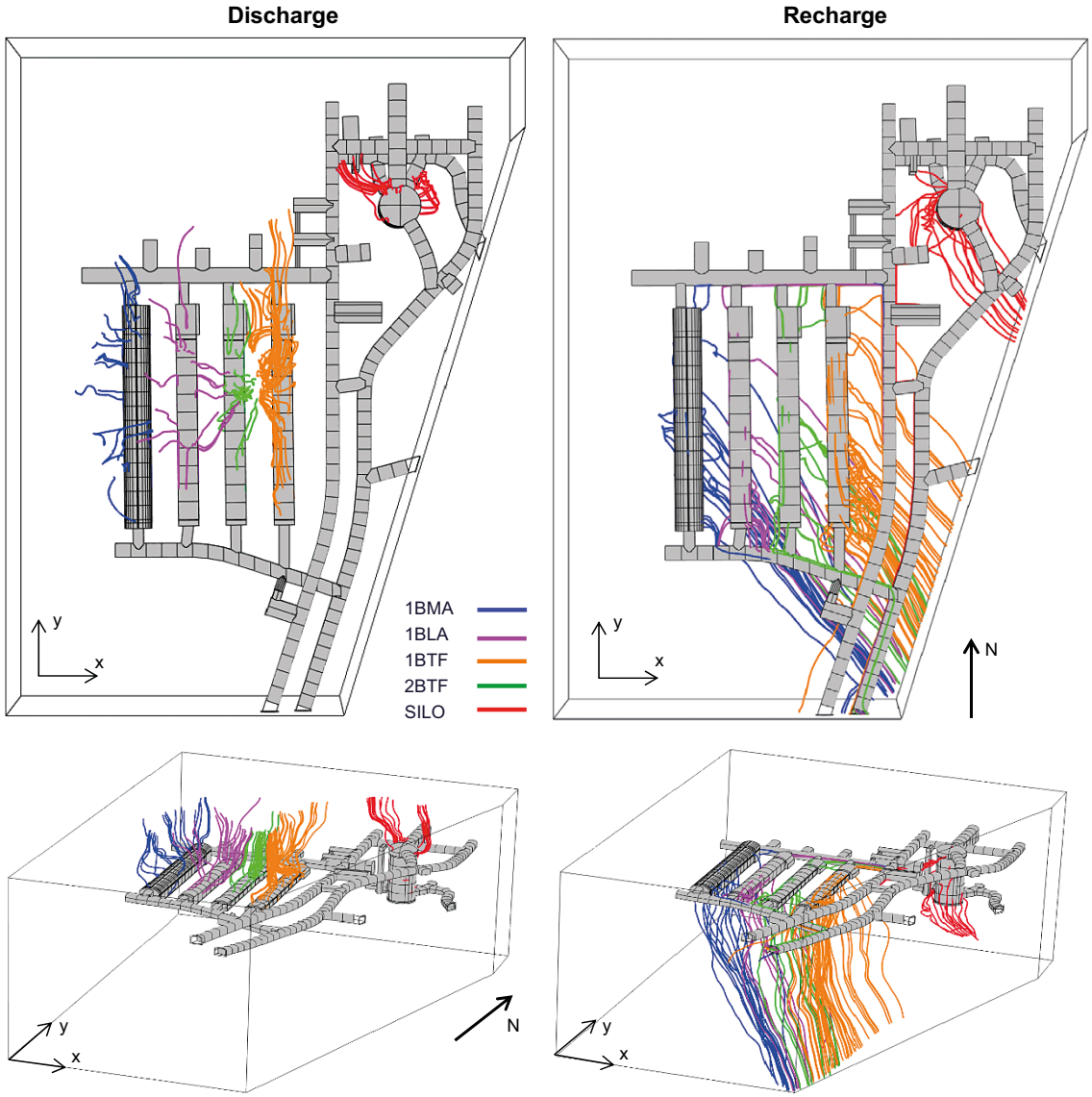

Figure 4-1. *Groundwater streamlines leaving (left) and reaching (right) the SFR1 vaults (colour tubes) for the initial state case and the shoreline position 1.*

Shoreline position 2 yields higher groundwater flows with a main vertical component. The groundwater reaching the vaults originates at the top boundary of the domain (Figure 4-2). The main source of water reaching the vaults is deformation zone ZFMNNW1209 (Abarca et al. 2013). The groundwater crosses the vaults from top to bottom and leaves the domain through the north–west boundaries. The silo is affected by water coming from deformation zone ZFMNNW1209 and the southern access tunnels. The water exits the silo mainly through its upper boundary and migrates towards north. A lower amount of water leaves the silo also through the lower boundaries moving towards the north–west (Figure 4-2).

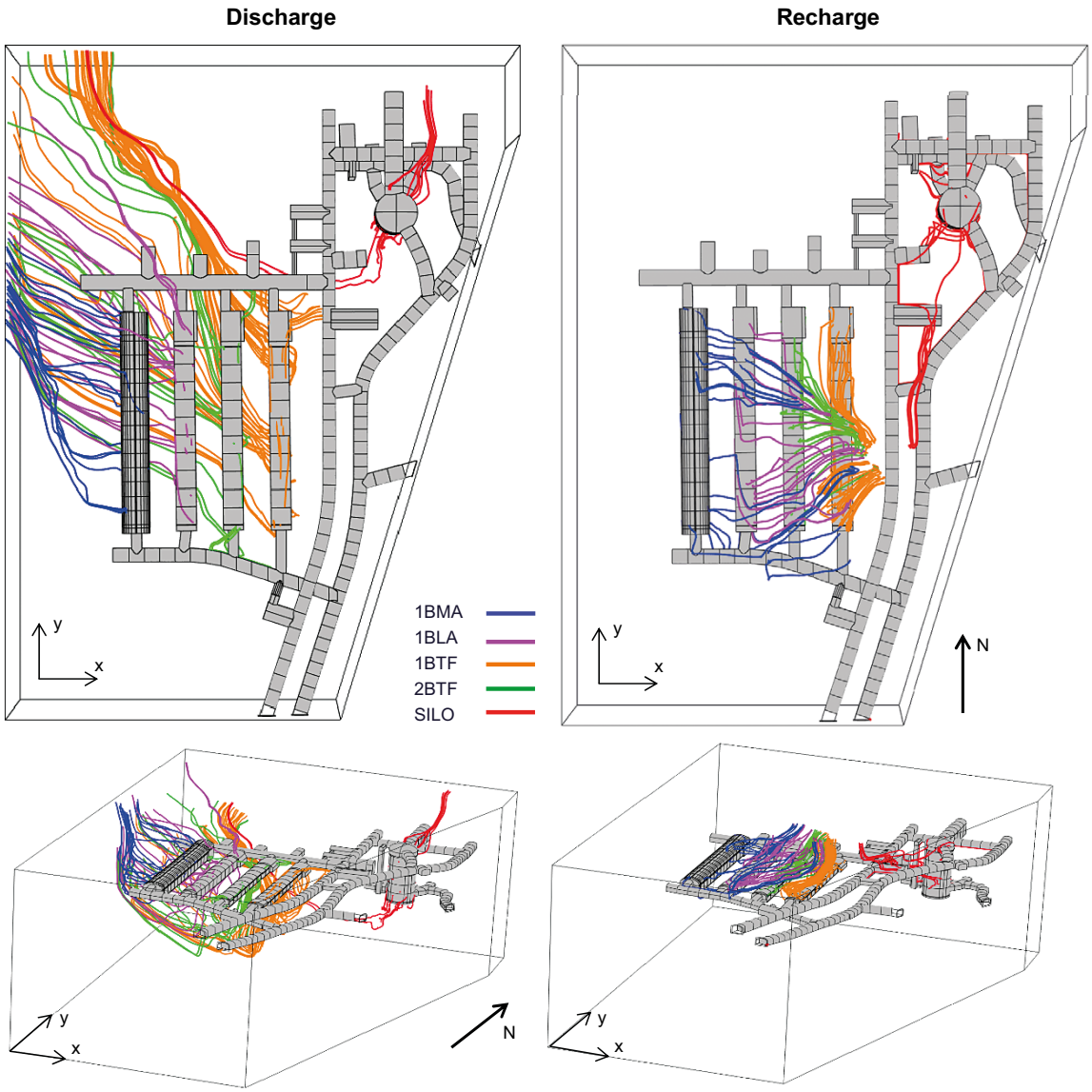

Figure 4-2. *Groundwater streamlines leaving (left) and reaching (right) the SFR1 vaults (colour tubes) for the initial state case and the shoreline position 2.*

The groundwater flow field for shoreline position 3 is similar to that observed for the shoreline position 2. However, in this case the streamlines show longer pathways within the domain, indicating that the main recharge zone has moved south and the discharge zone is further north (Figure 4-3). Most of the groundwater reaching the vaults originates at the top boundary in the deformation zone ZFMNNW1209, as in shoreline 2. However, part of the water entering 1BMA and, to a lesser extent, 1BLA comes from the southern boundary of the domain. The water entering the silo originates from the deformation zone ZFMNNW1209 or comes through the southern access tunnel. The water that exits the silo through its upper boundaries migrates towards north, while the water that discharges through the lower boundaries moves towards the north–west, converging with the water leaving the other vaults (Figure 4-3).

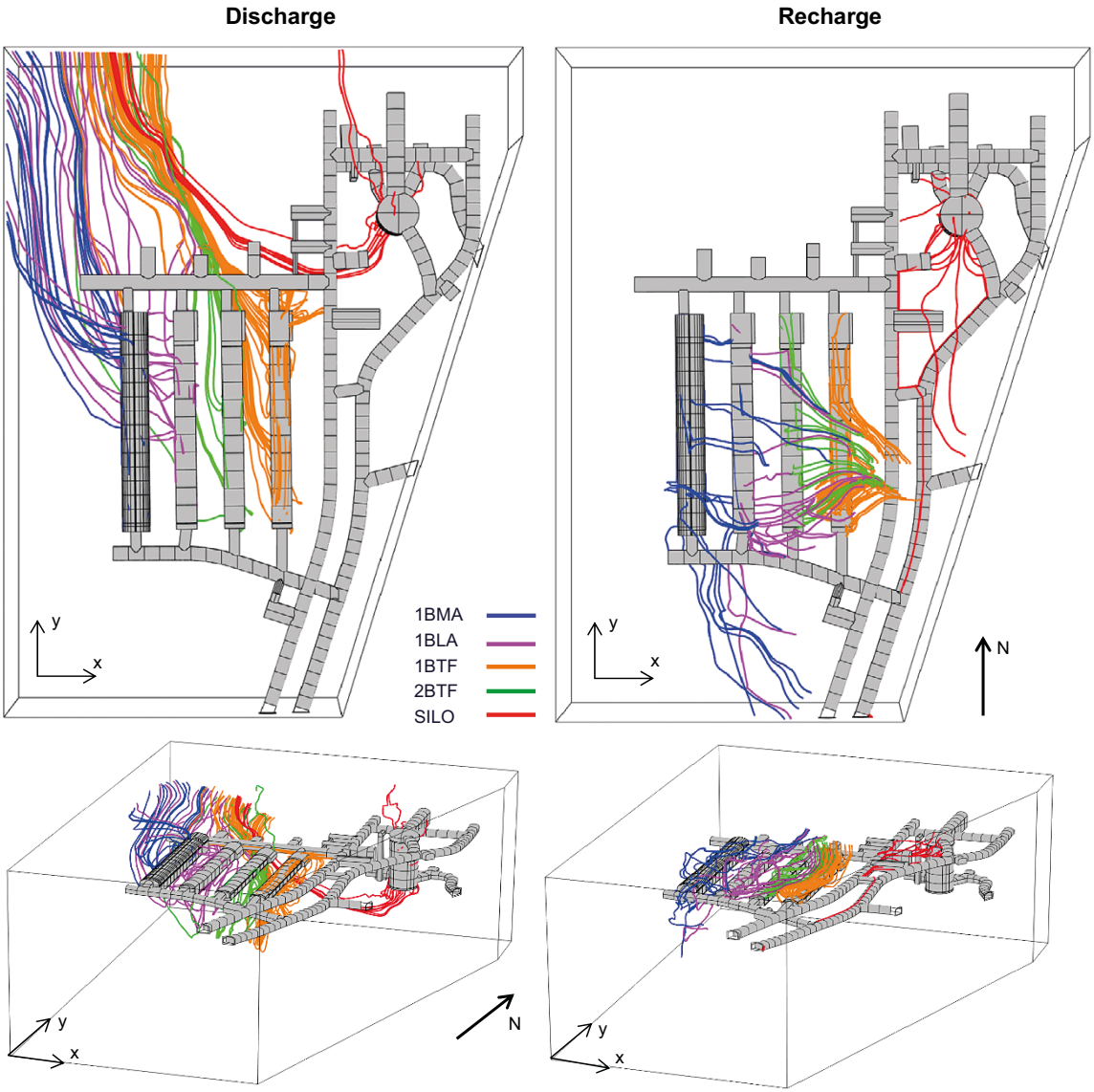

Figure 4-3. *Groundwater streamlines leaving (left) and reaching (right) the SFR1 vaults (colour tubes) for the initial state case and the shoreline position 3.*

4.1.2 Total flow rates through the vaults and waste

The calculated total flow through the vaults and waste domains for the three shoreline positions is shown in Figure 4-4. Shoreline 1 is characterized by flow rates two orders of magnitude lower than those for shoreline 2 and 3.

The flow rate through the waste is lower than the flow rate through the vaults where engineered barriers are installed. 1BLA has no internal barriers to restrict flow. Therefore, 1BLA has the largest flow rates and the waste flow rate represents around 90 % of the flow rate through the vault.

The flow rate through 2BTF vault is more than twice the flow rate through 1BTF. The reason is that the permeability of the surrounding rock is higher around 2BTF (Figure 3-6) and transfers more groundwater to the vault. However, the internal configuration of 1–2BTF reduces the flow rate through the waste to similar amounts. The waste flow rate represents more than 30 % of the vault flow rate in 1BTF, and less than 20 % of the vault flow rate in 2BTF.

The silo collects the lowest vault flow rate and the waste flow rate is really similar to the tunnel flow rate. The gravel dome located at the top of the silo has not been considered for the tunnel flow rates.

Flow rates through 1BMA are presented for the case of low and high permeable beams beneath the concrete floor, labelled 1BMA LPB and 1BMA HPB, respectively. The tunnel flow rate for both cases is similar being the second highest after 1BLA. However, the waste flow rate in 1BMA HPB is 3 orders of magnitude lower than for 1BMA LPB. The difference lies in the hydraulic properties of the foundation for the concrete structure. The highly permeable material assumed for the 1BMA HPB case redirects the water entering from the vault floor, causing it to pass by the concrete floor rather than go through it.

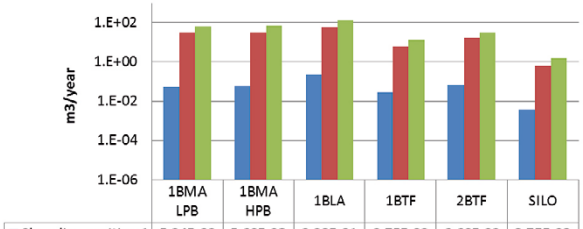

	1BMA LPB	1BMA HPB	1BLA	1BTF	2BTF	SILO
Shoreline position 1	5.24E-02	5.60E-02	2.23E-01	2.75E-02	6.60E-02	3.75E-03
Shoreline position 2	2.99E+01	3.08E+01	5.93E+01	5.91E+00	1.69E+01	6.40E-01
Shoreline position 3	6.49E+01	6.72E+01	1.29E+02	1.24E+01	3.03E+01	1.51E+00

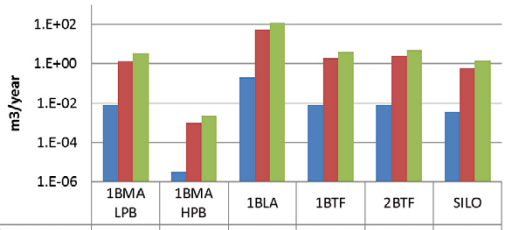

	1BMA LPB	1BMA HPB	1BLA	1BTF	2BTF	SILO
Shoreline position 1	7.90E-03	3.14E-06	1.98E-01	8.14E-03	8.39E-03	3.64E-03
Shoreline position 2	1.30E+00	9.51E-04	5.56E+01	1.87E+00	2.55E+00	5.85E-01
Shoreline position 3	3.44E+00	2.11E-03	1.21E+02	3.91E+00	4.95E+00	1.47E+00

Figure 4-4. *Total flow through the SFR1 vaults (left) and waste (right) domains (m^3/year) for the initial state case with low permeable beams in the 1BMA vault. The value for the Silo excludes the flow through the gravel dome, as defined for the radionuclide transport simulations. The vertical axis is logarithmic. Results correspond to the simulation with low permeable 1BMA beams except for 1BMA HPB results.*

4.1.3 Comparison with alternative closure case

The initial state case with concrete plugs is similar to the alternative closure case reported in Section 6.3 of Abarca et al. (2013). The alternative closure case in Abarca et al. (2013) had the same distribution of sealing plugs but the hydraulic conductivity of the plugs was 5×10^{-10} m/s, a bit lower than the hydraulic conductivity of the plugs considered here (8.3×10^{-10} m/s).

Table 4-1 shows the relation between the groundwater flow entering the different vaults for the repository closure with concrete plugs and for the alternative closure case in Abarca et al. (2013). Both simulations generate equal results for shoreline 2 and 3. For shoreline position 1, the vault flow rates are slightly higher for the closure with concrete plugs. However, the groundwater flow entering the waste is equal for both cases (Table 4-1). It can be concluded that small variations in the hydraulic conductivity of the sealing plugs have little influence in the hydraulic behaviour of the near-field.

Table 4-1. Ratio of the total flow through the SFR1 vault and waste domains between the initial state case with low permeable beams in 1BMA and the values reported in the alternative closure case of Abarca et al. (2013).

Ratio BC/TR-13-08		1BMA	1BLA	1BTF	2BTF	SILO
Tunnel	Shoreline position 1	1.003	1.003	1.003	1.001	1.002
	Shoreline position 2	1.001	1.000	1.001	1.000	1.006
	Shoreline position 3	1.001	1.001	1.001	1.000	0.999
Waste	Shoreline position 1	1.000	1.001	1.000	1.000	0.999
	Shoreline position 2	1.001	1.000	1.000	1.000	1.007
	Shoreline position 3	1.001	1.000	1.001	1.000	1.000

4.2 SFR3

4.2.1 Groundwater streamlines

For shoreline position 1, the repository is submerged and groundwater flows upwards from the south east towards the north–west (Figure 4-5). Water enters the domain through the southern end of the bottom boundary. There are two areas of water discharge from the vaults (Figure 4-5 left). South from the access tunnels ramp, water flows vertically upwards from vaults 1BRT, 5BLA, 4BLA and 3BLA. North of the ramp, diffuse discharge from all vaults flows mostly towards the north–west. Part of the discharge from 2BMA migrates eastwards.

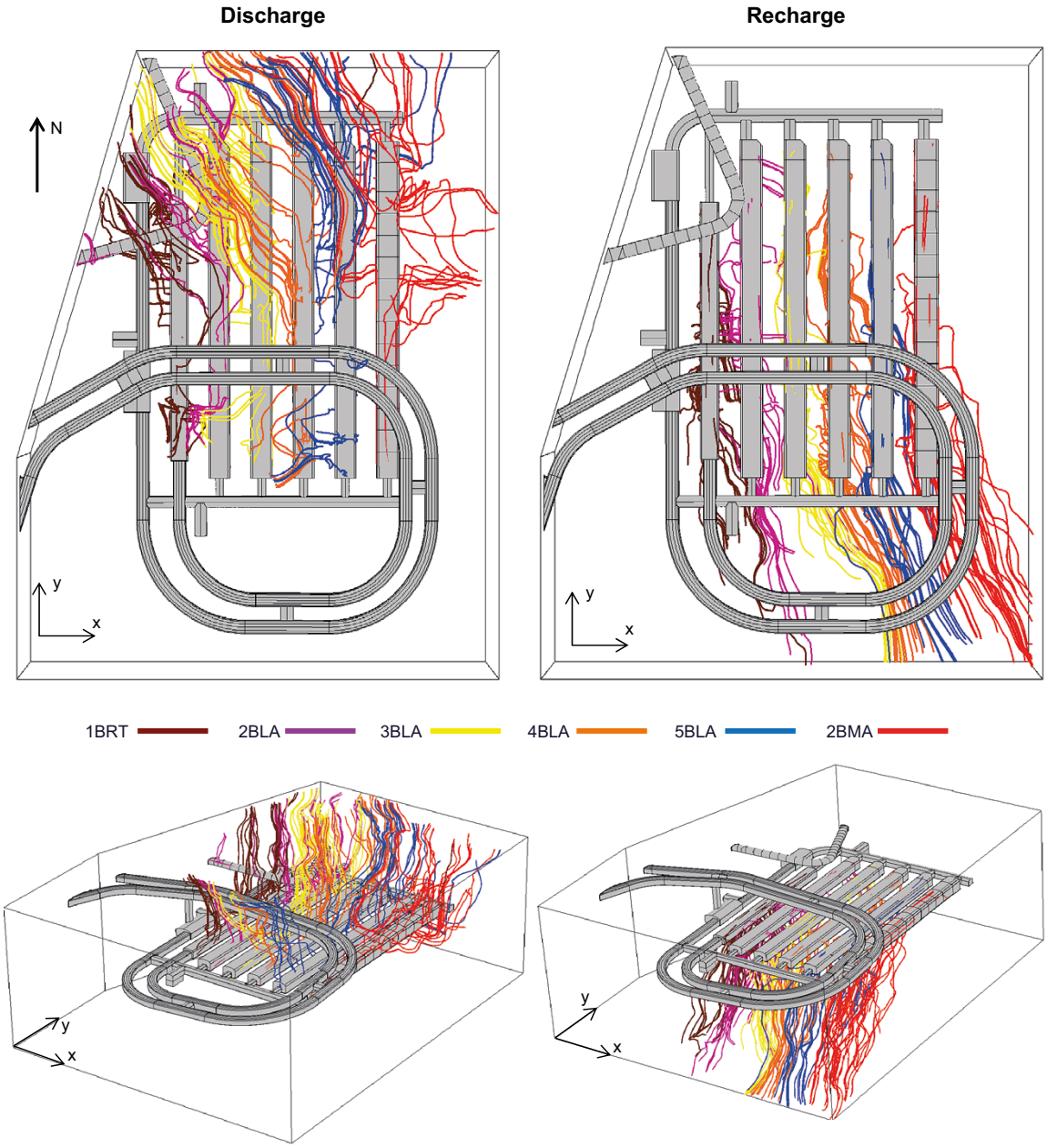

Figure 4-5. *Groundwater streamlines leaving (left) and reaching (right) the SFR3 vaults (colour tubes) for the initial state case and the shoreline position 1.*

At shoreline position 2, the main direction of the groundwater flow is from top to bottom of the model domain. The water enters the vaults through their southern half (Figure 4-6 right). Groundwater flows through the most permeable zones in the upper part of the domain and reaches the vaults vertically through small fracture zones. Part of the inflow to the vaults, especially towards 1BRT, comes from the access tunnels.

The outflow from the vaults migrates vertically downwards. At depth, it becomes horizontal following deformation zone ZFM871 and leaves the system through the northern boundary. 2BMA, 5BLA, 4BLA and part of 3BLA discharge flows towards the north–east, while the discharge from 1BRT, 2BLA and part of 3BLA flows towards the north–west. Part of the water leaves the vaults through their upper surfaces and migrates towards the north boundary.

The groundwater flow field for shoreline position 3 shows the same patterns than for shoreline position 2 (Figure 4-7).

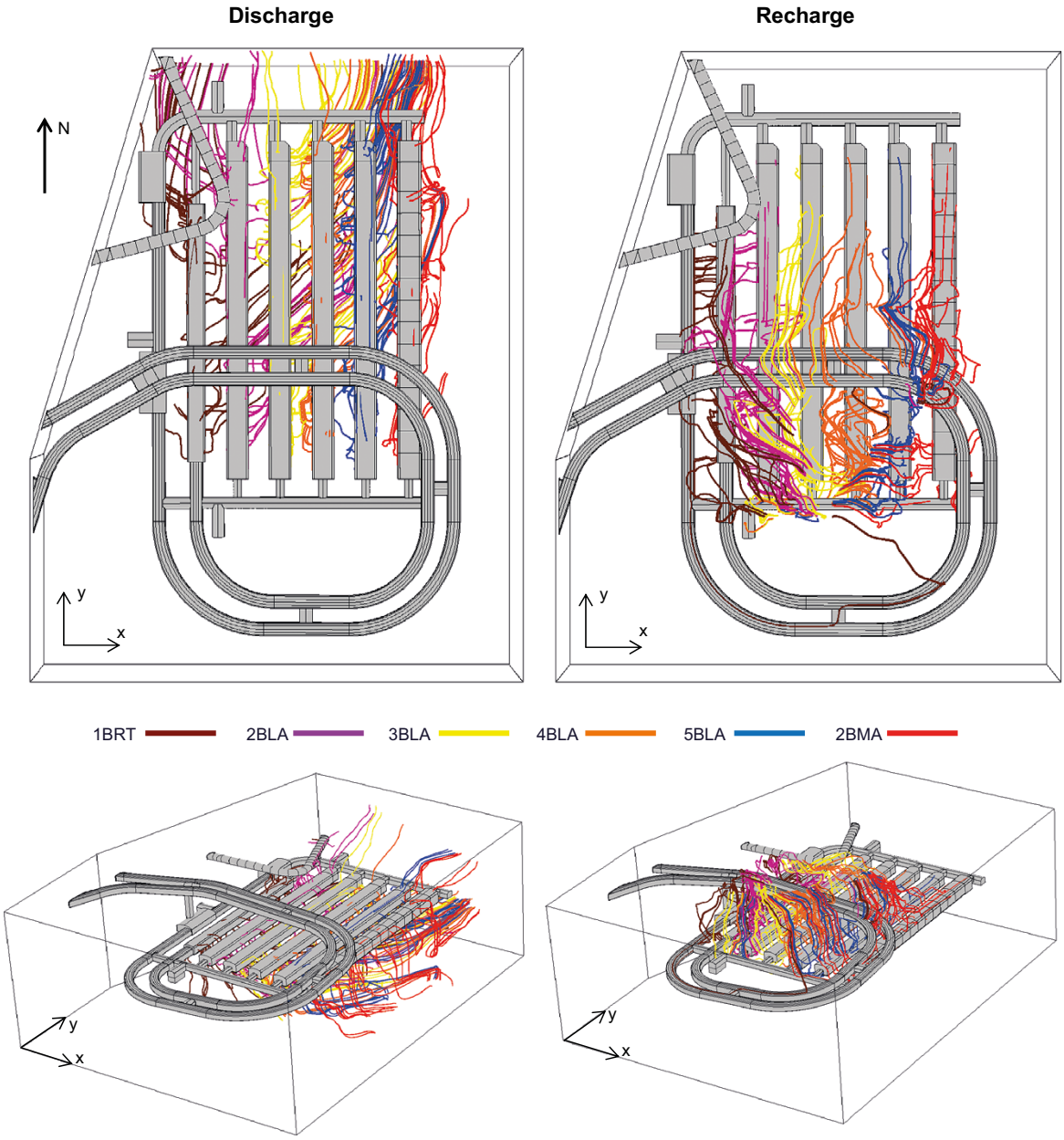

Figure 4-6. *Groundwater streamlines leaving (left) and reaching (right) the SFR3 vaults (colour tubes) for the initial state case and the shoreline position 2.*

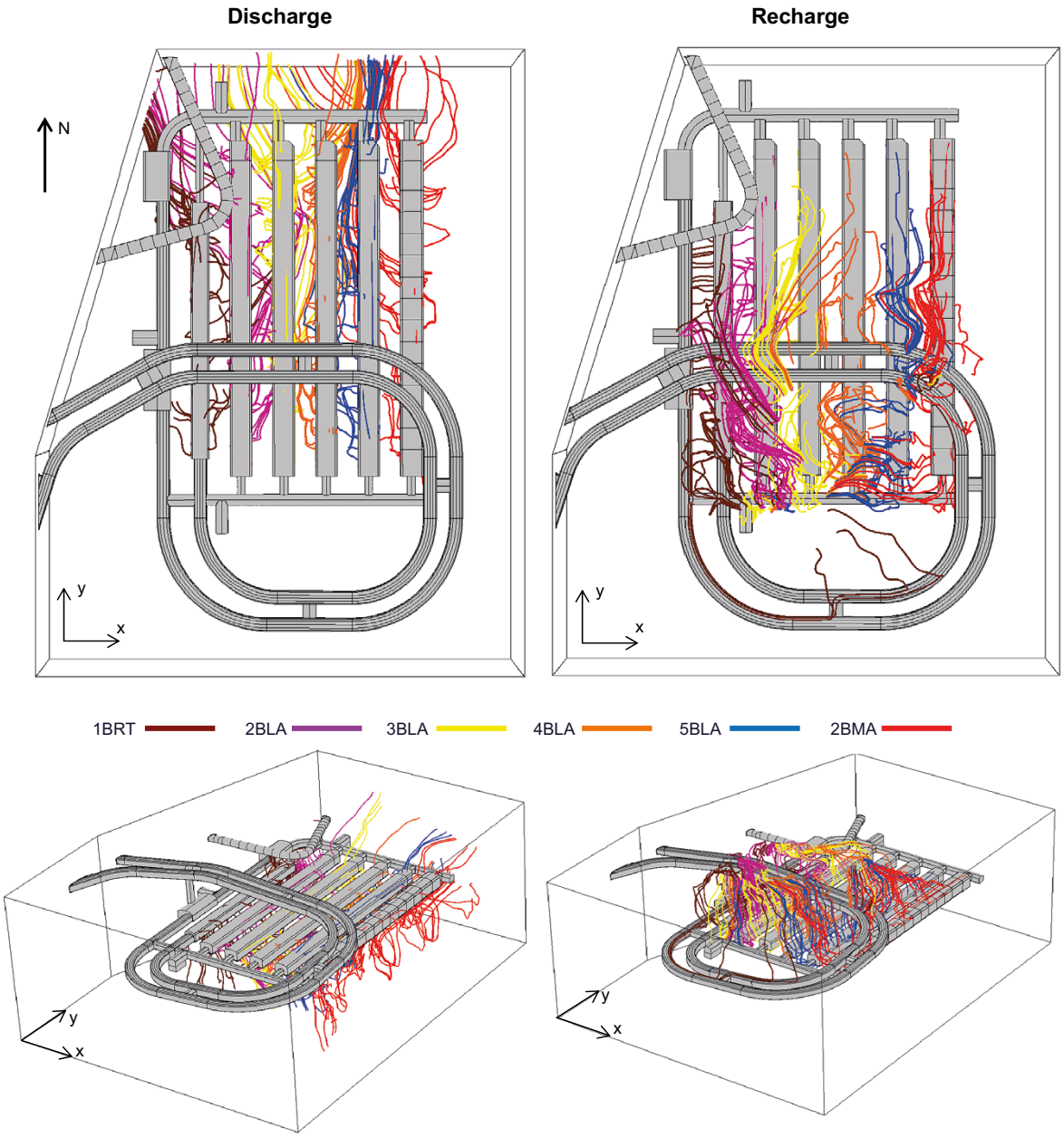

Figure 4-7. *Groundwater streamlines leaving (left) and reaching (right) the SFR3 vaults (colour tubes) for the initial state case and the shoreline position 3.*

4.2.2 Total flow through the vaults and waste

The total flow through vaults and waste domains is presented in Figure 4-8. The vault flow rate is of the same order of magnitude for all vaults for a given shoreline position. The 2–5BLA vaults have a waste flow rate very similar to the vault flow rate due to the absence of engineered barriers. In 1BRT the waste flow rate is less than 19 % of the tunnel flow rate.

Even though 2BMA collects the highest vault flow rate for all shoreline positions, its waste flow rate is the lowest. The concrete barriers and the hydraulic cage surrounding the individual waste compartments significantly reduce waste flow rate. Each waste compartment of 2BMA is surrounded by a highly permeable backfill material that collects groundwater flow rate. For 2BMA, the total flow rate per waste is normalized with respect to the number of waste compartments (14) (see Abarca et al. 2013 for more details). The normalized waste flow rate represents the 0.0009 % of the tunnel flow rate in 2BMA for the three shoreline positions.

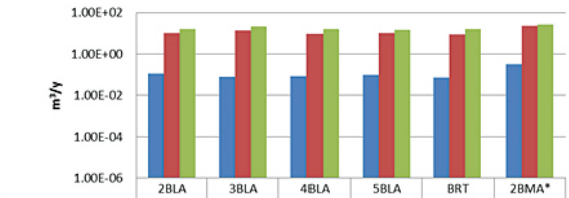

	2BLA	3BLA	4BLA	5BLA	BRT	2BMA*
Shoreline position 1	1.15E-01	8.04E-02	8.29E-02	9.65E-02	7.21E-02	3.07E-01
Shoreline position 2	1.02E+01	1.38E+01	9.41E+00	1.05E+01	9.08E+00	2.24E+01
Shoreline position 3	1.60E+01	2.06E+01	1.61E+01	1.52E+01	1.59E+01	2.74E+01

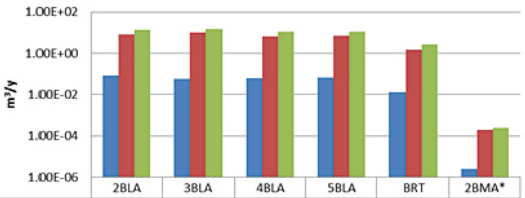

	2BLA	3BLA	4BLA	5BLA	BRT	2BMA*
Shoreline position 1	8.39E-02	5.99E-02	6.19E-02	6.88E-02	1.29E-02	2.56E-06
Shoreline position 2	8.42E+00	1.03E+01	6.53E+00	7.18E+00	1.48E+00	1.97E-04
Shoreline position 3	1.33E+01	1.51E+01	1.11E+01	1.13E+01	2.64E+00	2.46E-04

Figure 4-8. *Total flow through the SFR3 vaults (left) and waste (right) (m^3/year) for the initial state case, for the three shoreline positions. The waste flow for 2BMA* corresponds to the normalized flow per waste package. The vertical axis is logarithmic.*

5 Homogeneous concrete degradation

5.1 Degradation cases

This section explores the effect of homogeneous concrete degradation on the groundwater flow in the near field of SFR1 and SFR3. It is assumed that the full volume of the concrete plugs degrades simultaneously. A moderate, severe, and complete concrete degradation case are compared with the initial state case. The total flow entering the vaults, the waste compartments and the loading area (in the SFR3) is evaluated for each case.

The hydraulic conductivities of the different degradation states are defined in Table 5-1 and Table 5-2 for the SFR1 and SFR3, respectively. A hydraulic conductivity contrast of three orders of magnitude is maintained between the concrete and the waste until reaching a maximum conductivity of 10^{-3} m/s. Figure 5-1 and Figure 5-2 illustrate the hydraulic conductivity of the vault materials for the SFR1 and the SFR3, respectively.

In 1BMA with low permeable beams (LPB), the beams degrade together with other concrete structures. In the case of high permeable beams (HPB) the hydraulic conductivity of the beams remains constant at 10^{-3} m/s. The results presented in this section correspond to the LPB case. The results of the HPB case are reported in Appendix A.

Table 5-1. Hydraulic conductivity (m/s) of the different materials composed, at least partially, by concrete for all degradation states considered.

Hydraulic conductivity (m/s)		Concrete Degradation		
	Initial state	Moderate	Severe	Complete
Concrete	8.30E−10	1.00E−07	1.00E−05	1.00E−03
Concrete Backfill	8.30E−09	1.00E−06	1.00E−04	1.00E−03
1BMA HPB	1.00E−03	1.00E−03	1.00E−03	1.00E−03
1BMA LPB*	8.30E−10	1.00E−07	1.00E−05	1.00E−03
Backfill	1.00E−03	1.00E−03	1.00E−03	1.00E−03
Waste	8.30E−07	1.00E−04	1.00E−03	1.00E−03
Sand Floor	1.00E−07	1.00E−07	1.00E−07	1.00E−07
Concrete plugs	8.30E−10	1.00E−07	1.00E−05	1.00E−03

* High permeable beams considered as an alternative case. Its results are shown in Appendix A.

Table 5-2. Hydraulic conductivity (m/s) of the materials of the SFR3 for the different concrete degradation cases.

Hydraulic conductivity (m/s)		Concrete Degradation		
	Initial state	Moderate	Severe	Complete
Concrete	8.30E−10	1.00E−07	1.00E−05	1.00E−03
Backfill	1.00E−03	1.00E−03	1.00E−03	1.00E−03
1BRT grouted waste	8.30E−09	1.00E−06	1.00E−04	1.00E−03
2BMA waste	8.30E−07	1.00E−04	1.00E−03	1.00E−03
Sand layer	1.00E−07	1.00E−07	1.00E−07	1.00E−07
2BMA sand Floor	1.00E−03	1.00E−03	1.00E−03	1.00E−03
Concrete plugs	8.30E−10	1.00E−07	1.00E−05	1.00E−03

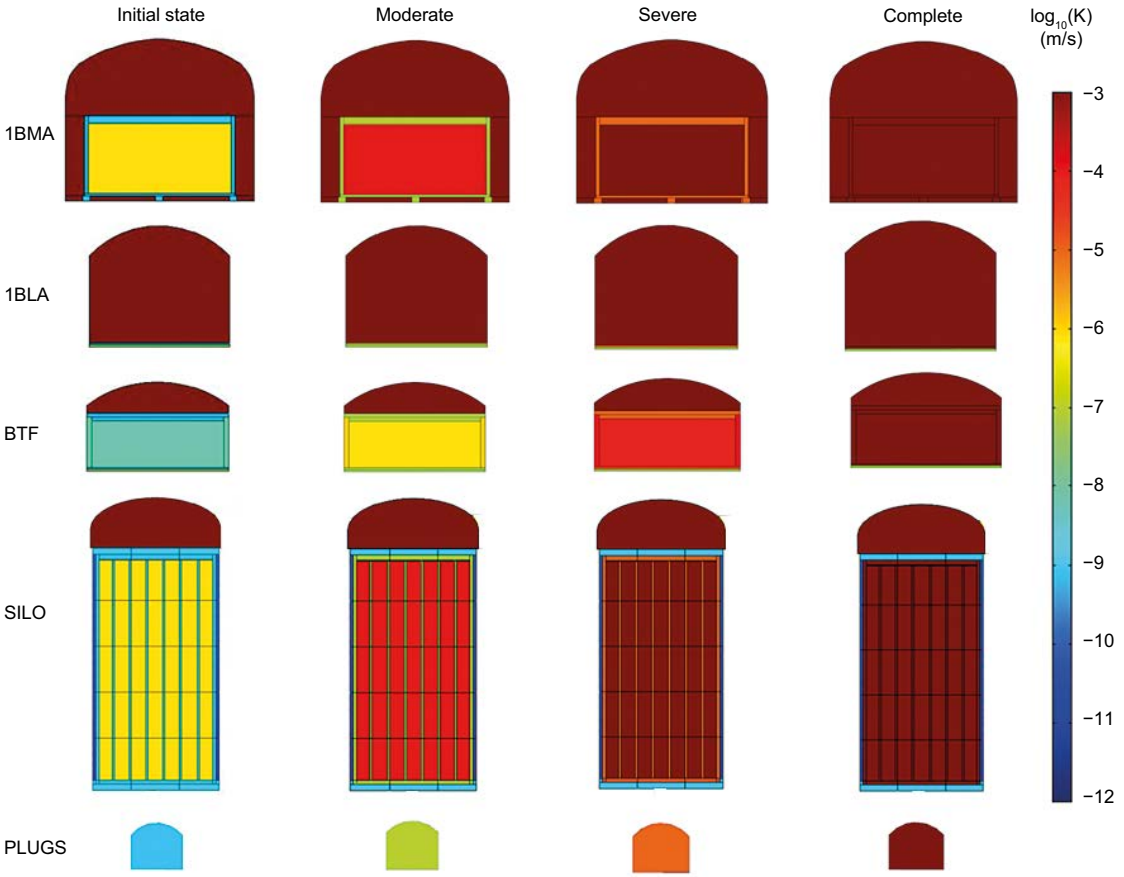

Figure 5-1. *Hydraulic conductivity parameterization for the different concrete degradation cases for the SFR1.*

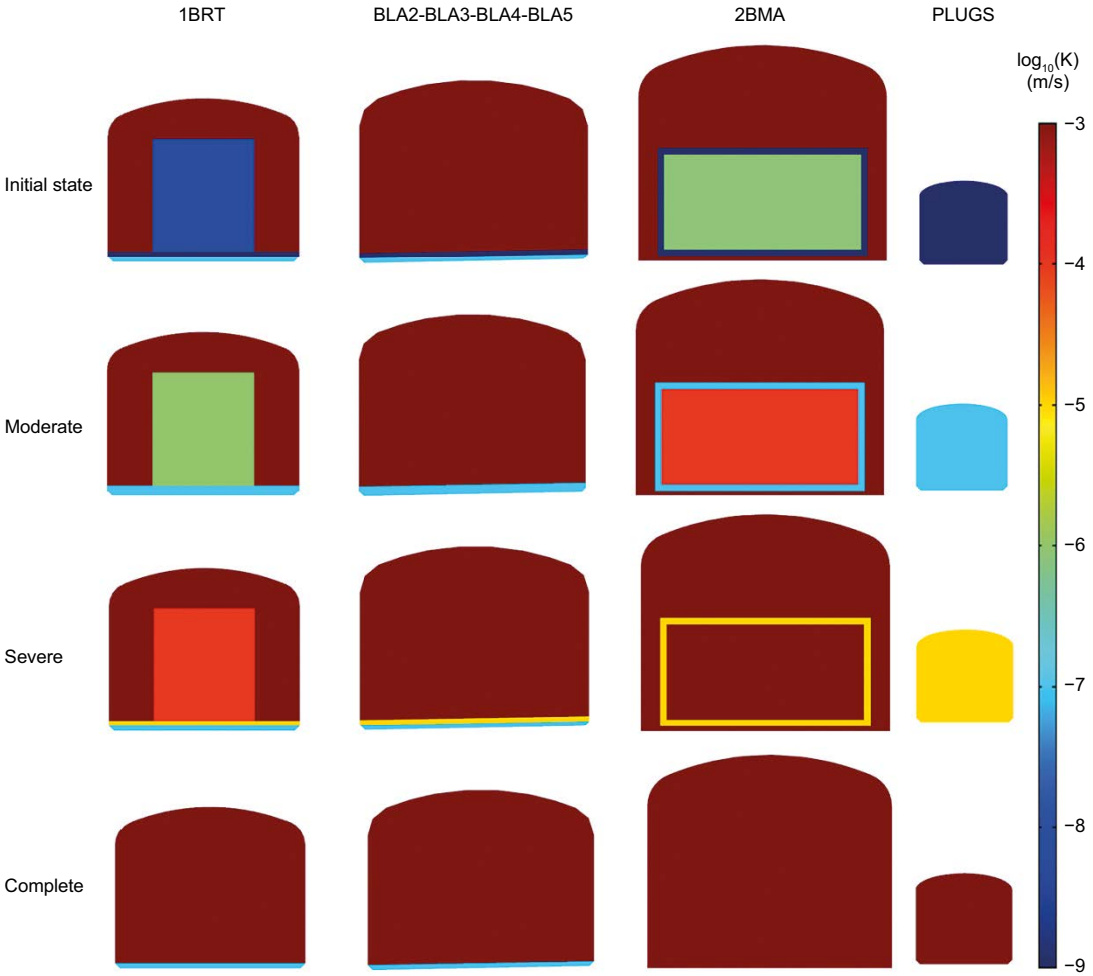

Figure 5-2. *Hydraulic conductivity parameterization for the different concrete degradation cases for the SFR3.*

5.2 SFR1

The calculated vault and waste flow rates for the different concrete degradation cases are presented in Figure 5-3. Table 5-3 shows the flow rate ratio with respect to the initial state case.

The vault flow rate increases progressively in all vaults as concrete degrades. The largest change in flow rate occurs between the completely degraded case and the severely degraded case. This is different compared to previous reported results (Abarca et al. 2013), and is due the degradation of the sealing plugs. The concrete plugs in this study are assumed to degrade with time, while in Abarca et al. (2013), the plugs delimit sections of bentonite that are considered as non-degradable. The concrete plug degradation connects the vaults with the access tunnels and increases the groundwater inflow to the vaults.

The increase in vaults flow rates in 1–2BTF is especially significant: in the complete degradation case, the tunnel flow rate is between 6.9 times (2BTF at shoreline position 1) and 57 times larger (1BTF at shoreline position 3) than for the initial state.

The flow rates for 1BMA with high and low permeable beams are similar. The water entering the vaults increases significantly for the severe and complete degradation cases. The flow rate in the tunnels is at least 4 times larger in the completely degraded case compared to the initial state, for all shoreline positions.

a) Shoreline position 1
Total flow per vault (m3/year)

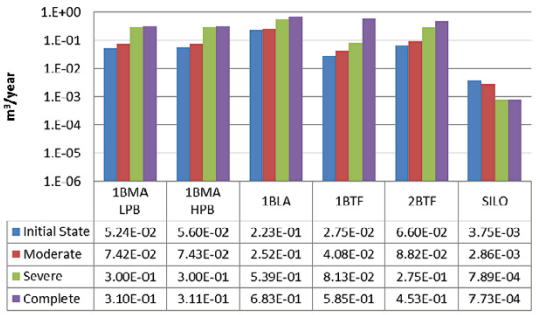

	1BMA LPB	1BMA HPB	1BLA	1BTF	2BTF	SILO
Initial State	5.24E-02	5.60E-02	2.23E-01	2.75E-02	6.60E-02	3.75E-03
Moderate	7.42E-02	7.43E-02	2.52E-01	4.08E-02	8.82E-02	2.86E-03
Severe	3.00E-01	3.00E-01	5.39E-01	8.13E-02	2.75E-01	7.89E-04
Complete	3.10E-01	3.11E-01	6.83E-01	5.85E-01	4.53E-01	7.73E-04

b) Shoreline position 1
Total flow per waste (m³/year)

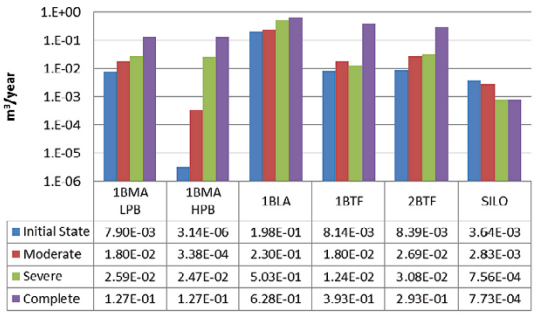

	1BMA LPB	1BMA HPB	1BLA	1BTF	2BTF	SILO
Initial State	7.90E-03	3.14E-06	1.98E-01	8.14E-03	8.39E-03	3.64E-03
Moderate	1.80E-02	3.38E-04	2.30E-01	1.80E-02	2.69E-02	2.83E-03
Severe	2.59E-02	2.47E-02	5.03E-01	1.24E-02	3.08E-02	7.56E-04
Complete	1.27E-01	1.27E-01	6.28E-01	3.93E-01	2.93E-01	7.73E-04

c) Shoreline position 2
Total flow per vault (m³/year)

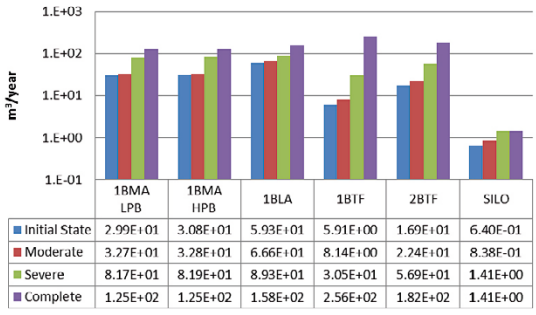

	1BMA LPB	1BMA HPB	1BLA	1BTF	2BTF	SILO
Initial State	2.99E+01	3.08E+01	5.93E+01	5.91E+00	1.69E+01	6.40E-01
Moderate	3.27E+01	3.28E+01	6.66E+01	8.14E+00	2.24E+01	8.38E-01
Severe	8.17E+01	8.19E+01	8.93E+01	3.05E+01	5.69E+01	1.41E+00
Complete	1.25E+02	1.25E+02	1.58E+02	2.56E+02	1.82E+02	1.41E+00

d) Shoreline position 2
Total flow per waste (m³/year)

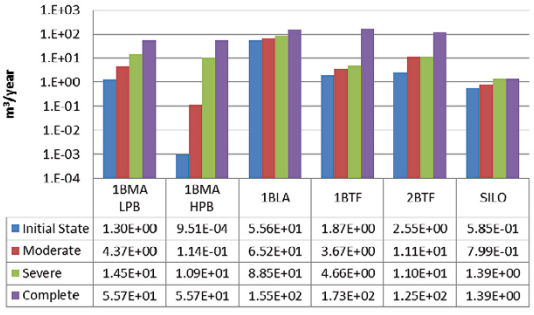

	1BMA LPB	1BMA HPB	1BLA	1BTF	2BTF	SILO
Initial State	1.30E+00	9.51E-04	5.56E+01	1.87E+00	2.55E+00	5.85E-01
Moderate	4.37E+00	1.14E-01	6.52E+01	3.67E+00	1.11E+01	7.99E-01
Severe	1.45E+01	1.09E+01	8.85E+01	4.66E+00	1.10E+01	1.39E+00
Complete	5.57E+01	5.57E+01	1.55E+02	1.73E+02	1.25E+02	1.39E+00

e) Shoreline position 3
Total flow per vault (m³/year)

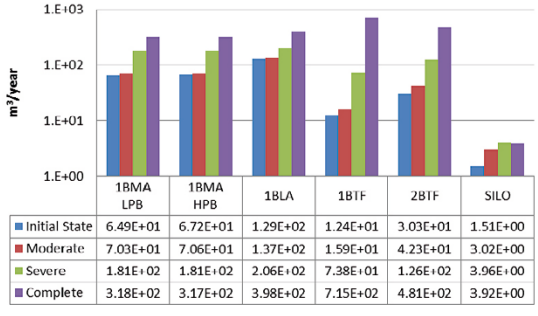

	1BMA LPB	1BMA HPB	1BLA	1BTF	2BTF	SILO
Initial State	6.49E+01	6.72E+01	1.29E+02	1.24E+01	3.03E+01	1.51E+00
Moderate	7.03E+01	7.06E+01	1.37E+02	1.59E+01	4.23E+01	3.02E+00
Severe	1.81E+02	1.81E+02	2.06E+02	7.38E+01	1.26E+02	3.96E+00
Complete	3.18E+02	3.17E+02	3.98E+02	7.15E+02	4.81E+02	3.92E+00

f) Shoreline position 3
Total flow per waste (m³/year)

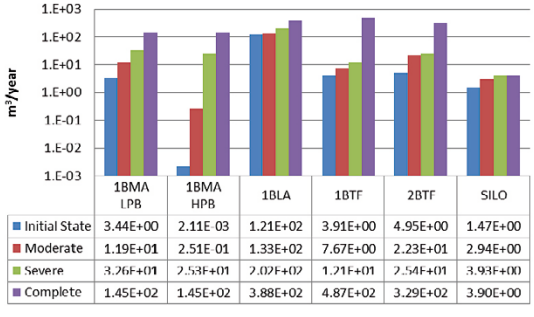

	1BMA LPB	1BMA HPB	1BLA	1BTF	2BTF	SILO
Initial State	3.44E+00	2.11E-03	1.21E+02	3.91E+00	4.95E+00	1.47E+00
Moderate	1.19E+01	2.51E-01	1.33E+02	7.67E+00	2.23E+01	2.94E+00
Severe	3.26E+01	2.53E+01	2.02E+02	1.21E+01	2.54E+01	3.93E+00
Complete	1.45E+02	1.45E+02	3.88E+02	4.87E+02	3.29E+02	3.90E+00

Figure 5-3. *Total flow (m^3/year) through the SFR1 vaults (left) and waste domains (right) for the different concrete degradation cases and the three shoreline positions. The vertical axis is logarithmic. Results of the simulation with low permeable 1BMA beams except for the 1BMA HPB case.*

The vault flow rate through the silo decreases with degradation of the concrete at shoreline position 1. It decreases 20 % in the completely degraded case, compared to the initial state. Note that the gravel dome located at top of the silo is not included in the vault flow rate calculations. As explained for the initial state case (Section 4), at shoreline position 1, the groundwater enters the silo through its south boundaries. When the concrete plug degrades the highly permeable access tunnels connect with the gravel dome, redirecting the flow and by-passing the Silo vault. However, at shoreline position 2 and 3, the groundwater flows from top to bottom, entering the Silo through the access tunnels and leaving through its upper and bottom boundaries. When the plugs are completely degraded, the flow rate through the silo increases by more than a factor 2 compared to the initial state.

The flow rate through the waste control volumes suffers also an increase due to concrete degradation. The effect on the waste flow rates is larger than in the vaults control volumes except in 1BLA and the silo. The flow rates through the waste increase due to the combination of two effects: the degradation of concrete plugs that lead to larger flow through the tunnels and the degradation of inner concrete structures in the vaults.

The 1BLA vault has no internal engineering barriers and, therefore, the increase in the waste flow rate correlates directly with the increase in the vault flow rate. The waste flow rate is approximately three times higher for the complete degradation case compared to the initial state.

The waste flow rate in the silo is not affected by the concrete degradation due to the external bentonite walls that are considered as non-degradable. The waste flow rate for the severely and completely degraded states is similar for all the shorelines. As occurs with the tunnel flow rate, for the shoreline 1 the waste flow rate decreases from the initial to the severely degraded state.

1–2BTF and 1BMA are the most affected by the degradation of concrete. The waste flow rate in 1–2BTF increases two orders of magnitude from the initial to the completely degraded state. Most of this difference stems from the transition from severely to the completely degraded concrete. The location of the BTF vaults, directly below the recharge area (see Section 4.1.1), leads to higher flow rates within these vaults as the concrete sealing at the access tunnels degrade.

The flow rate through 1BMA waste increases significantly for both low permeable and high permeable beams; however, the actual flow rates are low in spite of the large relatively large increase. The waste flow rate at the initial state is three orders of magnitude lower for the HPB case due to the hydraulic cage effect. The flow rate through the waste increases 5 orders of magnitude for the completely degraded state. This flow rate increase is lower for the LPB case. It increases one order of magnitude at shoreline position 2 and two orders of magnitude at shoreline positions 1 and 3. The waste flow rate at the complete degradation case is equal for both 1BMA configurations.

Table 5-3. Total flow ratio normalized with respect to the Base case for the three concrete degradation cases: Moderate (M), Severe (S), Complete (C).

		Shoreline position 1			Shoreline position 2			Shoreline position 3		
		M	S	C	M	S	C	M	S	C
Vaults	1BMA LPB	1.42	5.72	5.92	1.09	2.73	4.17	1.08	2.79	4.89
	1BMA HPB	1.33	5.36	5.54	1.06	2.66	4.05	1.05	2.70	4.72
	1BLA	1.13	2.42	3.06	1.12	1.51	2.67	1.06	1.59	3.08
	1BTF	1.49	2.96	21.32	1.38	5.16	43.32	1.29	5.97	57.84
	2BTF	1.34	4.17	6.87	1.33	3.37	10.80	1.40	4.15	15.88
	Silo	0.76	0.21	0.21	1.31	2.20	2.20	2.01	2.63	2.60
Waste	1BMA LPB	2.28	3.28	16.10	3.37	11.14	42.86	3.45	9.48	42.25
	1BMA HPB	107	7846	40480	119	11447	58553	119	12014	68907
	1BLA	1.16	2.54	3.17	1.17	1.59	2.78	1.10	1.67	3.20
	1BTF	2.21	1.53	48.32	1.97	2.50	92.66	1.96	3.10	124.71
	2BTF	3.21	3.67	34.97	4.38	4.31	48.91	4.52	5.13	66.61
	Silo	0.78	0.21	0.21	1.36	2.38	2.38	2.00	2.67	2.65

5.3 SFR3

The calculated flow rates though the vaults, waste and loading areas for the different concrete degradation states are presented in Figure 5-4. Table 5-4 shows the flow rate ratio with respect to the initial state case.

In general, the flow through the vaults increases progressively with the degradation of the concrete for the three shoreline positions. The flow rate increase is more pronounced between the severe and the complete degradation cases. In 1BRT and 2BLA vaults, the tunnel flow rate for the complete degradation case is four times the flow rate of the initial state. The exception is 2BMA where the flow rate increase is lower. At shoreline position 1, 2BMA presents even a slightly decrease in flow rate with the concrete degradation, which was also observed in Abarca et al. (2013). In the moderate degradation case, there is no significant increase in flow rate for any vault at shoreline positions 2 and 3.

a) Shoreline position 1
Total flow per vault (m³/y)

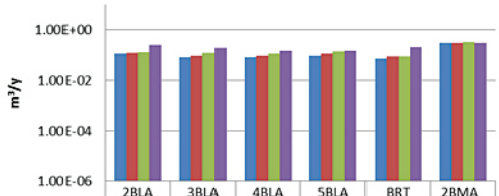

	2BLA	3BLA	4BLA	5BLA	BRT	2BMA
Initial State	1.15E-01	8.04E-02	8.29E-02	9.65E-02	7.21E-02	3.07E-01
Moderately degraded	1.23E-01	9.61E-02	9.26E-02	1.14E-01	8.94E-02	3.05E-01
Severely degraded	1.34E-01	1.25E-01	1.15E-01	1.39E-01	8.84E-02	3.19E-01
Completely degraded	2.45E-01	1.91E-01	1.52E-01	1.53E-01	2.13E-01	2.97E-01

b)Shoreline position 1
Total flow per waste (m³/y)

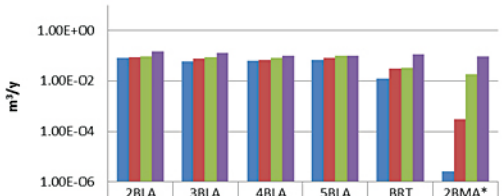

	2BLA	3BLA	4BLA	5BLA	BRT	2BMA*
Initial State	8.39E-02	5.99E-02	6.19E-02	6.88E-02	1.29E-02	2.56E-06
Moderately degraded	9.02E-02	7.60E-02	6.89E-02	8.16E-02	3.08E-02	3.03E-04
Severely degraded	9.20E-02	8.98E-02	8.11E-02	9.78E-02	3.30E-02	1.90E-02
Completely degraded	1.53E-01	1.27E-01	1.01E-01	1.04E-01	1.13E-01	9.66E-02

c) Shoreline position 2
Total flow per vault (m³/y)

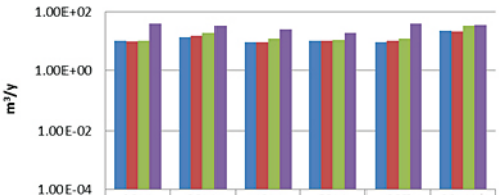

	2BLA	3BLA	4BLA	5BLA	BRT	2BMA
Initial State	1.02E+01	1.38E+01	9.41E+00	1.05E+01	9.08E+00	2.24E+01
Moderately degraded	1.01E+01	1.52E+01	9.50E+00	1.03E+01	1.06E+01	2.14E+01
Severely degraded	1.06E+01	1.95E+01	1.23E+01	1.10E+01	1.23E+01	3.29E+01
Completely degraded	3.92E+01	3.30E+01	2.49E+01	1.94E+01	3.99E+01	3.63E+01

d) Shoreline position 2
Total flow per waste (m³/y)

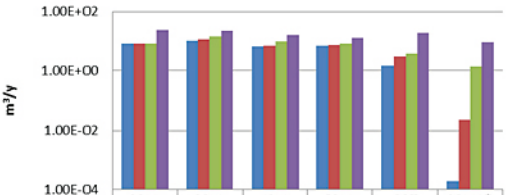

	2BLA	3BLA	4BLA	5BLA	BRT	2BMA*
Initial State	8.42E+00	1.03E+01	6.53E+00	7.18E+00	1.48E+00	1.97E-04
Moderately degraded	8.48E+00	1.15E+01	6.97E+00	7.42E+00	3.10E+00	2.31E-02
Severely degraded	8.09E+00	1.42E+01	9.72E+00	8.16E+00	3.70E+00	1.41E+00
Completely degraded	2.46E+01	2.28E+01	1.66E+01	1.27E+01	1.90E+01	9.49E+00

e) Shoreline position 3
Total flow per vault (m³/y)

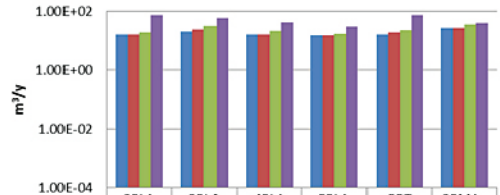

	2BLA	3BLA	4BLA	5BLA	BRT	2BMA
Initial State	1.60E+01	2.06E+01	1.61E+01	1.52E+01	1.59E+01	2.74E+01
Moderately degraded	1.59E+01	2.34E+01	1.63E+01	1.53E+01	1.88E+01	2.62E+01
Severely degraded	1.97E+01	3.18E+01	2.12E+01	1.72E+01	2.33E+01	3.62E+01
Completely degraded	7.20E+01	5.80E+01	4.25E+01	3.08E+01	7.43E+01	3.96E+01

f) Shoreline position 3
Total flow per waste (m³/y)

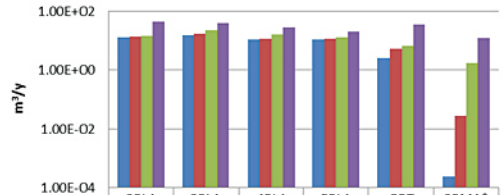

	2BLA	3BLA	4BLA	5BLA	BRT	2BMA*
Initial State	1.33E+01	1.51E+01	1.11E+01	1.13E+01	2.64E+00	2.46E-04
Moderately degraded	1.34E+01	1.72E+01	1.18E+01	1.17E+01	5.43E+00	2.87E-02
Severely degraded	1.48E+01	2.32E+01	1.64E+01	1.27E+01	6.78E+00	1.73E+00
Completely degraded	4.52E+01	3.95E+01	2.78E+01	1.98E+01	3.53E+01	1.24E+01

Figure 5-4. *Total flow (m^3/year) through the SFR3 vaults (left) and waste domains (right) for the different concrete degradation cases and the three shoreline positions. The vertical axis is logarithmic.*

The flow rate in the waste in 2–5BLA reflects the vault flow rate increase due to the absence of engineered barriers. The ratios between the waste and vault flow rate does not vary significantly. On the other hand, the waste flow rate in 1BRT and, especially, in 2BMA increases significantly with the degradation of the concrete. In 1BRT, the waste flow rate increases from 17 % of the vault flow rate in the initial state to 50 % in the complete degradation case. In 2BMA, the waste flow rate increases four orders of magnitude from the initial to the completely degraded concrete state. It should be notice, however, that the actual flow rates are low in spite of the large relatively large increase. The waste flow rate increase is linear in log-log scale with respect to the concrete hydraulic conductivity from the initial to the severely degraded state (Figure 5-5). However, in the complete degradation case, the slope decreases as the rock surrounding the vault becomes the active flow barrier.

Table 5-4. Total flow ratio normalized with respect to the Base case for the different concrete degradation cases: Moderate (M), Severe (S), Complete (C).

		Shoreline position 1			Shoreline position 2			Shoreline position 3		
		M	S	C	M	S	C	M	S	C
Vaults	2BLA	1.07	1.17	2.13	0.98	1.04	3.83	1.00	1.23	4.51
	3BLA	1.19	1.55	2.38	1.10	1.41	2.39	1.14	1.54	2.81
	4BLA	1.12	1.39	1.84	1.01	1.31	2.65	1.01	1.32	2.64
	5BLA	1.18	1.44	1.59	0.98	1.05	1.85	1.01	1.13	2.03
	1BRT	1.24	1.23	2.95	1.17	1.35	4.39	1.18	1.46	4.66
	2BMA	0.99	1.04	0.97	0.96	1.47	1.62	0.96	1.32	1.45
Waste	2BLA	1.08	1.10	1.83	1.01	0.96	2.92	1.01	1.12	3.41
	3BLA	1.27	1.50	2.13	1.12	1.38	2.22	1.14	1.54	2.62
	4BLA	1.11	1.31	1.63	1.07	1.49	2.54	1.06	1.47	2.50
	5BLA	1.18	1.42	1.51	1.03	1.14	1.77	1.04	1.12	1.75
	BRT	2.38	2.55	8.76	2.10	2.51	12.87	2.06	2.57	13.38
	2BMA	118	7419	37726	117	7177	48201	116	7041	50313
Loading Area	2BLA	1.04	0.96	3.15	1.05	2.09	9.03	1.02	2.18	9.58
	3BLA	1.53	5.16	10.87	1.11	3.06	3.26	1.13	2.87	4.00
	4BLA	1.27	2.40	4.06	1.07	1.70	3.23	1.05	1.52	3.73
	5BLA	1.29	3.32	3.84	0.87	1.28	2.75	0.86	1.12	3.35
	2BMA	1.27	4.20	3.29	0.71	5.54	3.81	0.69	3.38	1.18

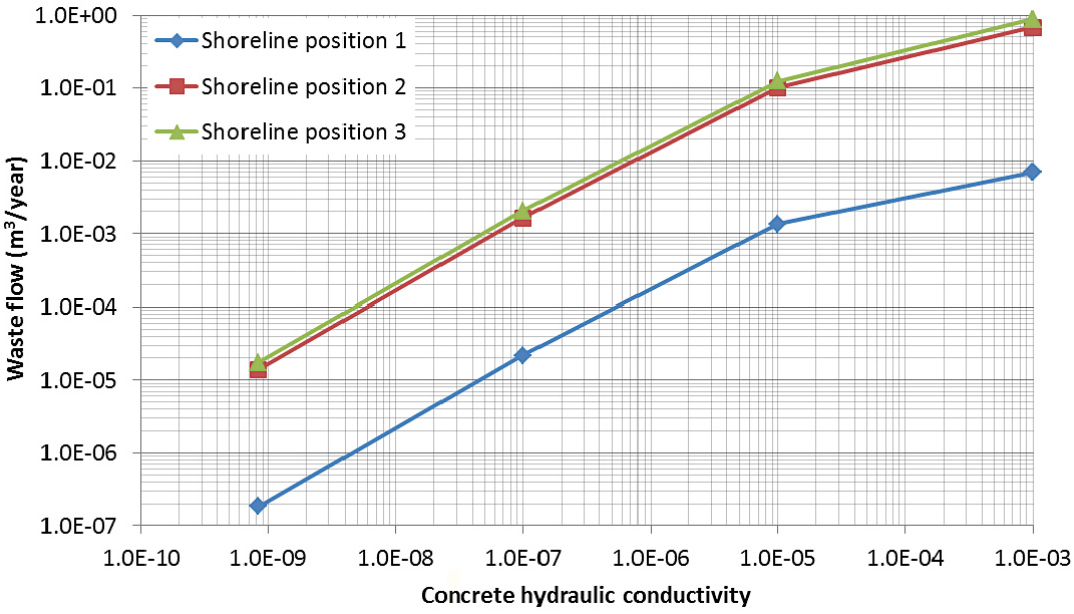

Figure 5-5. *Normalized 2BMA waste flow versus concrete hydraulic conductivity for the three different shoreline positions analysed.*

5.4 Discussion

The degradation of concrete leads to an increase in the groundwater flow rates through the tunnels and wastes except for the silo at shoreline position 1. The degradation of the concrete plugs connects the vaults with the access tunnels, increasing the inflow through the vaults. The plug degradation affects all the vault flow rates and the waste flow rates in vaults without concrete engineered barriers (1–5BLA and silo). The increase in flow rate is proportional to the distance to the access-tunnels. This increase is most significant in the severely and completely degraded cases.

The waste flow rates in the vaults with internal concrete barriers (1–2BTF, 1–2BMA and 1BRT) are influenced by the degradation of the internal barriers. They suffer the most significant increase in the complete degradation case. Groundwater increases more in the SFR1 than in the SFR3 vaults.

The flow rates for both 1BMA with high and low permeable beams are reported in this section. The influence of the permeability of the beams in the tunnel flow rates is minor and their impact in the other vaults is limited. The vault and waste flow rates for both cases are reported in the Appendix A. The HPB 1BMA induces a hydraulic cage effect for the initial case. This configuration is highly sensitive to concrete degradation. However, the flow rates are never higher than for the LPB configuration for the same degradation state. It should be noticed that faster concrete degradation is expected in the HPB case due to the larger flow induced by the high permeable beams.

The hydraulic conductivity of the concrete at the complete degradation case is higher than the rock conductivity around the vaults. The surrounding rock becomes, then, the active flow barrier driving the groundwater flow through the vaults.

6 Shrinking core plug degradation

This section explores the effect of axial concrete degradation on the evolution of the groundwater flow in the near field of SFR1 and SFR3. The degradation of the concrete plugs sealing the access tunnels advances from the concrete/rock interface towards the interior. The remaining concrete structures in the repository vaults are assumed to degrade homogeneously.

The time-dependent penetration depth of the concrete leaching and its implementation is first evaluated in a sub-model representing a single plug (Section 6.1). The single plug model helps to determine the leaching depth when repository scale models are considered, where the influence on the groundwater flow is assessed through the vaults and waste total flow (Section 6.2). Due to the extended times required for concrete leaching, the shoreline position 3 (5000 AD) pressure field is assumed as boundary condition in all the cases presented in this section.

6.1 Single plug model

A plug located between 4BLA and the southern access tunnel in SFR3 is selected as a representative modelling domain. The single plug model evaluates the evolving groundwater flow past the plug as function of concrete leaching. Further details on the model description can be found in Section 3.

6.1.1 Studied cases

The penetration depth of the concrete degradation is calculated using a diffusion-controlled shrinking core model for the portlandite leaching (see Section 3.4.2). The degradation rate depends on the effective diffusion coefficient in the weathered zone of the concrete (see Equation 3-4). Different values of the effective diffusivity are presented in Table 6-1. The resulting evolution of the penetration depth is shown Figure 6-1. In this work it is cautiously assumed that the maximum effective diffusivity (De) of weathered concrete applies (5×10^{-10} m^2/s). This De is expected for completely degraded concrete. In this study, it has been assumed that the access to water is homogenously distributed along the concrete plug, while it is expected that the flow and presence of freshwater able to degrade the concrete will be larger in the backfill than in the surrounding rock.

Table 6-1. Concrete effective diffusivities (m^2/s) used to evaluate the leaching depth with the diffusivity shrinking core model.

Description	Effective diffusivity (m^2/s)	Reference
Average concrete	1.6E−11	Average value (Idiart and Laviña 2019)
Weakly weathered concrete	3.0E−11	Aged concrete (Thompson et al. 2008)
Severely weathered concrete	5.0E−11	Higher than aged concrete (Höglund 2014)
Weathered concrete with maximum diffusivity	5.0E−10	Table 4-2 in SKB (2015) and Figure 8-1 in Höglund (2014)

As described in Section 3.4.3, two profiles of the advancing degradation front are analysed. One profile considers a step function to describe the changing porosity. It is assumed that both portlandite and CSH weathers simultaneously, leaving a skeleton of the initial aggregate material. This assumption is not realistic but is employed to represent a bounding case. A second profile assumes a gradual change of the porosity, based on the sequential leaching of portlandite and CSH. This represents realistic conditions and a profile based on the reactive transport models of concrete degradation developed on Idiart and Shafei (2019) and Idiart and Laviña (2019) is implemented. The different degradation profiles are illustrated in Figure 3-10.

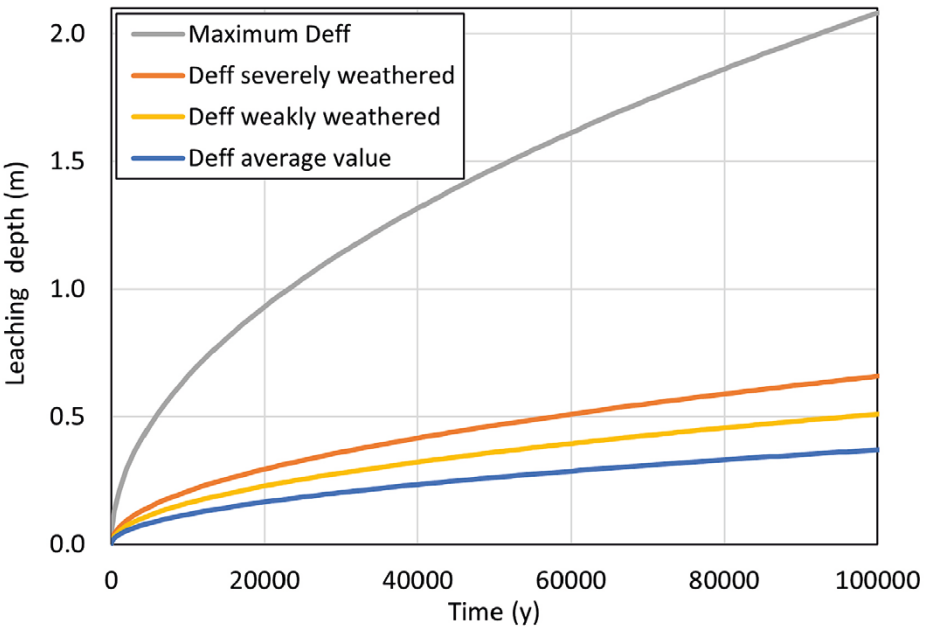

Figure 6-1. *Time evolution of the leaching depth for various types of concrete. The effective diffusivity values for each concrete type are described in Table 6-1.*

For both degradation profiles, the modified Kozeny-Carman is used to relate the porosity variation with the hydraulic conductivity of the concrete (Figure 3-12). The concrete plug degradation is evaluated with a transient model for 100 000 years assuming the hydraulic boundary conditions of shoreline position 3.

6.1.2 Results

The simulations analyse the influence of the leaching depth on the groundwater flow past the concrete plug. Pressure boundary conditions are extracted from the repository scale model of SFR3, assuming shoreline position 3. Due to the small size of the single plug model, it is expected that a large variation in the hydraulic properties of the concrete plug will affect the pressure conditions at the model boundaries. Hence, imposing a prescribed pressure field at the boundaries will give reasonable results for the initial states of the plug degradation. However, for advanced degradation states it may exaggerate groundwater fluxes through the model (further details are described in Section 6.3 and Figure 6-12).

The natural systems would evolve similarly to the gradual degradation case and, thus, this model is used in the repository scale case (Section 6.2). Several assumptions of the gradual degradation, such as the maximum effective diffusivity value for the weathered concrete used for the shrinking core model or the maximum hydraulic conductivity value of the modified Kozeny-Carman, are conservative and can account for the uncertainties that may arise from the theoretical models. The stepwise degradation is overly conservative and its results (Appendix B) add little to the understanding of the system.

The gradual degradation front model assumes that portlandite leaching happens first, followed by leaching of CSH minerals. The transition between the intact concrete and the totally degraded concrete results in intermediate conductivities along the plug (Figure 6-2). The penetration of the concrete leaching front is 2.1 m after 100 000 years, leading to an intact concrete core of around 2 m. Due to the imposed pressure at the boundaries, the pressure field remains nearly constant during the simulation (Figure 6-2).

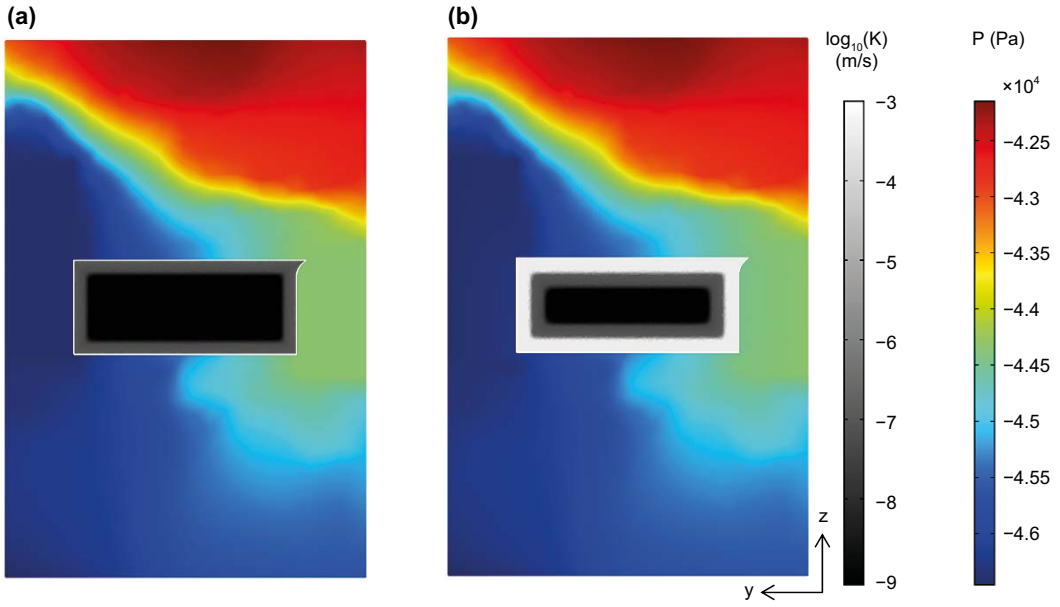

Figure 6-2. *Driving pressure field (P-ρ·g·z) and hydraulic conductivity of the concrete plug (grey scale) after 25 000 y (a) and after 100 000 y (b) for the gradual degradation front case.*

The range of conductivities leads to a zonation of Darcy velocities across the plug (Figure 6-3) with velocities of the order of 1×10^{-11} m/s in the intact concrete and of the order of 1×10^{-5} m/s in the degraded concrete. Intermediate velocities occur between them. High flow velocities along the plug (i.e., 1×10^{-5} m/s) arise when the leaching front penetration is higher than 1.16 m and the degraded concrete rim reaches a conductivity of the order of 1×10^{-4} m/s.

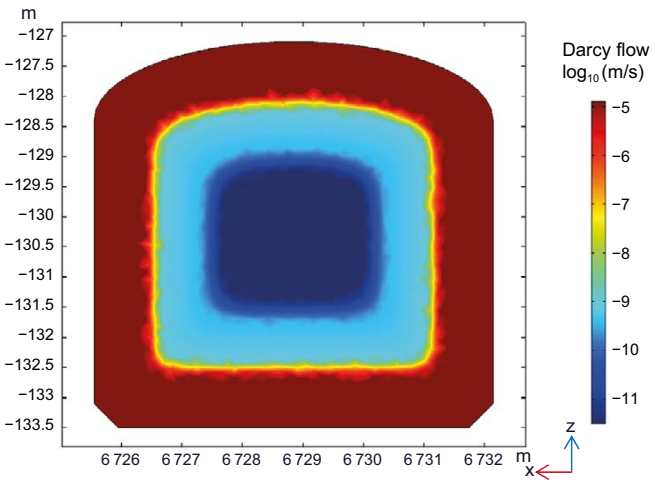

Figure 6-3. *Darcy flow velocity (m/s) in a vertical cross-section of the concrete plug after 100 000 y for the gradual degradation front in the single plug model.*

Streamlines that originate from 200 points located at the outer boundary of the model are calculated for each time step to illustrate the evolving groundwater flow paths (Figure 6-4). Initially, the concrete plug is intact and no flow is observed through the low permeable plug (Figure 6-4a). The water flows from the southern top boundary towards the northern bottom boundary of the domain and enters the vault from the surrounding rock. Most of the streamlines concentrate in the highly permeable backfill of the loading area of the vault. High Darcy velocities occur also within the highly permeable access tunnel.

When the concrete plug degrades (Figure 6-4b), groundwater flow is redirected through the plug. The degraded plug rim connects the highly permeable vault and access tunnels, creating a preferential flow path. Due to the gradual increase of the conductivity of the degraded concrete, the flow concentrates in the plug after 30 000 years (Figure 6-5). After 31 800 years, the groundwater flow crossing the interface between the concrete plug and the vault exceeds 100 m^3/y.

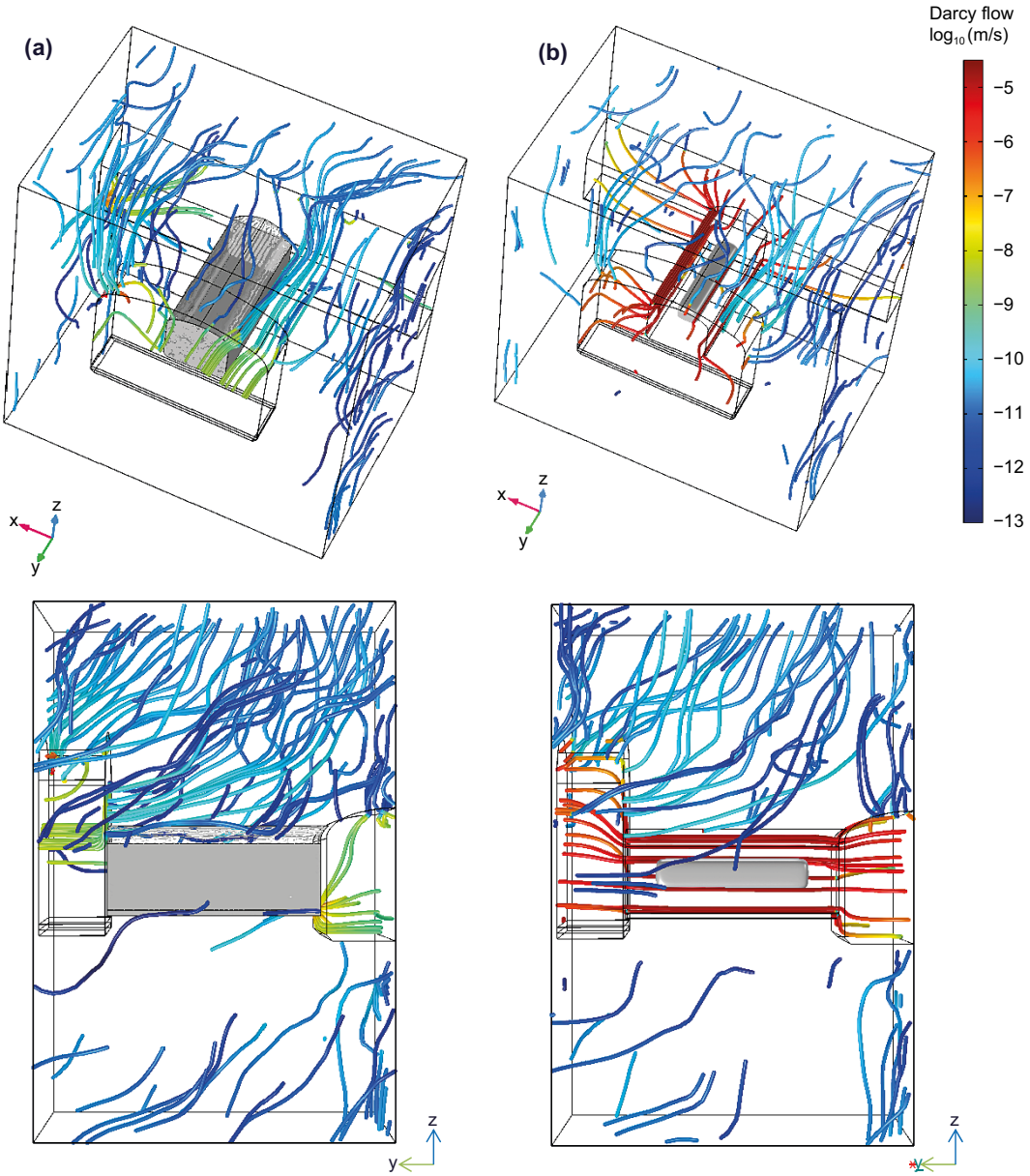

Figure 6-4. *Groundwater streamlines at the initial time (a) and after 100 000 y for the gradual degradation front case. The streamlines correspond to 200 particles released uniformly at the model boundaries. The streamlines are coloured by its Darcy flow velocity. The size of the intact concrete is shown in grey.*

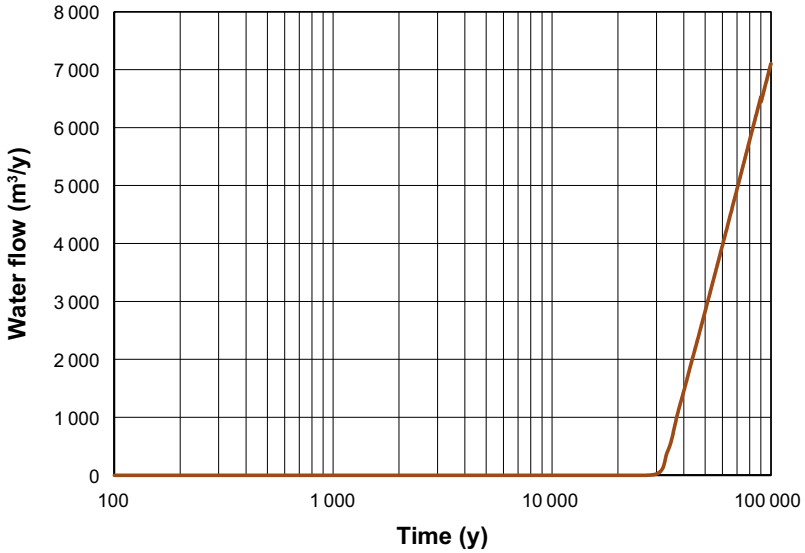

Figure 6-5. *Evolution of the groundwater flow (m^3/y) through the interface between the concrete plug and the vault for the gradual degradation case.*

6.2 Repository scale model

6.2.1 Degradation cases

The temporal evolution of the degradation of the concrete plugs is combined with the homogenous degradation of the remaining concrete structures in the repository scale models. The temporal evolution of the properties of the concrete in the different SFR vaults is described in Table 4-1 of SKB (2015). The initial state, which lasts up to 3000 AD, and the complete degradation state, which begins at 52 000 AD were analysed in Section 5. Here, the evolution in between these two states is analysed considering three intermediate degradation states: A, from 3000 to 12 000 AD; B, from 12 000 to 22 000 AD; and C, from 22 000 to 52 000 AD.

The A, B and C degradation states for the concrete in the vaults are combined with a gradual degradation of the concrete plugs. The leaching depths corresponding to the lower and upper limit of each temporal interval are calculated assuming a weathered concrete with a maximum diffusivity (Table 6-1). The spatial distribution of the hydraulic conductivity in the sealing plugs corresponding to the resulting 5 leaching depths are shown in Figure 6-7. The maximum concrete hydraulic conductivity of the plugs is around 1×10^{-7} m/s except for the last degradation case that have a leaching depth of 1.501 m and a maximum hydraulic conductivity of 1×10^{-3} m/s. The combination leads to a set of 6 degradation cases (Figure 6-6). The cases are named degradation case 1 to 6 (DC 1–6). The hydraulic conductivity values of the concrete structures in each vault are described in Table 6-2. All these cases are simulated using the pressure field corresponding to shoreline position 3 as boundary condition.

A sensitivity analysis to the impact in the vault and waste flow rate of the axial plug degradation is presented in Appendix C. In this analysis, only the concrete plugs degrade while the other concrete structures remain intact.

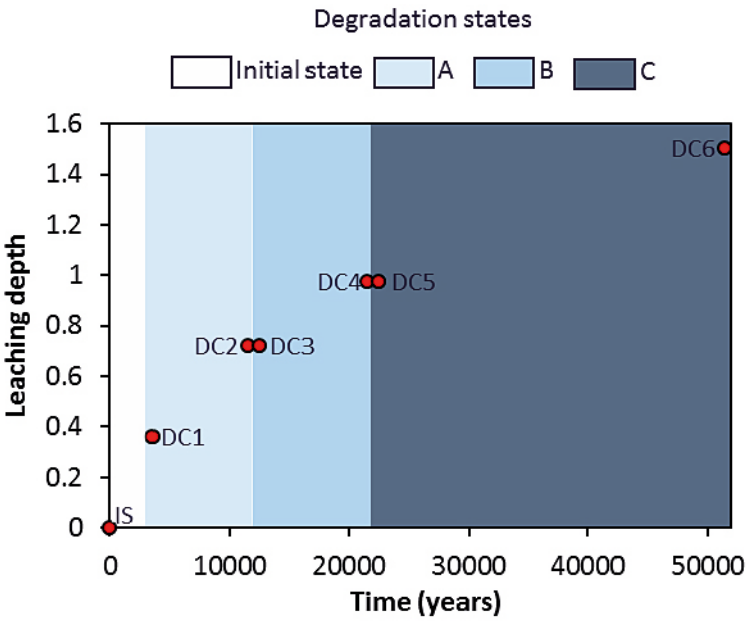

Figure 6-6. *Temporal sequence of cases (DC 1–6) given by the combination of the leaching depths and the degradation states with the concrete in the vaults (A,B,C).*

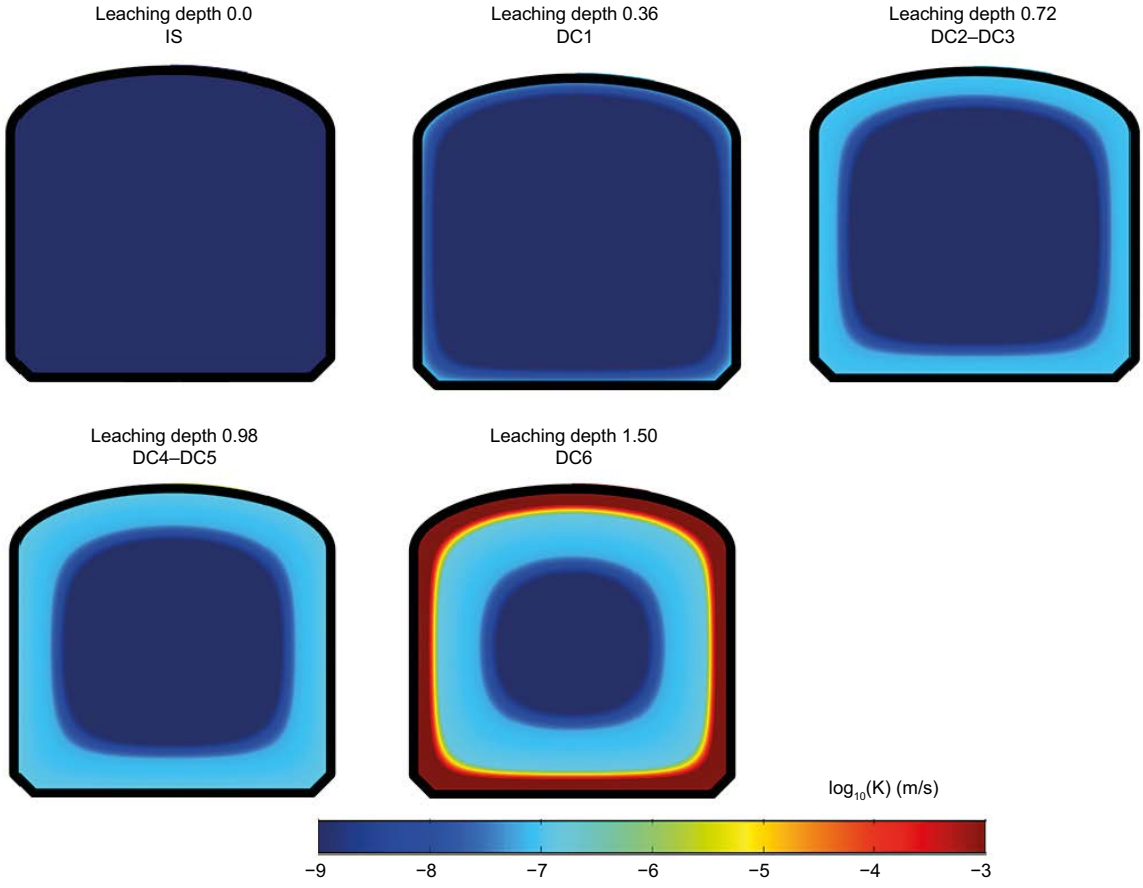

Figure 6-7. *2D perpendicular cross-section of the hydraulic conductivity of the sealing plugs for the considered leaching depths.*

Table 6-2. Hydraulic conductivity of the materials and leaching depth in the plugs for the different models studied. The hydraulic conductivity of the different materials is obtained from SKB (2015).

Degradation state	ID	Year	Leaching depth (m)	Hydraulic conductivity m/s		
				Concrete (BMA, BTF, BLA)	Silo	BTF, 1BRT
Initial state	IS	0	0	8.30E−10	8.30E−10	8.30E−09
A	DC1	3000	0.36	1.00E−07	1.00E−05	1.00E−05
	DC2	12000	0.721	1.00E−07	1.00E−05	1.00E−05
B	DC3	12000	0.721	1.00E−07	1.00E−05	1.00E−03
	DC4	22000	0.976	1.00E−07	1.00E−05	1.00E−03
C	DC5	22000	0.976	1.00E−05	1.00E−05	1.00E−03
	DC6	52000	1.501	1.00E−05	1.00E−05	1.00E−03

6.2.2 SFR1

Figure 6-8 shows the computed flow rates through the vaults and waste for each degradation case. The flow rate ratios with respect to the initial state case are shown in Table 6-3.

Vault flow rates are similar for all degradation states except for DC6 (Figure 6-8 left). These results imply that the plug degradation does not affect the vault flow rates until the maximum hydraulic conductivity set for the concrete (1×10^{-3} m/s) is achieved. This value of hydraulic conductivity occurs after 50 000 years, considering that the advancement of the degradation zone is controlled by the maximum effective diffusivity of the weathered zone ($De = 5 \times 10^{-10}$ m^2/s). This is a conservative estimate. The maximum increase in the vault flow rate is observed in 1–2BTF at the DC6 (Table 6-3). The vault flow rate increases 34 and 13 times at 1BTF and 2BTF, respectively. The lowest increase (2.6 times) occurs in the silo due to the surrounding bentonite walls.

The flow rate through the waste increases between the initial state and the DC1 and between the DC5 and the DC6 (Figure 6-8 right). The flow rate increase in the DC1 is due to the degradation of the concrete structures within the vaults. It is observed in all vaults except 1BLA, which does not have any internal concrete barriers. The 1BMA with high permeability beams case follows the trend of the homogeneous degradation case (Figure 5-3). It should be noticed that the actual flow rates are low in spite of the large relatively large increase. The flow rate in the waste is driven by the degradation of the concrete barriers. Thus, the waste flow rate at DC1–CD4 is similar to the moderate homogeneous degradation case in Section 5.2 because the permeability of the concrete barriers is the same for all cases. At DC6, the flow rates are similar for both 1BMA with high (HPM) and low permeability beams (LPB). In this case, the increase in waste flow rates is uniquely controlled by vault flow rate increase due to the plugs degradation. Local and minor increases of waste flow rate due to the degradation of concrete structures are also evident in 1–2BTF between the DC2 and the DC3. Similar to the vault flow rate, the influence of the concrete sealing plugs degradation is only evident at the transition between the DC5 and the DC6. Waste flow rate clearly increases in all vaults except for the silo where the interior bentonite barriers prevent a significant flow rate increase.

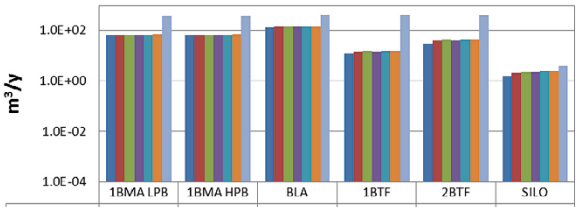

	1BMA LPB	1BMA HPB	BLA	1BTF	2BTF	SILO
IS h=0	6.49E+01	6.72E+01	1.29E+02	1.24E+01	3.03E+01	1.51E+00
DC1 h=0.36	6.71E+01	6.73E+01	1.37E+02	1.44E+01	4.14E+01	2.09E+00
DC2 h=0.721	6.74E+01	6.76E+01	1.37E+02	1.48E+01	4.18E+01	2.28E+00
DC3 h=0.721	6.74E+01	6.76E+01	1.37E+02	1.46E+01	4.15E+01	2.28E+00
DC4 h=0.976	6.83E+01	6.84E+01	1.37E+02	1.49E+01	4.21E+01	2.47E+00
DC5 h=0.976	6.85E+01	6.86E+01	1.39E+02	1.49E+01	4.21E+01	2.47E+00
DC6 h=1.501	3.69E+02	3.71E+02	4.33E+02	4.26E+02	4.07E+02	3.96E+00

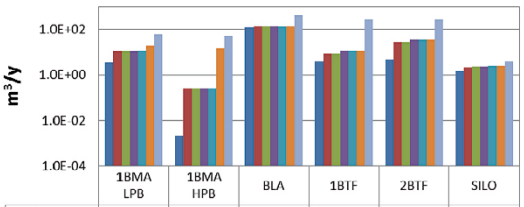

	1BMA LPB	1BMA HPB	BLA	1BTF	2BTF	SILO
IS h=0	3.44E+00	2.11E-03	1.21E+02	3.91E+00	4.95E+00	1.47E+00
DC1 h=0.36	1.11E+01	2.48E-01	1.34E+02	8.38E+00	2.64E+01	2.06E+00
DC2 h=0.721	1.12E+01	2.50E-01	1.34E+02	8.30E+00	2.63E+01	2.23E+00
DC3 h=0.721	1.12E+01	2.50E-01	1.34E+02	1.16E+01	3.51E+01	2.23E+00
DC4 h=0.976	1.14E+01	2.52E-01	1.34E+02	1.19E+01	3.58E+01	2.41E+00
DC5 h=0.976	1.86E+01	1.42E+01	1.38E+02	1.19E+01	3.58E+01	2.41E+00
DC6 h=1.501	5.92E+01	5.39E+01	4.24E+02	2.76E+02	2.65E+02	3.93E+00

Figure 6-8. *Total flow (m^3/year) through the SFR1 vaults (left) and waste domains (right) for the different concrete degradation cases. The vertical axis is logarithmic. Note that the results refer to the simulation with low permeable 1BMA beams except for the 1BMA HPB case.*

Table 6-3. Total flow ratio normalized with respect to the Base case for the different degradation cases.

	Case	1BMA LPB	1BMA HPB	BLA	1BTF	2BTF	SILO
Tunnel	DC1 h = 0.36	1.03	1.00	1.06	1.17	1.37	1.39
	DC2 h = 0.721	1.04	1.01	1.06	1.19	1.38	1.51
	DC3 h = 0.721	1.04	1.01	1.06	1.18	1.37	1.51
	DC4 h = 0.976	1.05	1.02	1.06	1.21	1.39	1.64
	DC5 h = 0.976	1.06	1.02	1.07	1.21	1.39	1.64
	DC6 h = 1.501	5.69	5.52	3.35	34.51	13.43	2.63
Waste	DC1 h = 0.36	3.22	117	1.10	2.14	5.34	1.40
	DC2 h = 0.721	3.27	118	1.10	2.12	5.32	1.51
	DC3 h = 0.721	3.27	118	1.10	2.98	7.11	1.51
	DC4 h = 0.976	3.33	119	1.10	3.04	7.25	1.64
	DC5 h = 0.976	5.41	6748	1.13	3.04	7.23	1.64
	DC6 h = 1.501	17.24	25567	3.49	70.69	53.60	2.67

Streamlines illustrating the general flow field evidence similar patterns at the initial state (Figure 4-3) and the DC6 (Figure 6-9). Pathways of groundwater discharging from the vaults are the same. However, the pathways of water entering the vaults differ. At the initial state, water enters the vaults through the surrounding rock while water enters 1BMA, 1BLA and silo through the access tunnels at the DC6. The degradation of the plugs creates preferential flow paths and prompts the water flow through the tunnels.

6.2.3 SFR3

Figure 6-10 shows the vault and waste flow rates at each degradation case. The flow rate ratios with respect to the initial state case are reported in Table 6-4. The flow rates through the vaults (Figure 6-10 left) are not significantly affected by the plug degradation until the last degradation state (DC6) in which the maximum hydraulic conductivity of 1×10^{-3} m/s is reached. In SFR3, the vault flow rate is less than 4 times larger than for the initial state. Therefore, the increase in flow rate through the vaults is lower in SFR3 than in SFR1.

The waste flow rate in BLA vaults is not affected by concrete degradation until the DC6 state (Figure 6-10 right). BLA vaults do not have internal concrete barriers and, therefore, their waste flow rate is controlled by the hydraulic conductivity of the sealing plugs. For the DC6, the waste flow rate in BLAs is less than 3 times the flow rate at the initial state. In 2BMA and 1BRT vaults the waste flow rate increases for the DC1, the DC3 (1BRT) and the DC5 (2BMA). These flow rate increments are due to the degradation of the internal concrete structures. Notice that the actual flow rates are low in spite of the large relatively large increase.

Table 6-4. Flow ratios normalized with respect to the flow at the initial state.

		2BMA	2BLA	3BLA	4BLA	5BLA	1BRT
Tunnel	DC1 h = 0.36	0.99	1.08	1.17	1.02	1.08	1.23
	DC2 h = 0.721	0.99	1.06	1.17	1.02	1.07	1.23
	DC3 h = 0.721	0.99	1.06	1.17	1.02	1.07	1.23
	DC4 h = 0.976	0.98	1.05	1.16	1.02	1.06	1.23
	DC5 h = 0.976	0.98	1.05	1.16	1.02	1.06	1.23
	DC6 h = 1.501	1.47	3.35	2.60	2.60	2.21	2.89
Waste	DC1 h = 0.360	119	1.06	1.15	1.06	1.10	5.13
	DC2 h = 0.721	118	1.05	1.15	1.06	1.09	5.12
	DC3 h = 0.721	118	1.05	1.15	1.06	1.09	14.00
	DC4 h = 0.976	118	1.04	1.15	1.06	1.08	14.18
	DC5 h = 0.976	7648	1.04	1.14	1.06	1.08	14.18
	DC6 h = 1.501	14992	2.70	2.52	2.53	1.93	22.12

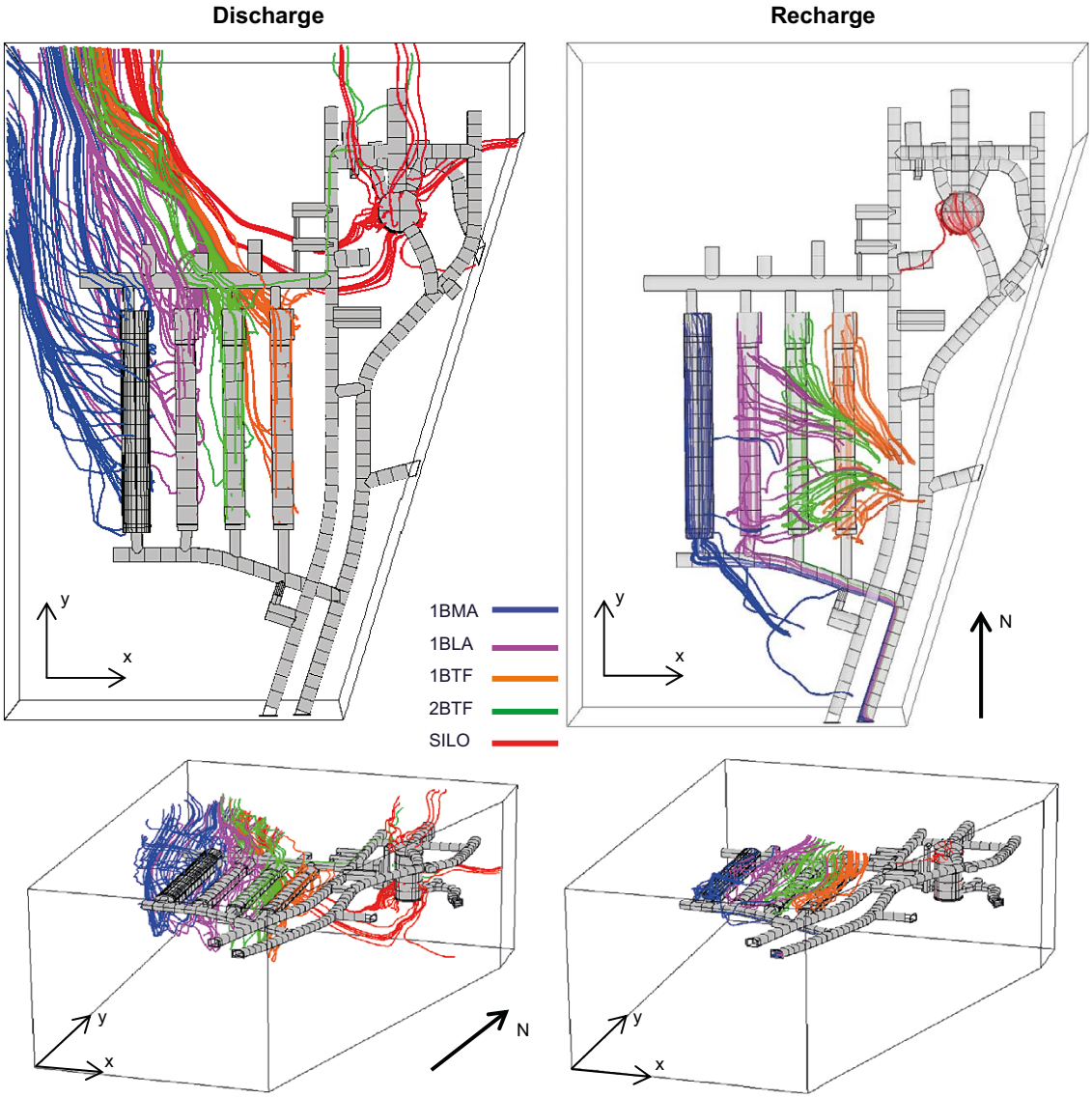

Figure 6-9. *Groundwater streamlines leaving (left) and reaching (right) individual vaults (colour tubes) in the SFR1 for the DC6 at shoreline position 3.*

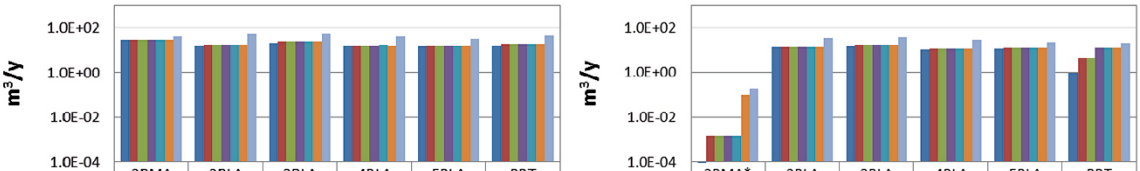

	2BMA	2BLA	3BLA	4BLA	5BLA	BRT
IS h=0	2.73E+01	1.58E+01	2.06E+01	1.61E+01	1.50E+01	1.54E+01
DC1 h=0.36	2.71E+01	1.71E+01	2.41E+01	1.64E+01	1.63E+01	1.88E+01
DC2 h=0.721	2.69E+01	1.68E+01	2.40E+01	1.64E+01	1.61E+01	1.88E+01
DC3 h=0.721	2.69E+01	1.68E+01	2.40E+01	1.64E+01	1.61E+01	1.88E+01
DC4 h=0.976	2.68E+01	1.66E+01	2.39E+01	1.65E+01	1.59E+01	1.88E+01
DC5 h=0.976	2.68E+01	1.66E+01	2.38E+01	1.64E+01	1.59E+01	1.88E+01
DC6 h=1.501	4.03E+01	5.30E+01	5.34E+01	4.19E+01	3.33E+01	4.44E+01

	2BMA*	2BLA	3BLA	4BLA	5BLA	BRT
IS h=0	1.30E-05	1.31E+01	1.50E+01	1.11E+01	1.12E+01	9.11E-01
DC1 h=0.36	1.55E-03	1.40E+01	1.72E+01	1.17E+01	1.24E+01	4.67E+00
DC2 h=0.721	1.54E-03	1.38E+01	1.72E+01	1.17E+01	1.23E+01	4.66E+00
DC3 h=0.721	1.54E-03	1.38E+01	1.72E+01	1.17E+01	1.23E+01	1.28E+01
DC4 h=0.976	1.54E-03	1.37E+01	1.72E+01	1.18E+01	1.21E+01	1.29E+01
DC5 h=0.976	9.97E-02	1.36E+01	1.70E+01	1.18E+01	1.22E+01	1.29E+01
DC6 h=1.501	1.95E-01	3.55E+01	3.78E+01	2.82E+01	2.17E+01	2.01E+01

Figure 6-10. *Total flow (m^3/year) through the SFR3 vaults (left) and waste domains (right) for the different concrete degradation cases. The vertical axis is logarithmic. *2BMA waste flow is normalized with respect the number of waste compartments.*

Comparing the streamlines for the DC6 case (Figure 6-11) and for the initial state (Figure 4-7) it can be concluded that the local groundwater flow around the SFR3 is not affected by concrete degradation. The major difference is the increase of groundwater entering the vaults through the access tunnels due to the degradation of the plugs, which leads to the connection of the vaults and the access tunnels.

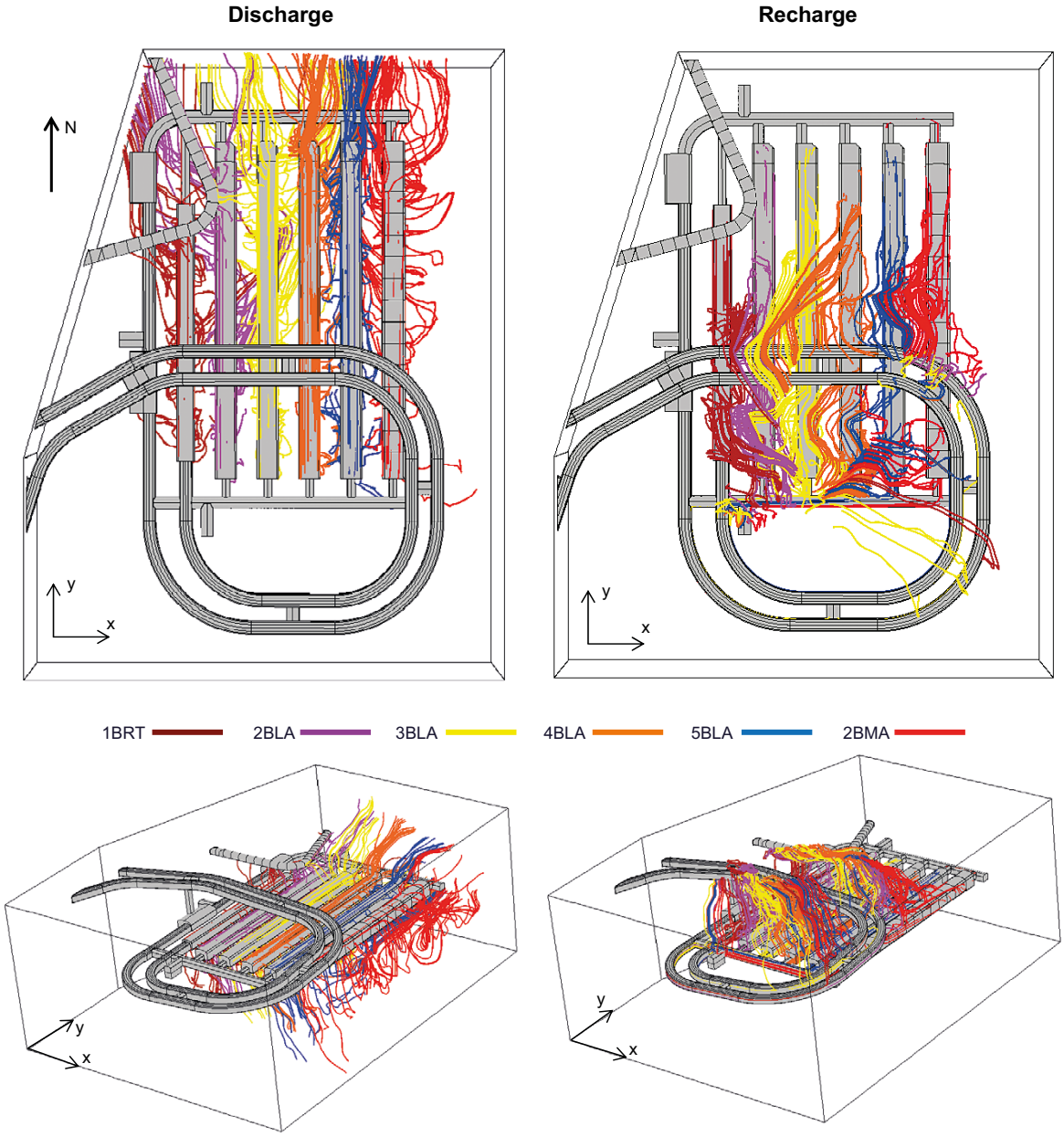

Figure 6-11. *Groundwater streamlines leaving (left) and reaching (right) individual vaults (colour tubes) in the SFR3 for the case DC6 at shoreline position 3.*

6.3 Discussion

An axial degradation of the concrete plugs has been investigated, where the degradation front advances from the rock/concrete interface towards the interior of the plugs. The implementation of such degradation process is tested in a transient plug-scale model. The information gained from this single-plug model is applied to a repository-scale model where the water flow rates through the tunnel and waste domains are calculated.

The leaching of the concrete plugs is modelled using a shrinking core model to compute the penetration depth following from portlandite leaching. The advancement of the degradation zone is controlled by the maximum effective diffusivity of the weathered zone. An effective diffusivity of $De = 5 \times 10^{-10}$ m^2/s has been used, corresponding to completely degraded concrete in the weathered zone. This is a cautiously selected value that exaggerates the penetration depth of portlandite leaching (see Figure 6-1).

The presence of other calcium-rich minerals (i.e., CSH phases) when portlandite is exhausted is considered in a gradual degradation model. In the gradual degradation model, the porosity of the degraded concrete evolves progressively from its initial state (0.11) to a maximum value (0.3). The modified Kozeny-Karman relation links the hydraulic conductivity of the concrete with its porosity. It scales the hydraulic conductivity between the initial conductivity of the intact concrete (assumed $K = 8.3 \times 10^{-10}$ m/s) and the maximum conductivity when all calcium minerals have been depleted (assumed $K = 1 \times 10^{-3}$ m/s). For the study of the hydraulic sealing capability of concrete plugs this is a cautious approach, as a high hydraulic conductivity is forced in severely and completely degraded regions (see also Section 3).

In this study the maximum porosity and, therefore, the maximum conductivity occurs when the leaching depth is 1.2 m or higher. A significant increase of the flow rate in the access tunnel occurs only after 26 000 years (Figure 6-12). Figure 6-12 shows the groundwater flow that enters the 4BLA vault through the access tunnel in the single-plug model and the repository scale model. The flow rates are similar for both models up to 22 000 years. The repository-scale model yields lower flow rates than the single-plug model for DC6. For extended times, the realistic values are those calculated with the repository scale model. The single-plug model domain is too small and its boundary conditions are compromised under severe degradation scenarios.

The full degradation of a rim in the concrete plugs connects the vaults with the access tunnels, generating preferential flow paths and increasing the groundwater flow entering the vaults (Figure 6-9 and Figure 6-11). These preferential paths lead to relevant water flow rates only when the maximum hydraulic conductivity of the degraded plugs is around 1×10^{-3} m/s.

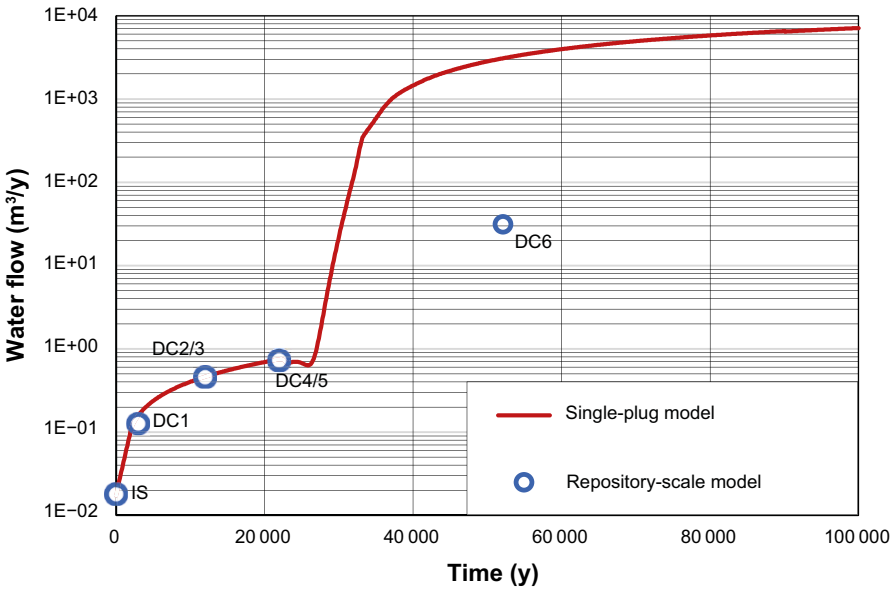

Figure 6-12. *Evolution of the groundwater flow entering 2–5BLA for the single plug and the repository scale models for the different degradation cases assuming a gradual degradation profile.*

7 Conclusion

The main objective of this work is to evaluate the implications of using concrete as sealing material on the plugs of the SFR1 and SFR3 repositories. Two conceptualizations of the degradation of the hydraulic properties of the concrete plugs are considered: the homogeneous degradation, where the properties of the whole plugs vary homogeneously; and the axial degradation, where the degradation front advances from the rock/concrete interface towards the interior of the plugs. The flow rates through predefined control volumes are computed and tabulated as input to radionuclide transport calculations following the procedure in Abarca et al. (2013).

The homogeneous degradation concept has been used previously to assess the impact of different design decision (Abarca et al. 2013, 2014). It can be seen as a conservative case as the degradation of concrete will not occur simultaneously in the whole plug.

In the axial degradation of the concrete plugs the degradation front advances from the rock/concrete interface towards the interior of the plugs. This approach uses recent results of reactive transport models of concrete degradation (Idiart and Shafei 2019). First a plug-scale model has been implemented to test such degradation process and then, the information gained from this single-plug model is applied to a repository-scale model. This last repository-scale model can serve for comparison with the homogenous degradation case and other design options.

In the axial degradation models, a shrinking core model of the leaching of the concrete plugs is used to compute the penetration depth of the degradation front. In this study, it is assumed that the availability of water able to degrade the concrete plugs is homogenously distributed while it is expected that the access to water will be larger in the backfill materials than in the host rock. The degradation front is assumed to be controlled by diffusion where the concentration of Ca at the concrete/rock boundary is considered to be 0. This would imply that a high groundwater flow, parallel to the surface of the weathered concrete, flushes out the dissolved calcium. Furthermore, the effective diffusivity used corresponds to that of the completely degraded concrete. These assumptions can be seen as conservative. It should be kept in mind, however, that after several thousands of years of degradation, an advection-controlled leaching would lead to larger degradation front penetration. The hydraulic conductivity of the degraded concrete follows the modified Kozeny-Karman relation that scales the hydraulic conductivity between the initial conductivity of the intact concrete and the maximum conductivity when all calcium minerals have been depleted. This is also a cautious approach, as a high hydraulic conductivity is forced in severely and completely degraded regions.

In both, the homogeneous and axial degradation models, the groundwater flow rates through the tunnels and wastes (except for the silo at shoreline position 1) increase due to the degradation of concrete. The degradation of the concrete plugs connects the vaults with the access tunnels, increasing the inflow through the vaults. The vault and waste flow rates of all the vaults without concrete engineered barriers (1–5BLA and silo) are affected by the plug degradation. In these vaults, the increase in flow rate is proportional to the distance to the access-tunnels. This increase is most significant in the severely and completely degraded cases. In vaults with internal concrete barriers (1–2BTF, 1–2BMA and 1BRT), the waste flow rates are also influenced by the degradation of the internal barriers. Despite the large increase in waste flow at advanced degraded states in 1–2BMA, it should be kept in mind that the flow rates are low. The presence of high or low permeable beams in 1BMA have minor influence in the tunnel groundwater flow and its impact in other vaults is limited. The highly permeable beams (HPB) generate a hydraulic cage effect at the initial case that do not occur at the low permeable beams (LPB). The HPB configuration is highly sensitive to concrete degradation; however, the flow rates are never higher in the HPB than in the LPB. It should be noticed that faster concrete degradation is expected in the HPB case due to the larger flow induced by the high permeable beams.

The flow rates estimated in this work can be compared with the flow rates estimated for the plug degradation case of Abarca et al. (2013, Section 6.2.2). That study analyses the flow rates through the SFR1 case considering the shoreline position 3. The initial state is comparable for all the vaults and waste control volumes. For the degradation cases, only the vault flow rates are comparable as no degradation of concrete inner structures was considered in Abarca et al. (2013). The vault flow rates of the silo are also not comparable as its bentonite walls were considered as degradable in Abarca et al. (2013).

For the initial state, the flow rates calculated for the cases with concrete and bentonite plugs are similar. The vault and waste flow rates are slightly larger in the case with bentonite for all the cases except for the waste control volume of 1BTF. In the completely degraded case, the flow rates through the vaults is also larger in the case with bentonite plugs except in the 2BTF. In the moderate and severe degradation cases, the flow rates at the vaults are lager in the concrete plugs except in 1–2BTF and 1BLA at the moderate degradation case. In general, the differences between the flow rates are not critical, indicating that both materials are suitable for the plug sealing if the same degradation state is considered. In order to answer which system would be the most adequate, it would be necessary to pay attention to the rate of degradation of the bentonite and the concrete. The material with the highest resistance to degradation would be the most suitable for the plug sealing.

References

SKB's (Svensk Kärnbränslehantering AB) publications can be found at www.skb.com/publications.

Abarca E, Idiart A, de Vries L M, Silva O, Molinero J, von Schenck H, 2013. Flow modelling on the repository scale for the safety assessment SR-PSU. SKB TR-13-08, Svensk Kärnbränslehantering AB.

Abarca E, Silva O, Idiart A, Nardi A, Font J, Molinero J, 2014. Flow and transport modelling on the vault scale for the safety assessment SR-PSU. SKB R-14-14, Svensk Kärnbränslehantering AB.

Benbow S, Watson C, Savage D, 2005. Investigating conceptual models for physical property couplings in solid solution models of cement. SKI Report 2005:64, Statens kärnkraftinspektion (Swedish Nuclear Power Inspectorate).

Carman P, 1937. Fluid flow through a granular bed. Transactions, Institution of Chemical Engineers, London 15, 150–167.

COMSOL, 2015. COMSOL Multiphysics® v. 5.2. COMSOL AB, Stockholm, Sweden.

Höglund L O, 2014. The impact of concrete degradation on the BMA barrier functions report. SKB R-13-40, Svensk Kärnbränslehantering AB.

Idiart A, Laviña M, 2019. Modelling of concrete degradation in a one-million-year perspective – Hydro-chemical processes. Report for the safety evaluation SE-SFL. SKB R-19-13, Svensk Kärnbränslehantering AB.

Idiart A, Shafei B, 2019. Modelling of concrete degradation – Hydro-chemical processes. Report for the safety evaluation SE-SFL. SKB R-19-11, Svensk Kärnbränslehantering AB.

Levenspiel O, 1972. Chemical reaction engineering. 2nd ed. New York: Wiley.

Odén M, Follin S, Öhman J, Vidstrand P, 2014. SR-PSU Bedrock hydrogeology. Groundwater flow modelling methodology, setup and results. SKB R-13-25, Svensk Kärnbränslehantering AB.

SKB, 2013. Site description of the SFR area at Forsmark at completion of the site investigation phase. SDM-PSU Forsmark. SKB TR-11-04, Svensk Kärnbränslehantering AB.

SKB, 2015. Radionuclide transport and dose calculation for the safety assessment SR-PSU. Revised edition. SKB TR-14-09, Svensk Kärnbränslehantering AB.

Thomson G, Miller A, Smith G, Jackson D, 2008. Radionuclide release calculations for SAR-08. SKB R-08-14, Svensk Kärnbränslehantering AB.

Öhman J, Follin S, Odén M, 2014. SR-PSU Hydrogeological modelling. TD11 – Temperate climate conditions. SKB P-14-04, Svensk Kärnbränslehantering AB.

Appendix A

Homogeneous concrete degradation

The flow rates through the Waste and vaults of SFR1 and SFR3 are presented in the following appendix. The results presented for the SFR1 present two different simulation cases: one with low permeable beams at 1BMA and other with high permeable beams at 1BMA.

A1 SFR1

A1.1 Low permeable 1BMA beams

Table A-1. Total flow (m^3/year) through the vaults and waste compartments for the initial state case and the three homogeneous degradation cases studied at shoreline position 1. Note: These results correspond with the Low permeable 1BMA beams.

		Shoreline position 1			
		Initial State	Moderate	Severe	Complete
Vaults	1BMA	5.24E−02	7.42E−02	3.00E−01	3.10E−01
	1BLA	2.23E−01	2.52E−01	5.39E−01	6.83E−01
	1BTF	2.75E−02	4.08E−02	8.13E−02	5.85E−01
	2BTF	6.60E−02	8.82E−02	2.75E−01	4.53E−01
	Silo	3.75E−03	2.86E−03	7.89E−04	7.73E−04
Waste	1BMA	7.90E−03	1.80E−02	2.59E−02	1.27E−01
	1BLA	1.98E−01	2.30E−01	5.03E−01	6.28E−01
	1BTF	8.14E−03	1.80E−02	1.24E−02	3.93E−01
	2BTF	8.39E−03	2.69E−02	3.08E−02	2.93E−01
	Silo	3.64E−03	2.83E−03	7.56E−04	7.73E−04

Table A-2. Total flow (m^3/year) through the vaults and waste compartments for the initial state case and the three homogeneous degradation cases studied at shoreline position 2. Note: These results correspond with the Low permeable 1BMA beams.

		Shoreline position 2			
		Initial State	Moderate	Severe	Complete
Vaults	1BMA	2.99E+01	3.27E+01	8.17E+01	1.25E+02
	1BLA	5.93E+01	6.66E+01	8.93E+01	1.58E+02
	1BTF	5.91E+00	8.14E+00	3.05E+01	2.56E+02
	2BTF	1.69E+01	2.24E+01	5.69E+01	1.82E+02
	Silo	6.40E−01	8.38E−01	1.41E+00	1.41E+00
Waste	1BMA	1.30E+00	4.37E+00	1.45E+01	5.57E+01
	1BLA	5.56E+01	6.52E+01	8.85E+01	1.55E+02
	1BTF	1.87E+00	3.67E+00	4.66E+00	1.73E+02
	2BTF	2.55E+00	1.11E+01	1.10E+01	1.25E+02
	Silo	5.85E−01	7.99E−01	1.39E+00	1.39E+00

Table A-3. Total flow (m^3/year) through the vaults and waste compartments for the initial state case and the three homogeneous degradation cases studied at shoreline position 3. Note: These results correspond with the Low permeable 1BMA beams.

		Shoreline position 3			
		Initial State	Moderate	Severe	Complete
Vaults	1BMA	6.49E+01	7.03E+01	1.81E+02	3.18E+02
	1BLA	1.29E+02	1.37E+02	2.06E+02	3.98E+02
	1BTF	1.24E+01	1.59E+01	7.38E+01	7.15E+02
	2BTF	3.03E+01	4.23E+01	1.26E+02	4.81E+02
	Silo	1.51E+00	3.02E+00	3.96E+00	3.92E+00
Waste	1BMA	3.44E+00	1.19E+01	3.26E+01	1.45E+02
	1BLA	1.21E+02	1.33E+02	2.02E+02	3.88E+02
	1BTF	3.91E+00	7.67E+00	1.21E+01	4.87E+02
	2BTF	4.95E+00	2.23E+01	2.54E+01	3.29E+02
	Silo	1.47E+00	2.94E+00	3.93E+00	3.90E+00

A1.2 High permeable 1BMA beams

Table A-4. Total flow (m^3/year) through the vaults and waste compartments for the initial state case and the three homogeneous degradation cases studied at shoreline position 1. Note: These results correspond with the high permeable 1BMA beams.

		Shoreline position 1			
		Base case	Moderate	Severe	Complete
Vaults	1BMA	5.60E−02	7.43E−02	3.00E−01	3.11E−01
	1BLA	2.23E−01	2.52E−01	5.40E−01	6.84E−01
	1BTF	2.75E−02	4.09E−02	8.14E−02	5.86E−01
	2BTF	6.60E−02	8.82E−02	2.76E−01	4.54E−01
	Silo	3.75E−03	2.86E−03	7.86E−04	7.70E−04
Waste	1BMA	3.14E−06	3.38E−04	2.47E−02	1.27E−01
	1BLA	1.98E−01	2.31E−01	5.04E−01	6.29E−01
	1BTF	8.14E−03	1.80E−02	1.24E−02	3.94E−01
	2BTF	8.38E−03	2.69E−02	3.08E−02	2.94E−01
	Silo	3.65E−03	2.83E−03	7.74E−04	7.70E−04

Table A-5. Total flow (m^3/year) through the vaults and waste compartments for the initial state case and the three homogeneous degradation cases studied at shoreline position 2. Note: These results correspond with the high permeable 1BMA beams.

		Shoreline position 2			
		Base case	Moderate	Severe	Complete
Vaults	1BMA	3.08E+01	3.28E+01	8.19E+01	1.25E+02
	1BLA	5.92E+01	6.66E+01	8.93E+01	1.58E+02
	1BTF	5.91E+00	8.14E+00	3.05E+01	2.56E+02
	2BTF	1.69E+01	2.24E+01	5.69E+01	1.82E+02
	Silo	6.40E−01	8.39E−01	1.41E+00	1.41E+00
Waste	1BMA	9.51E−04	1.14E−01	1.09E+01	5.57E+01
	1BLA	5.55E+01	6.52E+01	8.84E+01	1.55E+02
	1BTF	1.86E+00	3.67E+00	4.67E+00	1.73E+02
	2BTF	2.55E+00	1.11E+01	1.10E+01	1.25E+02
	Silo	5.85E−01	7.99E−01	1.39E+00	1.39E+00

Table A-6. Total flow (m^3/year) through the vaults and waste compartments for the initial state case and the three homogeneous degradation cases studied at shoreline position 3. Note: These results correspond with the high permeable 1BMA beams.

		Shoreline position 3			
		Base case	Moderate	Severe	Complete
Vaults	1BMA	6.72E+01	7.06E+01	1.81E+02	3.17E+02
	1BLA	1.29E+02	1.37E+02	2.06E+02	3.98E+02
	1BTF	1.24E+01	1.59E+01	7.38E+01	7.15E+02
	2BTF	3.03E+01	4.23E+01	1.26E+02	4.81E+02
	Silo	1.51E+00	3.02E+00	3.96E+00	3.92E+00
Waste	1BMA	2.11E−03	2.51E−01	2.53E+01	1.45E+02
	1BLA	1.21E+02	1.33E+02	2.02E+02	3.88E+02
	1BTF	3.91E+00	7.68E+00	1.21E+01	4.88E+02
	2BTF	4.94E+00	2.24E+01	2.54E+01	3.30E+02
	Silo	1.47E+00	2.94E+00	3.93E+00	3.91E+00

A2 SFR3

Table A-7. Total flow (m^3/year) through the vaults and waste compartments for the initial state case and the three homogeneous degradation cases studied at shoreline position 1. Note: 2BMA waste flows are normalized per waste compartment.

			Shoreline position 1		
		Base case	Moderate	Severe	Complete
Vaults	2BLA	1.15E−01	1.23E−01	1.34E−01	2.45E−01
	3BLA	8.04E−02	9.61E−02	1.25E−01	1.91E−01
	4BLA	8.29E−02	9.26E−02	1.15E−01	1.52E−01
	5BLA	9.65E−02	1.14E−01	1.39E−01	1.53E−01
	BRT	7.21E−02	8.94E−02	8.84E−02	2.13E−01
	2BMA	3.07E−01	3.05E−01	3.19E−01	2.97E−01
Waste	2BLA	8.39E−02	9.02E−02	9.20E−02	1.53E−01
	3BLA	5.99E−02	7.60E−02	8.98E−02	1.27E−01
	4BLA	6.19E−02	6.89E−02	8.11E−02	1.01E−01
	5BLA	6.88E−02	8.16E−02	9.78E−02	1.04E−01
	1BRT	1.29E−02	3.08E−02	3.30E−02	1.13E−01
	2BMA*	1.83E−07	2.17E−05	1.36E−03	6.90E−03
Loading Area	2BLA	4.78E−02	4.98E−02	4.59E−02	1.50E−01
	3BLA	1.19E−02	1.82E−02	6.15E−02	1.30E−01
	4BLA	2.15E−02	2.72E−02	5.14E−02	8.71E−02
	5BLA	2.98E−02	3.83E−02	9.89E−02	1.14E−01
	2MBA	2.14E−02	2.72E−02	8.97E−02	7.04E−02

Table A-8. Total flow (m^3/year) through the vaults and waste compartments for the initial state case and the three homogeneous degradation cases studied at shoreline position 2. Note: 2BMA waste flows are normalized per waste compartment.

			Shoreline position 2		
		Base case	Moderate	Severe	Complete
Vaults	2BLA	1.02E+01	1.01E+01	1.06E+01	3.92E+01
	3BLA	1.38E+01	1.52E+01	1.95E+01	3.30E+01
	4BLA	9.41E+00	9.50E+00	1.23E+01	2.49E+01
	5BLA	1.05E+01	1.03E+01	1.10E+01	1.94E+01
	BRT	9.08E+00	1.06E+01	1.23E+01	3.99E+01
	2BMA	2.24E+01	2.14E+01	3.29E+01	3.63E+01
Waste	2BLA	8.42E+00	8.48E+00	8.09E+00	2.46E+01
	3BLA	1.03E+01	1.15E+01	1.42E+01	2.28E+01
	4BLA	6.53E+00	6.97E+00	9.72E+00	1.66E+01
	5BLA	7.18E+00	7.42E+00	8.16E+00	1.27E+01
	1BRT	1.48E+00	3.10E+00	3.70E+00	1.90E+01
	2BMA*	1.41E−05	1.65E−03	1.01E−01	6.78E−01
Loading Area	2BLA	3.11E+00	3.26E+00	6.49E+00	2.81E+01
	3BLA	3.64E+00	4.05E+00	1.11E+01	1.19E+01
	4BLA	3.73E+00	4.00E+00	6.34E+00	1.20E+01
	5BLA	3.14E+00	2.72E+00	4.02E+00	8.64E+00
	2MBA	2.87E+00	2.05E+00	1.59E+01	1.09E+01

Table A-9. Total flow (m^3/year) through the vaults and waste compartments for the initial state case and the three homogeneous degradation cases studied at shoreline position 3. Note: 2BMA waste flows are normalized per waste compartment.

			Shoreline position 3		
		Base case	Moderate	Severe	Complete
Vaults	2BLA	1.60E+01	1.59E+01	1.97E+01	7.20E+01
	3BLA	2.06E+01	2.34E+01	3.18E+01	5.80E+01
	4BLA	1.61E+01	1.63E+01	2.12E+01	4.25E+01
	5BLA	1.52E+01	1.53E+01	1.72E+01	3.08E+01
	BRT	1.59E+01	1.88E+01	2.33E+01	7.43E+01
	2BMA	2.74E+01	2.62E+01	3.62E+01	3.96E+01
Waste	2BLA	1.33E+01	1.34E+01	1.48E+01	4.52E+01
	3BLA	1.51E+01	1.72E+01	2.32E+01	3.95E+01
	4BLA	1.11E+01	1.18E+01	1.64E+01	2.78E+01
	5BLA	1.13E+01	1.17E+01	1.27E+01	1.98E+01
	1BRT	2.64E+00	5.43E+00	6.78E+00	3.53E+01
	2BMA*	1.75E−05	2.05E−03	1.24E−01	8.83E−01
Loading Area	2BLA	5.33E+00	5.44E+00	1.17E+01	5.11E+01
	3BLA	5.87E+00	6.62E+00	1.68E+01	2.35E+01
	4BLA	6.14E+00	6.46E+00	9.34E+00	2.29E+01
	5BLA	4.52E+00	3.89E+00	5.08E+00	1.51E+01
	2MBA	3.71E+00	2.58E+00	1.25E+01	4.37E+00

Appendix B

Single plug model with the stepwise degradation front

The stepwise degradation front model assumes that portlandite and CSH are leached simultaneously. Once the minerals are removed, the concrete reaches a maximum porosity value of 0.3 and a hydraulic conductivity value of 1×10^{-3} m/s (Section 3.4.3). Considering the maximum effective diffusivity of the weathered zone (De = 5×10^{-10} m^2/s) the penetration of the concrete leaching front is 2.1 meters after 100 000 years (see Figure 6-1). That means that the width of the intact concrete is around 2 meters at the end of the simulation. Due to the imposed pressure at the boundaries, the pressure field remains nearly constant during the simulation (Figure B-1).

Water flow streamlines (Figure B-2) evolve similarly to the gradual degradation case (Section 6.1.2). At the initial time, the flow paths do not cross the plug and water enters the vault through the surrounding rock. When the concrete degrades, a rim with high hydraulic conductivity appears on the plug. This degraded plug rim connects the highly permeable access tunnel and the vault and the water flow is redirected through the plug (Figure B-2b).

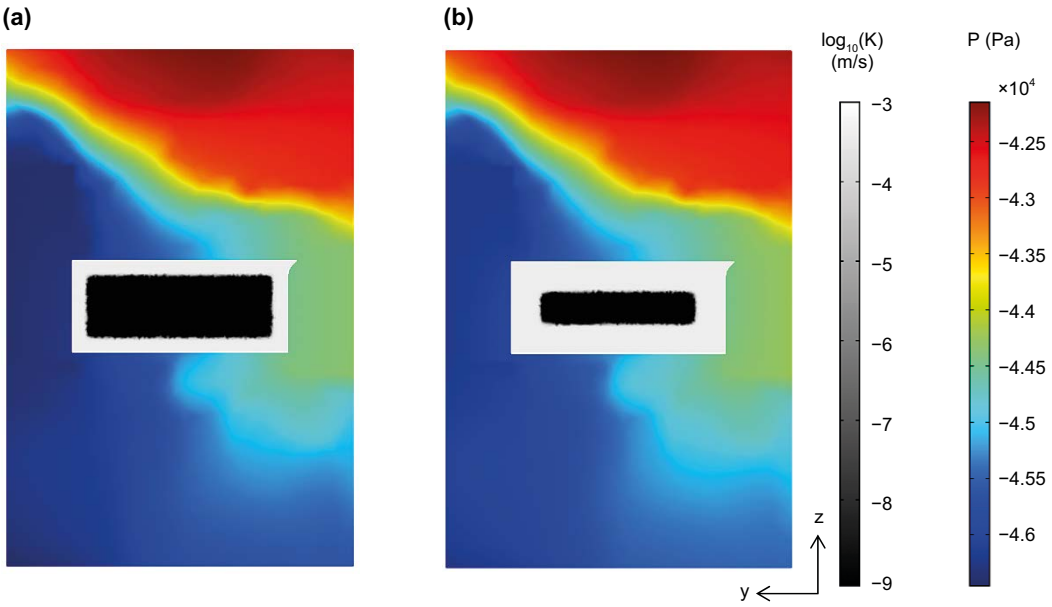

Figure B-1. *Driving pressure field (P-ρ·g·z) and hydraulic conductivity of the concrete plug (gray scale) after 25 000 y (a) and 100 000 y (b) for a step degradation front in the plug.*

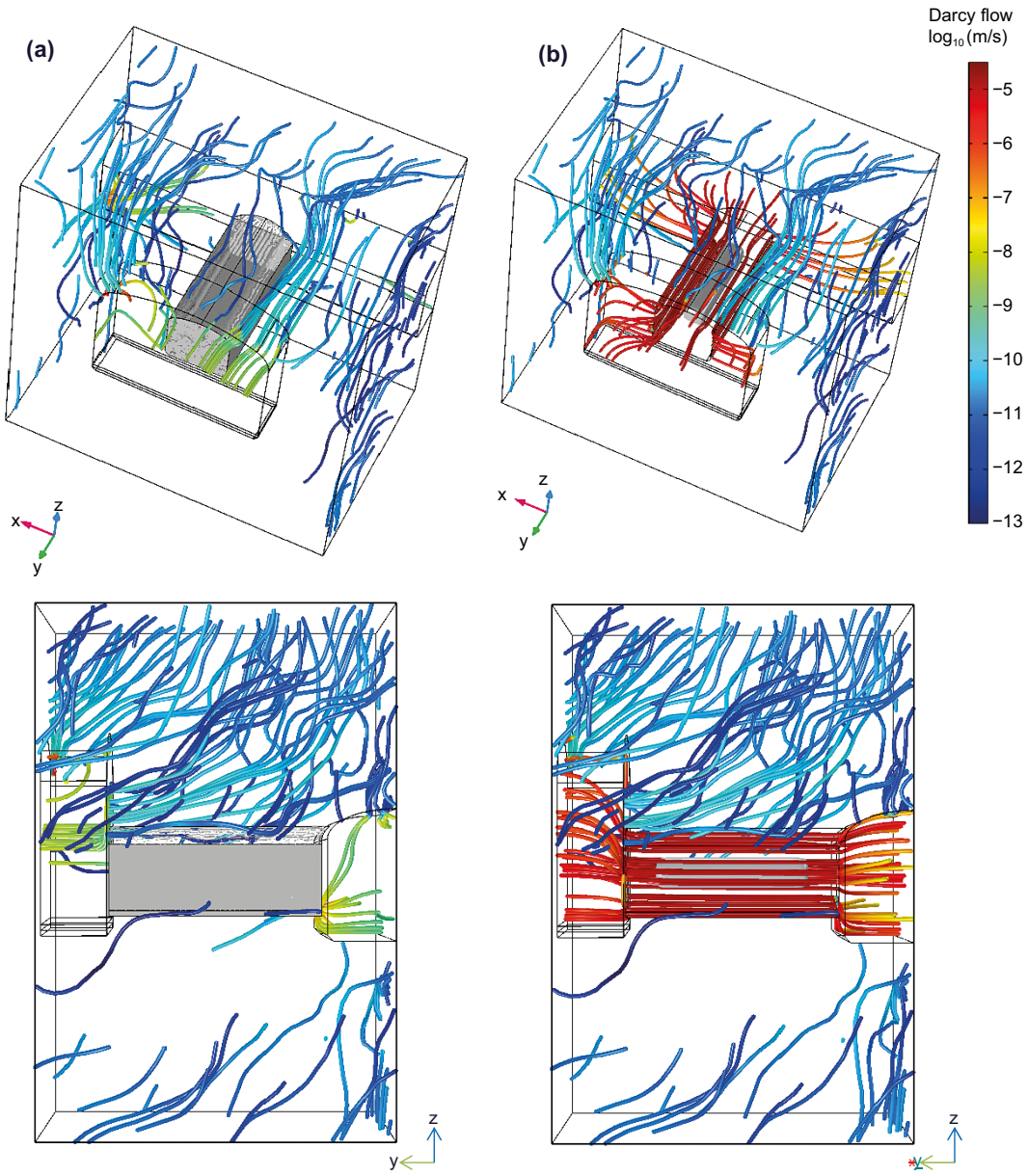

Figure B-2. *Groundwater streamlines at the initial time (a) and after 100 000 y for a step degradation front in the plug. The streamlines correspond to 200 particles released uniformly at the model boundaries. The streamlines are coloured by its Darcy flow velocity. The size of the intact concrete is shown in grey.*

B1 Comparison between stepwise and gradual degradation

The gradual degradation front differs from the step degradation front in the presence of a transition zone between the completely degraded and the intact concrete. The higher flow resistance of this transition zone affects the groundwater flow velocity (Figure B-3) and hence the amount of water crossing the plug (Figure B-4).

Darcy velocities along the plug of the order of 1×10^{-11} m/s in the intact concrete and of the order of 1×10^{-5} m/s in the degraded concrete are computed in the step degradation case (Figure B-3a). This increase of 6 orders of magnitude in the groundwater velocity occurs also at the gradual degradation case. However, the transition zone between the intact and the totally degraded concrete yields intermediate velocities (Figure B-3b). Flow through the intact concrete is slightly higher for the gradual degradation case. In the stepwise degradation case, the greater degraded volume surrounding the intact concrete acts as a hydraulic bypass, which reduces the flow through the intact concrete.

The groundwater flow crossing the interface between the concrete plug and the vault is shown in Figure B-4. This flow increases at early times in the stepwise degradation case while in the gradual degradation case, only after 30 000 y the groundwater flow between the plug and the vault is greater than 20 m^3/y.

The stepwise degradation case can be considered as an overly conservative case and its results should be analysed cautiously. The gradual degradation case is also a conservative case, e.g., the maximum effective diffusivity value used in the shrinking core model or the maximum hydraulic conductivity of the modified Kozeny-Carman relation.

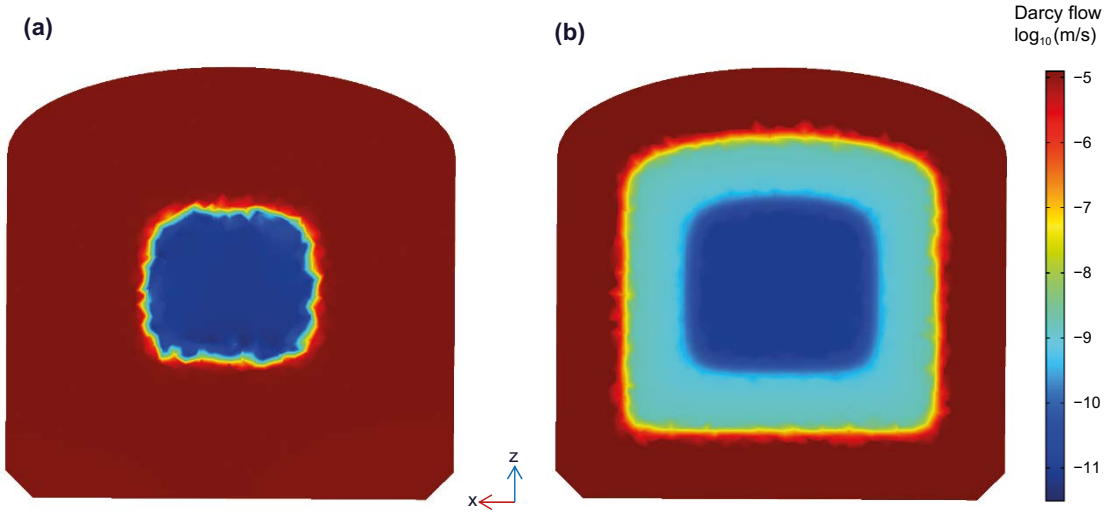

Figure B-3. *Darcy flow velocity in a vertical cross-section of the concrete plug after 100 000 y for the step degradation case (a) and for the gradual degradation case (b) single plug model.*

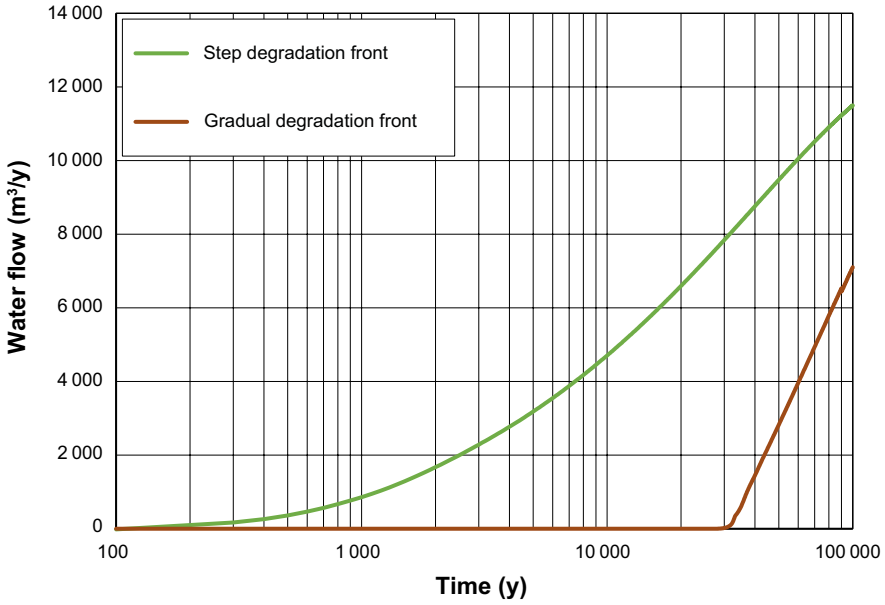

Figure B-4. *Evolution of the groundwater flow crossing the interface between the concrete plug and the vault for the stepwise degradation and the gradual degradation case.*

Appendix C

Axial concrete degradation

C1 Groundwater flow sensitivity to axial plug degradation

This appendix contains the results of a sensitivity analysis to the effect of the plug degradation using the shrinking core plug degradation over the waste and tunnel flow rates. This study contains a set of seven simulations with different leaching depths. The Figure C-1 shows the hydraulic conductivity of the plugs for the different studied cases. Note that this study evaluates only the effect of the plug degradation over the tunnel and waste flow rates. The rest of concrete structures remain intact for the different cases studied.

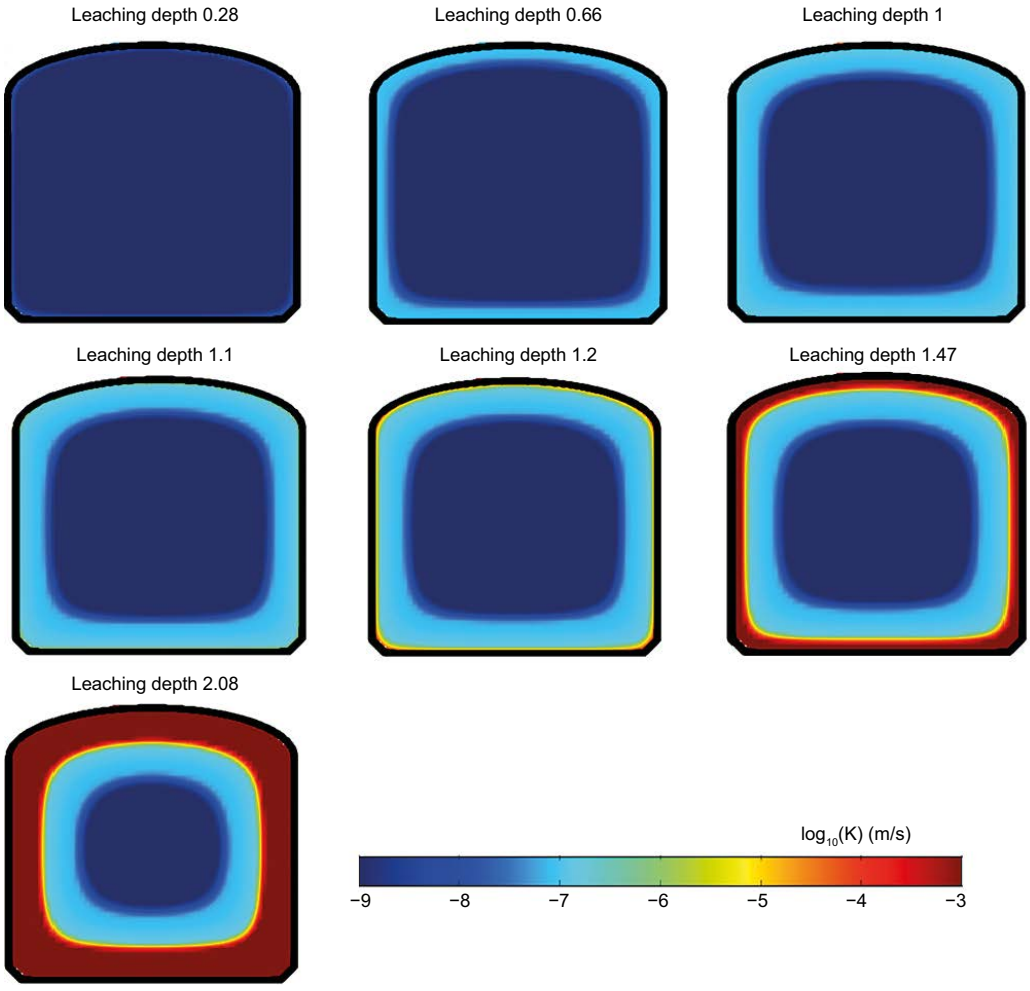

Figure C-1. *Hydraulic conductivity of the sealing plugs for the different leaching depth studied showed in a 2D perpendicular cross-section.*

The results of the simulations show that the plug degradation affects the tunnel flow rate from a leaching depth above 1.2 m (Figure C-2 and Figure C-4). With a leaching depth of 1.2 m or above, the maximum hydraulic conductivity of the plugs is 1×10^{-3} m/s and the amount of water entering the vaults increases significantly. The effect of the concrete degradation is lower in the waste flow rates of the vaults that contain concrete barriers (1–2BMA) or the vault with an homogenized waste (BRTs and BTFs) (Figure C-3 and Figure C-5).

The following section contains the groundwater flow entering in the vaults and waste control volumes for the different leaching depth studied in the and SFR 3. The results of the SFR 1 repository refer to the case of 1BMA with low permeable beams. However, the results of the 1BMA vault with high permeable beams (1BMA HPB) are also reported for completeness (Figure C-2 and Figure C-3).

C2 SFR 1

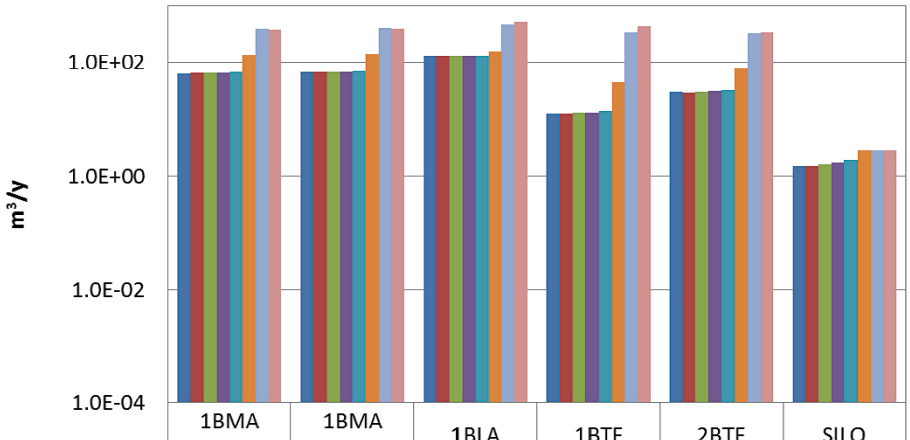

	1BMA LPB	1BMA HPB	1BLA	1BTF	2BTF	SILO
IS	6.49E+01	6.72E+01	1.29E+02	1.24E+01	3.03E+01	1.51E+00
LD 1 h=0.208	6.51E+01	6.73E+01	1.30E+02	1.25E+01	3.01E+01	1.50E+00
LD 2 h=0.66	6.55E+01	6.78E+01	1.30E+02	1.28E+01	3.08E+01	1.60E+00
LD 3 h=1	6.65E+01	6.88E+01	1.30E+02	1.31E+01	3.14E+01	1.77E+00
LD 4 h=1.1	6.90E+01	7.15E+01	1.29E+02	1.38E+01	3.28E+01	1.92E+00
LD 5 h=1.2	1.39E+02	1.44E+02	1.57E+02	4.47E+01	8.09E+01	2.85E+00
LD 6 h=1.47	3.89E+02	3.95E+02	4.69E+02	3.41E+02	3.27E+02	2.86E+00
LD 7 h=2.08	3.79E+02	3.86E+02	5.21E+02	4.35E+02	3.43E+02	2.85E+00

Figure C-2. *Total flow (m^3/year) through the SFR1 vaults for the different concrete degradation cases. The vertical axis is logarithmic. Note the results refer to the simulation with low permeable 1BMA beams except for the 1BMA HPB case.*

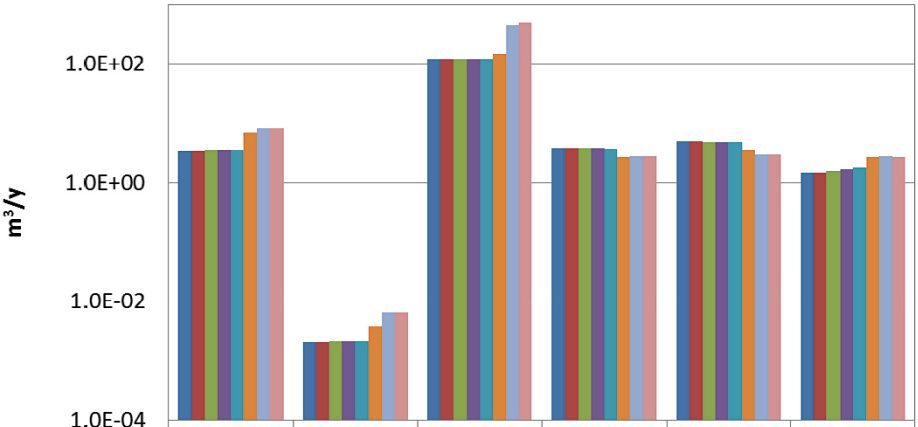

	1BMA LPB	1BMA HPB	1BLA	1BTF	2BTF	SILO
IS	3.44E+00	2.11E-03	1.21E+02	3.91E+00	4.95E+00	1.47E+00
LD 1 h=0.208	3.43E+00	2.11E-03	1.22E+02	3.90E+00	4.94E+00	1.45E+00
LD 2 h=0.66	3.48E+00	2.13E-03	1.22E+02	3.86E+00	4.91E+00	1.55E+00
LD 3 h=1	3.55E+00	2.15E-03	1.22E+02	3.81E+00	4.89E+00	1.71E+00
LD 4 h=1.1	3.68E+00	2.20E-03	1.22E+02	3.73E+00	4.83E+00	1.85E+00
LD 5 h=1.2	7.00E+00	3.70E-03	1.48E+02	2.73E+00	3.49E+00	2.75E+00
LD 6 h=1.47	8.43E+00	6.62E-03	4.52E+02	2.77E+00	2.97E+00	2.75E+00
LD 7 h=2.08	8.46E+00	6.51E-03	5.02E+02	2.81E+00	2.98E+00	2.75E+00

Figure C-3. *Total flow (m^3/year) through the SFR1 waste domains for the different concrete degradation cases. The vertical axis is logarithmic. Note the results refer to the simulation with low permeable 1BMA beams except for the 1BMA HPB case.*

C3 SFR3

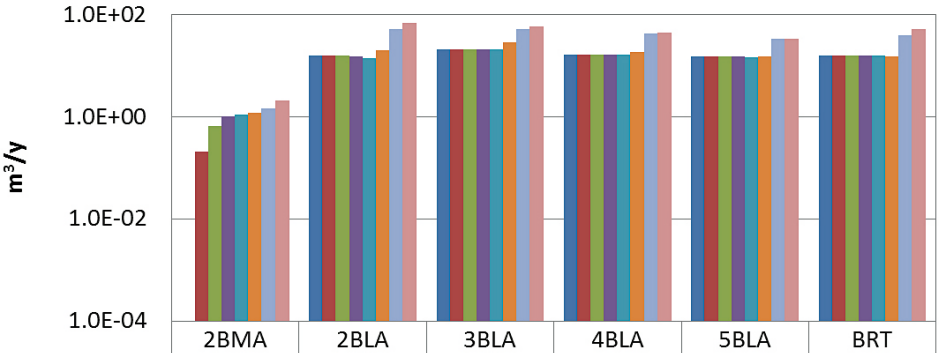

	2BMA	2BLA	3BLA	4BLA	5BLA	BRT
IS	0.00E+00	1.60E+01	2.06E+01	1.61E+01	1.52E+01	1.59E+01
LD1 h=0.208	2.08E-01	1.58E+01	2.06E+01	1.61E+01	1.50E+01	1.58E+01
LD2 h=0.66	6.60E-01	1.55E+01	2.04E+01	1.62E+01	1.50E+01	1.58E+01
LD3 h=1	1.00E+00	1.51E+01	2.04E+01	1.62E+01	1.49E+01	1.58E+01
LD4 h=1.1	1.10E+00	1.41E+01	2.05E+01	1.63E+01	1.46E+01	1.56E+01
LD5 h=1.2	1.20E+00	1.97E+01	2.88E+01	1.84E+01	1.49E+01	1.51E+01
LD6 h=1.47	1.47E+00	5.25E+01	5.26E+01	4.19E+01	3.33E+01	3.89E+01
LD7 h=2.08	2.08E+00	6.84E+01	5.79E+01	4.39E+01	3.30E+01	5.18E+01

Figure C-4. *Total flow (m^3/year) through the SFR3 vaults for the different leaching depths studied degradation cases. The vertical axis is logarithmic.*

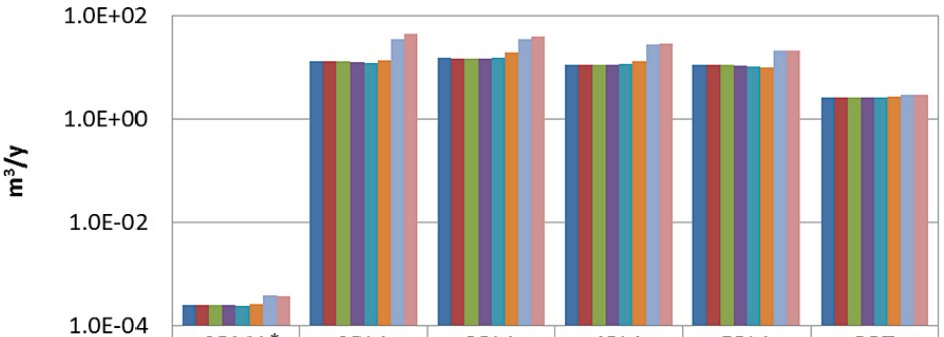

	2BMA*	2BLA	3BLA	4BLA	5BLA	BRT
IS	2.46E-04	1.33E+01	1.51E+01	1.11E+01	1.13E+01	2.64E+00
LD1 h=0.208	2.45E-04	1.31E+01	1.50E+01	1.11E+01	1.12E+01	2.60E+00
LD2 h=0.66	2.44E-04	1.29E+01	1.49E+01	1.12E+01	1.11E+01	2.58E+00
LD3 h=1	2.44E-04	1.27E+01	1.49E+01	1.13E+01	1.10E+01	2.58E+00
LD4 h=1.1	2.42E-04	1.20E+01	1.51E+01	1.15E+01	1.04E+01	2.56E+00
LD5 h=1.2	2.57E-04	1.37E+01	1.93E+01	1.31E+01	9.92E+00	2.72E+00
LD6 h=1.47	3.87E-04	3.44E+01	3.54E+01	2.75E+01	2.12E+01	2.91E+00
LD7 h=2.08	3.69E-04	4.40E+01	3.89E+01	2.89E+01	2.13E+01	2.90E+00

Figure C-5. *Total flow (m^3/year) through the SFR3 waste domains for the different concrete degradation cases. The vertical axis is logarithmic. 2BMA waste flow is normalized with respect the number of waste compartments.*

Arkitektkopia AB, Bromma, 2022

SKB is responsible for managing spent nuclear fuel and radioactive waste produced by the Swedish nuclear power plants such that man and the environment are protected in the near and distant future.

skb.se